



THE UCLA Undergraduate Science Journal

Volume 38 | Spring 2025

In Vitro Reconstituted Enveloped
Virus-Like Particles for Gene Delivery

Selina Juang • p. 34

Immunofluorescence of Mouse Fetal Ovary
Reveals Timing of Meiotic Progression

Azra Cruz • p. 43

Non-Invasive Analysis of Vessel Wall
Vibrations During Blood Flow

Ashwath Nayagadurai • p. 67

2024–2025 USJ Staff

Faculty Advisor

Jorge A. Avila, PhD

Editors in Chief

Dashrit K. Pandher
Sohan Talluri

Logistics Coordinator

Archi K. Patel

Review

Managing Editor
Malvika Iyer

Editorial

Managing Editor
Isabel Angres

Layout

Managing Editor
Dashrit K. Pandher

Asst. Managing Editors

Caden Chow
Kuan Heng Lin
Melody Jiang
Nyah Zhang
Oliver Wang

Asst. Managing Editors

Brynn Beatty
Chahak Gupta
Nhi H. Pham
Tanisha Lakhanpal
Timothy Liu

Asst. Managing Editor

Zenya Bian

Board

Aryan Law
Beverly Luring
Catherine Zhang
Felisha Kuo
Joanna Rhim
Katherine A. Morrisette
Ken Woo
Khushi Sharma
Miki Matsuoka
Naisha Agarwal
Nathan Abraham Joshua
Sofia Ando
Sumedha M. Shastry
Summer Kelso
Vedant V. Janapaty

Board

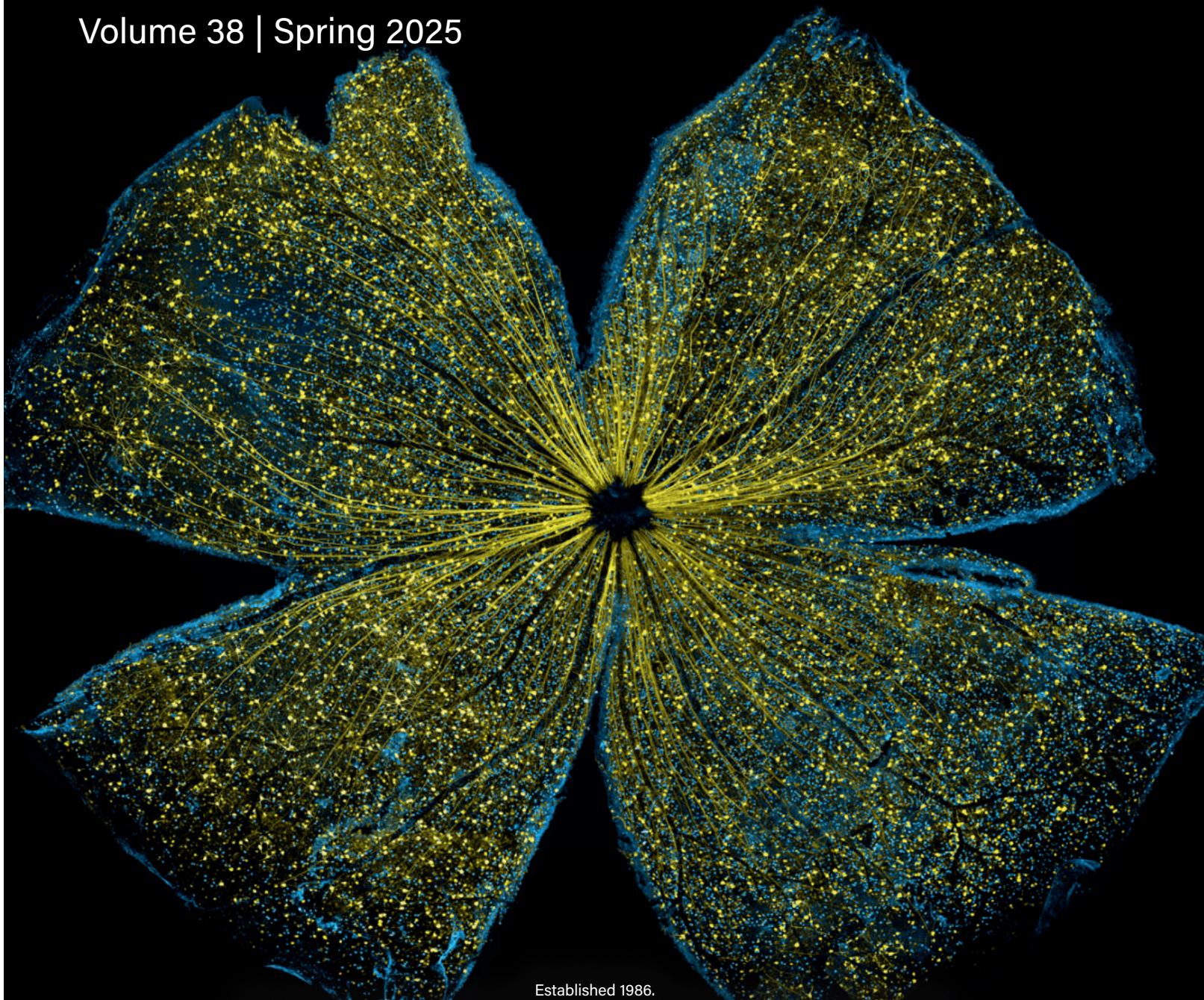
Andrew Tsui
Aniket Das
Emre Gürdal
Eshika Abbaraju
Gia Boisselier
Karch A. Borsa
Kavya M. Pandrangi
Lee Zucker-Murray
Marie Yang
Paul Zhang
Phillip Tang
Prannay Veerabahu
Priya Ravi
Ryan Wong
Siddhika Naik
Spencer Bergland
Truman Ma
Vyas Koduvayur
Yubin Kim

Board

Ahmad Ismail
Hongbo Zhu
Katelyn Mak
Lucas J. Kim
Megan Huang
Natalia Liang
Renee Chowdhry

THE UCLA Undergraduate Science Journal

Volume 38 | Spring 2025



Established 1986.

The UCLA Undergraduate Science Journal is an officially recognized student organization at UCLA.

The UCLA Undergraduate Science Journal is entirely managed and produced by students.

Its contributions are the original work of UCLA undergraduates.

FRONT COVER IMAGE TAKEN BY MEGAN HUANG.

INSIDE COVER IMAGE COURTESY OF KEUNYOUNG KIM, WONKYU JU AND MARK ELLISMAN, NATIONAL CENTER FOR MICROSCOPY AND IMAGING RESEARCH, UNIVERSITY OF CALIFORNIA, SAN DIEGO.



A Letter from the Editors

Dear Reader,

We are incredibly proud to present to you the 38th Volume of the UCLA Undergraduate Science Journal (USJ). The entirety of this volume is the direct result of undergraduate student effort, from the outstanding manuscripts to the peer review, editing, and layout of the journal. We are truly impressed with the caliber of research conducted by this year's undergraduate authors, as well as the tireless diligence and dedication of the staff members in our Review, Editorial, and Layout Boards. This volume of the USJ includes both original research and review articles, ranging from developing novel methods for the delivery of gene therapies to studying the Collatz conjecture, one of the most famous unsolved questions in mathematics. The articles featured in this journal may only offer a small glimpse into the breadth of research that undergraduates undertake at UCLA, but they are a true representation of the ingenuity and tenacity of our students. We are honored to be a part of this scientific collaboration and we are confident you will see these values exemplified in this year's volume of the USJ.

As Editors-in-Chief, we couldn't be more proud of the growth of the USJ throughout our time here. Continuing the efforts of last year's USJ leadership, one hallmark of our tenure is the summation of our revamp of the USJ seminar. Every year, USJ staff members enroll in a 2.0 unit seminar to learn the review, editorial, and layout skills necessary for their role in USJ, as well as experience the USJ's publication process outside of their board. This year, as Editors-in-Chief, we completed our overhaul of the course's training materials to be interactive, student-led, and better-aligned with the seminar's goals. Our revised training curriculum allows all members to not only learn about each step of the USJ publication process, but directly experience each step for themselves as they discover review, editorial, and layout errors in a series of sample articles and craft their Newsbeats, several of which are featured in the USJ. We hope this experience inspires future leadership teams to build on the foundations laid by their predecessors to effect change for the betterment of both the staff and journal.

Last year, the USJ also reinstated staff-written interview articles highlighting the experiences of the undergraduate authors and faculty advisors whose research is presented in the journal. Continuing this tradition, this year's interview articles feature the stories, advice, and scientific understanding of our authors and faculty advisors to further contextualize their published research, offer insight into the undergraduate research environment at UCLA, and encourage undergraduate students to take advantage of the many exciting research opportunities that UCLA has to offer.

This journal would not be possible without the labor and love of our entire team. We would like to especially commend the passion and dedication of all of our USJ staff members who worked with us to make this year's journal the best it could be. A huge thank you goes to our managing editors, assistant managing editors, and logistics coordinator for the amazing work and long hours you have all dedicated to the USJ. Of course, we would like to express our heartfelt gratitude to our faculty advisor, Dr. Jorge Avila, who supported us throughout the entire publication process and without whom the USJ would not exist. Dr. Avila has been extremely supportive and encouraging of our ideas to improve USJ, including completely refreshing our seminar. Additionally, we sincerely thank Dr. Tama Hasson, the director of the Undergraduate Research Center—Sciences, who provides pivotal support to publish our journal, and the UCLA Clinical and Translational Science Institute for their generous continued support. Finally, we would like to thank ColorNet Press for helping us produce this beautiful print journal.

We hope you are inspired while reading about the science featured in this journal, in fields that touch many aspects of our daily lives. At a time when the research enterprise has come under significant pressure, this journal stands as a testament to the sheer courage and determination of our journal staff and undergraduate authors—we could not be more honored to share this volume with you.

Warm regards,
Sohan Talluri and Dashrit Pandher

TABLE OF CONTENTS

- 06 Newsbeats**
USJ Staff



INTERVIEW

- 11 Improving Gene Therapy One Vector at a Time**
Tanisha Lakhanpal, Prannay Veerabahu, Khushi Sharma, Isabel Angres
- 14 The Endeavor to Restore Brain Health Through Neuroprotective Research**
Karch Borsa, Priya Ravi, Sumedha Shastry, Paul Zhang, Sohan Talluri
- 17 Fluid Dynamics Reveal the Physics of Aneurysms**
Vyas Koduvayur, Oliver Wang, Dashrit Pandher
- 20 Uncovering Metabolic Adaptations in Prostate Cancer**
Ken Woo, Joanna Rhim, Katherine Morrisette, Andrew Tsui, Malvika Iyer
- 24 Mapping the Future of Reproductive Biology**
Chahak Gupta, Melody Jiang, Phillip Tang, Archi Patel

REVIEW

- 26 Various Fruit Consumption Forms and Their Health Outcomes**
Shubhreet Bhullar

RESEARCH

- 34 *In Vitro* Reconstituted Enveloped Virus-Like Particles for Gene Delivery**
Selina Juang
- 43 Immunofluorescence of Mouse Fetal Ovary Reveals Timing of Meiotic Progression** 
Azra Cruz
- 48 Differential Effects of Iron Chelation on Ferroptosis and Neuroprotection**
Caterina Stoica
- 54 Collatz Conjecture: Odd Integers do not Strictly Increase**
Jiali Chen
- 58 Investigating Mitochondrial Evolution in Advanced Prostate Cancer** 
Kylie Heering
- 67 Non-Invasive Analysis of Vessel Wall Vibrations During Blood Flow**
Ashwath Nayagadurai

Addy and Mary Jane: Friends or Foes?

Zenya Bian

As recreational marijuana becomes increasingly accessible in the US, complications resulting from simultaneous usage with common medications such as Adderall have become a concern. A recent study showed that consistent exposure to inhaled cannabis may have the potential to reduce an individual's sensitivity to amphetamines. fMRI imaging of mice subjected to prolonged hotboxing revealed that areas of the brain typically stimulated by Adderall had significantly reduced activity compared to control mice. Interestingly, neurochemical sensitivity to Adderall returned to normal levels in the experimental group after two weeks of marijuana discontinuation. Given the widespread usage of marijuana and Adderall in today's society, more comprehensive studies behind this phenomenon are warranted. The next time you're getting ready to go out, it may be best to leave one of the girls behind.



Image: Green leaves growing in abundance.

Reference: J. M. Ognibene, R. I. Desai, P. P. Kulkarni, C. F. Ferris, Chronic exposure to inhaled vaporized cannabis high in Δ^9 -THC suppresses adderall-induced brain activity. *Front. Pharmacol.* **15**, 1413812 (2024). doi: 10.3389/fphar.2024.1413812

Image Source: Photo credit to Jeff W. Image is free to use under Unsplash license.

Meet DeTox: A Venomous Organism Toxin Detection Tool

Megan Huang



Meet DeTox—originally crafted for neogastropod mollusks, this versatile data pipeline adapts to any venomous organism, with an 88–100% toxin detection rate when applied to test transcriptome datasets. By combining both similarity and structure-based approaches, DeTox uses a more comprehensive toxin discovery process compared to existing tools, identifying both confirmed and novel toxins. This pipeline takes in RNA-seq transcriptome data and outputs a single file containing a table summarizing the found toxins, along with customizable key information (such as cysteine patterns, possible cell locations, and gene expression levels) that showcase DeTox's modular nature. With a simple and intuitive interface, the pipeline is suitable for both experienced bioinformaticians as well as novice researchers. By streamlining the toxin identification process, DeTox provides new insights into venom composition quicker than ever before and holds significant potential in advancing evolutionary biology and drug discovery.

Image: *Anthopleura elegantissima*—a venomous species of sea anemone.

Reference: A. Ringeval et al., DeTox: A pipeline for the detection of toxins in venomous organisms. *Brief. Bioinform.* **25**, bbae094 (2024). doi: 10.1093/bib/bbae094

Image Source: Aggregating anemone. *Animalia.bio*. Licensed under CC BY-SA 4.0.

Fat Cats: The Key to Human Obesity?

Gia Boisselier

In the United States, an astounding 60% of domestic cats are overweight or obese. Feline obesity comes with severe comorbidities including osteoarthritis, hip dysplasia, and numerous cardiovascular diseases. In a recent study, researchers scrutinized the effects of a calorie-restrictive diet on domestic cats, with a specific focus on gut microbial composition and short-chain fatty acids. Over a time period of 16 weeks, researchers administered a four phase diet to 7 cats while collecting fecal samples and monitoring their body weight. Over the course of the diet, the study identified an increase of propionic acid in fecal samples as weight decreased over time. This change was notably associated with a rise in the bacterium *Prevotella 9 copri*, a species that had been previously linked to human weight loss and blood sugar control. These findings suggest that understanding the feline gut microbiota may be a useful translational model for human obesity, as pet owners share similar environments and foods with their beloved cats.



Image: Artistic rendition of an obese cat and its gut microbiome.

Reference: J. C. Rowe et al., Gut microbiota promoting propionic acid production accompanies caloric restriction-induced intentional weight loss in cats. *Sci. Rep.* **14**, 11901 (2024). doi: 10.1038/s41598-024-62243-4

Image Source: Illustration by Gia Boisselier.

Interventions to Slow Myopia Are Closer Than They Appear

Caden Chow

Seemingly distant solutions are coming into focus. The rapid onset of childhood myopia—a global epidemic commonly known as nearsightedness—is strongly associated with increased time spent indoors. While scientists previously struggled to identify behaviors that accelerate myopia, Dr. Yuanyuan Hu's team in Shandong, China conducted a clinical trial to evaluate myopic onset in children who received vibrational reminders for adequate exposure to lighting, head positioning, and distance of eyes from work. The eye physiology of children who received behavioral interventions for proper eye use exhibited significantly lower myopic progression than that of children who did not receive interventions. Children in the intervention group also demonstrated significantly improved eye use in the short term. These results are promising for in-home myopia interventions, as these eye use reminders may be implemented by parents and caregivers without complex technology. Future studies establishing long-term behavioral changes may ensure that myopia stays out of sight.

Image: Artistic rendition of a human eye with the image of an autorefractor test inside the pupil.

Reference: Y. Hu et al., Behavioral intervention with eye-use monitoring to delay myopia onset and progression in children: A cluster randomized trial. *Ophthalmology* (2025). doi: 10.1016/j.optha.2025.01.003

Image Source: Illustration by Caden Chow.



What Does Your Dog Want? Just Ask!

Eshika Abbaraju



Dogs may have a greater cognitive ability than we think. A recent study at UCSD's Comparative Cognition Lab demonstrate that dogs trained with soundboards of buttons that “speak” when pressed can express their needs using two-button combinations. By comparing presses per each category of buttons between owners and their dogs using a Bayesian negative binomial model, researchers found the dogs were likely not simply repeating their owner's motions. Additionally, using a mixed effects model for each dog's presses, they found the dogs pressed certain combinations, such as “food” and “treat,” more, despite having different soundboards, suggesting the dogs' actions were deliberate. Calculated Randomness Index (RI) values, which indicate non-randomness when nearer to -1 than 1 , for networks of the dogs' presses were closer to -1 than for randomly generated networks. These findings highlight the potential for interspecies communication and offer owners a practical method to better comprehend their dog's needs.

Image: A dog speaking at a press conference into a set of microphones.

Reference: A. P. M. Bastos, Z. N. Houghton, L. Naranjo, F. Rossano, Soundboard-trained dogs produce non-accidental, non-random and non-imitative two-button combinations. *Sci. Rep.* **14**, 28771 (2024). doi: 10.1038/s41598-024-79517-6

Image Source: Free to use under the iStock License.

Metabolic Approaches to Understanding Neurodegenerative Disease

Malvika Iyer

The approach of studying neurodegenerative diseases has expanded past the realm of basic neuroscience as understanding the role of brain metabolism in maintaining healthy brain function is becoming more important. This is particularly relevant in preventing and treating complicated diseases, like Alzheimer's and Parkinson's. This article used mass spectrometry and quantitative -omics approaches to explore how disruptions in brain housekeeping functions like autophagy (cellular recycling) can lead to neuron damage and loss of motor function. ATG5, a crucial receptor on the autophagosome membrane, was found to have an important role in maintaining cerebellar Purkinje cell (PC) survival as it regulates glycolytic activity and glucose metabolism. Loss of ATG5 resulted in elevated lactate production and toxic metabolic byproducts from glycolysis, which caused neuronal death in ATG5-deficient PCs. While more research is required to understand the impact of ATG5 in human models of neurodegeneration, this study is a crucial step in the development of metabolic therapies for neurodegenerative diseases.

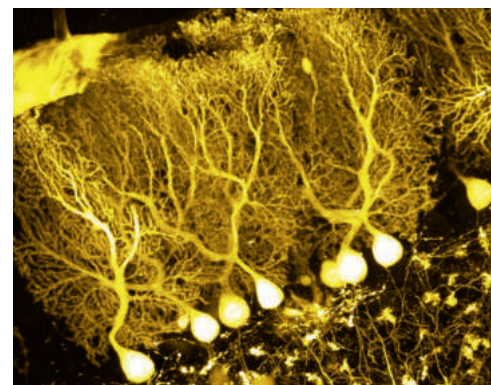


Image: Immunofluorescent stain of Purkinje cells.

Reference: J. Tutas et al., Autophagy regulator ATG5 preserves cerebellar function by safeguarding its glycolytic activity. *Nat. Metab.* **7**, 297–320 (2025). doi: 10.1038/s42255-024-01196-4

Image Source: BrainsRusDC. All that glitters in the brain. *Wikimedia Commons*. Licensed under CC BY-SA 4.0.

Dreams: Your Brain's Emotional Reset Button

Vyas Koduvayur

You've probably woken up before in cold sweats, panic setting in as you realize you missed your midterm—only to realize it was just a dream. Or maybe it's the opposite, where your grade is suddenly amazing, and for a moment, it feels like you've won the lottery. Why does this happen? New research suggests that dreams may help us process memories and reduce stress. In a study at UC Irvine, researchers asked 125 adults to rate emotional images before sleeping and then monitored their sleep. The next morning, participants were asked about their dreams and the images. Interestingly, "dream recallers" experienced a unique memory tradeoff: they retained negative emotional images while forgetting neutral ones. They also exhibited reduced emotional reactivity after waking, suggesting that dreaming actively helps regulate emotions and filter memories. So the next time you're pulling an all-nighter, just remember—your GPA isn't the only thing on the line.



Image: An artistic depiction of the neural pathways that bring about our dreams.

Reference: J. Zhang et al., Evidence of an active role of dreaming in emotional memory processing shows that we dream to forget. *Sci. Rep.* **14**, 8722 (2024). doi: 10.1038/s41598-024-58170-z

Image Source: Geralt. Abstract cerebrum. Pixabay. Licensed under CC0 1.0.

Can Wildfires Increase Mercury in the Water?

Joanna Rhim



After the containment of raging wildfires across Los Angeles County, many scientists turned their attention to a critical water source—headwater streams. These streams are the starting points of rivers that can influence downstream water quality. Researchers from the U.S. Geological Survey sampled soils in Pacific Northwest headwater streams to evaluate the impact of wildfires on methylmercury (MeHg) and mercury (Hg) levels, focusing on their transportation, methylation, and bioaccumulation. Total mercury (THg) increased by 89%, and MeHg by 178%, in burned watersheds compared to unburned watersheds. Filter-passing MeHg was also higher, with greater enrichment on particles, but filtered THg showed only minor differences between burned and unburned watersheds. Therefore, more frequent and severe wildfires can increase MeHg production and movement in headwaters, negatively affecting downstream areas. Further research on wildfires and abiotic or biotic mercury in headwater systems can help apply these findings to the recent fires in Los Angeles.

Image: Palisades Fire visible from the UCLA Centennial Hall.

Reference: A. K. Baldwin et al., Wildfires influence mercury transport, methylation, and bioaccumulation in headwater streams of the Pacific Northwest. *Environ. Sci. Technol.* **58**, 14396–14409 (2024). doi: 10.1021/acs.est.4c00789

Image Source: Photo by Joanna Rhim.

Flying Insects and Light: Attraction or Confusion?

Truman Ma

For centuries, insects' attraction to artificial light has remained a mystery with explanations ranging from warmth to lunar navigation. However, researchers from Imperial College London believe insects are disoriented and trapped by artificial light. In the lush rainforests of Costa Rica, field recordings revealed three insect flight behaviors around light: orbiting, stalling, and inverting. Motion captured videos also identified an interesting tendency: insects consistently tilt their back toward light sources. Combining this dorsal tilting with the insects' flight trajectories revealed that insects do not fly towards light. Instead, they maintain a perpendicular direction of flight around a light source, trapped in a planetary-like orbit. It is possible that insects mistake artificial light for the overhead sun, causing an incorrect sense of upward direction and gravity. Flying insect entrapment can devastate their ecology, so this research reveals unintended consequences of artificial light, potentially suggesting better open light placement and design.



Image: Moths circling an artificial light source.

Reference: S. T. Fabian, Y. Sondhi, P. E. Allen, J. C. Theobald, H. Lin, Why flying insects gather at artificial light. *Nat. Commun.* **15**, 689 (2024). doi: 10.1038/s41467-024-44785-3

Image Source: Евгения Егорова. White and black pendant lamp. Pexels. Licensed under CC0 1.0.

Fully Mapping the Fly Brain

Paul Zhang

In a milestone for neuroscience, researchers successfully created a complete model of an adult *Drosophila melanogaster* brain, consisting of 139,255 neurons and 50 million synapses. Using serial section transmission electron microscopy, they created cross-sections at minute intervals across the length of the fly brain. The cross sections were subsequently aligned, and each neuron's components were identified. Then, synapses were automatically detected and the rough brain model was proofread. This model of the *Drosophila* brain can be used to derive the underlying neural circuits governing *Drosophila* behavior. As a demonstration, the researchers used the model to trace a pathway from a subset of photoreceptors to descending motor neurons. However, several limitations still exist in the model, such as the exclusion of electrical synapses and underestimation of the number of chemical synapses.

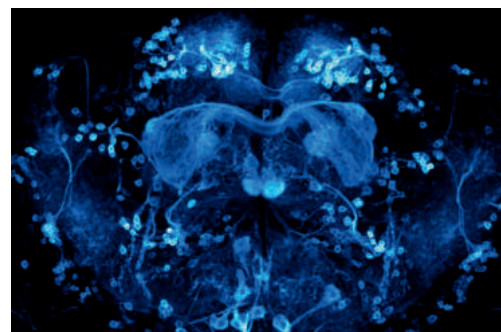


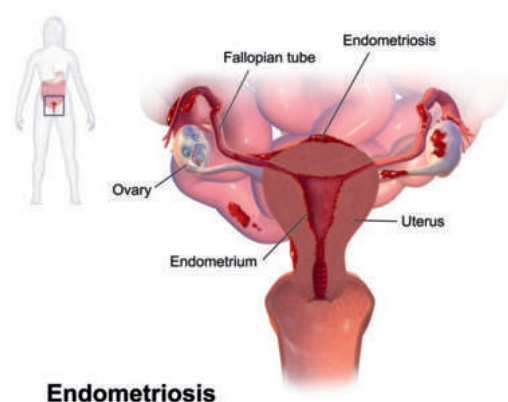
Image: Although relatively simple, the brain of *Drosophila melanogaster* has over 100,000 neurons.

Reference: S. Dorkenwald et al., Neuronal wiring diagram of an adult brain. *Nature* **634**, 124–138 (2024). doi: 10.1038/s41586-024-07558-y

Image Source: Photo by Vincent Croset. Licensed under the Creative Commons Attribution

Microbial Diversity as an Indicator of Disease in Endometriosis Patients

Katherine Morrisette



Approximately 10% of women suffer from endometriosis, a disease characterized by tissue similar to the endometrium (uterine lining) that proliferates and metastasizes like cancer. This leads to infertility, chronic pain, and organ damage. To develop more effective treatment protocols, it is critical to understand the disease's development. A recent study by Guo *et al.* examined how an altered endometrial microbiome composition can affect endometriosis progression. Researchers biopsied 43 participants (13 healthy and 30 with endometriosis) and employed various techniques, including immunohistochemistry and rRNA sequencing, to characterize the microbes found. Statistical analysis of the data showed that the endometriosis patients had significantly more diverse endometrial microbiomes, a likely indicator of pathology. This study did not factor participants' menstrual cycles into the analyses, despite previous research showing cycle influence on the endometrial microbiome. Despite this limitation, this study elucidated a potential driving factor of endometriosis, which could eventually be a therapeutic target.

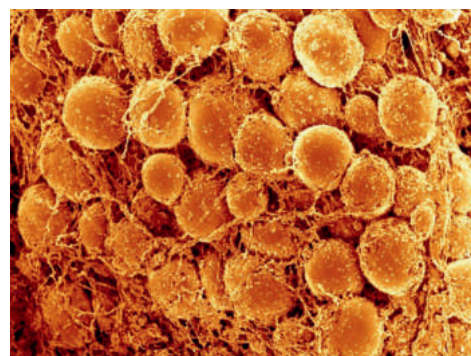
Image: Endometriosis. A diagram of a uterus, ovaries, and fallopian tubes with endometriosis lesions.

Reference: W. Guo, Z. Xu, S. Hu, Y. Shen, Exploring microbial signatures in endometrial tissues with endometriosis. *Int. Immunopharmacol.* **148**, 114072 (2025). doi: 10.1016/j.intimp.2025.114072

Image Source: Blausen.com staff. "Medical gallery of Blausen Medical 2014". *WikiJournal of Medicine*. Licensed under CC BY 3.0.

Can Fat Cells Remember Obesity?

Beverly Lauring



A recent study shows that even after losing weight, your fat cells might still "remember" obesity. Using single-nucleus RNA sequencing and epigenetic profiling on both human and mouse models, researchers found that chromatin modifications H3K4me1 and H3K27ac persist in fat cells, or adipocytes, post-weight loss. These lingering epigenetic marks maintain a regulatory environment that predisposes the body to regain weight. The study suggests that this epigenetic memory could influence gene expression linked to metabolism and inflammation, priming the body for weight regain. Targeting these epigenetic marks could offer new therapeutic targets for preventing weight cycling, though more research is needed to determine whether these modifications can be reversed. Obesity treatment is often challenged by persistent weight regain, and understanding how adipose tissue "remembers" past weight states could not only help patients lose weight, but leave their old weight behind for good.

Image: Adipose tissue, close-up showing adipocytes.

Reference: L. C. Hinte et al., Adipose tissue retains an epigenetic memory of obesity after weight loss. *Nature* **636**, 457–465 (2024). doi: 10.1038/s41586-024-08165-7

Image Source: David Gregory and Debbie Marshall. Adipose tissue. *Wellcome Collection*. Licensed under CC BY 4.0.

Microbial Resistant *E. coli* Strains From Swine Manure Affecting Human Health

Renee Chowdhry

Antimicrobial resistance found in *Escherichia coli* (*E. Coli*) strains from concentrated animal feeding operations (CAFOs), such as manure, biofertilizers, and runoff waterways, can indirectly affect human health. A recent study by M. Oliveira-Silva examined the presence of antimicrobial resistance genes, antimicrobial susceptibility, and virulence genes in *E. coli* isolates from swine manure biofertilizers in Brazil. Samples were collected from two pig farms that underwent sterilizing treatments and various microbial-resistant testing methods such as plate spreading, susceptibility testing, and PCR. The study's results showed that all 28 *E. coli* isolates were multi-drug resistant and resistant to at least ten antimicrobials. The resistance could be due to the use of antimicrobials as growth promoters for pigs—a common practice in animal farming. Thus, this study reveals that such CAFO practices can lead to resistance genes that can appear in meat products, sewage, and water runoff, impacting human health.



Image: Antimicrobial resistance testing *E. coli* isolates against antibiotics using the Kirby Bauer Disk Diffusion method.

Reference: M. Oliveira-Silva et al., Multidrug-resistant *Escherichia coli* strains isolated from swine manure biofertilizer in Brazil. *Environ. Monit. Assess.* **196**, 534 (2024). doi: 10.1007/s10661-024-12658-3

Image Source: Photo taken by Renee Chowdhry.

Could Light-Driven CO₂ Removal from Oceans be the Answer to CO₂ Mitigation?

Tanisha Lakhanpal



As global CO₂ emissions continue to rise, climate scientists are looking to the sustainable removal of dissolved atmospheric CO₂ from seawater, which contains almost 130 times more CO₂ per volume than air, for the future of CO₂ mitigation. The pH-dependent chemical changes in CO₂ that occur in aqueous environments previously motivated the manipulation of pH to remove dissolved inorganic carbon (DIC) from seawater. Electrochemical oceanic carbon capture takes advantage of these changes but requires a high energetic cost. Alternatively, driving CO₂ removal with light is less operationally complex and is possible in a two-compartment reactor using metastable photoacids (PAs). PAs are used to induce pH fluctuations across a membrane that allows for proton exchange between seawater and bicarbonate species in the PAs, releasing CO₂. Using this system, up to 60% DIC removal was demonstrated in synthetic seawater, showing significant potential for CO₂ mitigation on a large scale.

Image: Underwater shot of the Pacific Ocean taken at Bronte Beach, Sydney, Australia.

Reference: P. Saha et al., Enabling light-driven CO₂ removal from seawater using metastable photoacids. *J. Phys. Chem. C* **128**, 4914–4923 (2024). doi: 10.1021/acs.jpcc.3c08306

Image Source: Photo by Silas Baisch. Free to use under the Unsplash License.

Attosecond X-Ray Pulses Shed New Light on the Photoelectric Effect

Lee Zucker-Murray

The photoelectric effect, first described by Einstein in 1911, was long believed to be an instantaneous phenomenon wherein light causes the emission of photoelectrons from a metal. Recent studies made possible by innovative laser technologies are beginning to investigate the time scale of the photoelectric effect and have found that there are actually time delays between the incident light and the emission of electrons. A team of physicists at SLAC National Accelerator Laboratory utilized the Nobel Prize-winning breakthrough of attosecond light pulses to investigate photoemission delays, using attosecond soft X-ray pulses, about one quintillionth of a second in duration, to ionize nitrogen oxide gas. They measured surprisingly large delays of up to 700 attoseconds in the emission of core-level electrons, exposing significant inadequacies in current theoretical models of photoemission. By harnessing new technologies to investigate a phenomenon that was thought to be well understood, these scientists are literally illuminating the nature of the atom's inner workings.



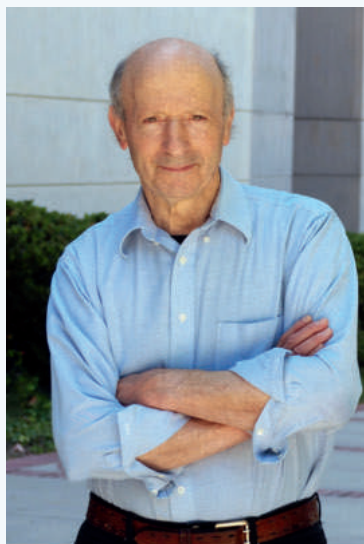
Image: SLAC and the lovely optical effects of sunlight Rayleigh scattering in the atmosphere (a sunset).

Reference: T. Driver et al., Attosecond delays in X-ray molecular ionization. *Nature* **632**, 762–767 (2024). doi: 10.1038/s41586-024-07771-9

Image Source: Image in the public domain from the United States Department of Energy.

Improving Gene Therapy One Vector at a Time: Using Virus-Like Particles for Gene Delivery

By Tanisha Lakhapal, Prannay Veerabahu, Khushi Sharma, Isabel Angres



Principal Investigator
William Gelbart, PhD
Department of Chemistry and Biochemistry,
University of California, Los Angeles.



Student
Selina Juang
Department of Molecular, Cell, and Developmental Biology,
University of California, Los Angeles.

Gene therapy is an ever-changing but increasingly important medical technology capable of treating or preventing diseases by altering individuals' genes. Through the use of gene-editing tools, gene therapy can address disease-causing mutations by replacing or inactivating their corresponding genes or by introducing new genetic material into the human body. In particular, gene delivery systems, which were developed to introduce new material into the human genome, can be effectively optimized for therapeutic applications. Utilizing either viral or non-viral vectors, these systems are used to treat a wide range of diseases, from cancers to cardiovascular diseases.

Viruses, which, over centuries of evolution, have developed the natural ability to protect and deliver genes to specific target cells, are the basis for many therapeutic gene delivery systems. Viruses are capable of co-opting cellular machinery to reproduce its own genetic material en masse. Using naturally occurring viruses for gene delivery, however, poses a significant risk to individuals, in the form of uncontrollable viral growth. Having recognized the utility of viruses for gene delivery systems as well as the dangers of their direct application, author Selina Juang and her advisor Dr. William Gelbart investigate the implementation of virus-like particles (VLPs) for a novel gene delivery system. VLPs are non-infectious forms of viruses that contain genes of interest, in the form of single-stranded RNA (ssRNA), to be introduced to the human genome.

Juang, an MCDB senior, developed her interest in viruses during COVID, researching at home to understand how viruses can be used as tools, specifically for vaccines and gene delivery. Immunology deeply interested Selina. She views autoimmune diseases as fascinating because the body is not naturally designed to target its own antigens, which trigger immune responses. However, these diseases still occur, highlighting the complexities of the human body. This led her to dive deep into viral research, and she came across Dr. Gelbart's work, which focused on using viral components to deliver genes into cells. She reached out to him before attending UCLA and began working in the lab after coming to campus.

In the Gelbart/Knobler Lab, stoichiometrically precise VLPs are designed and synthesized using purified components *in vitro*. VLPs are synthesized with RNA, rather than DNA, to allow for the spontaneous self-assembly of the gene of interest into a virus-like particle when combined with the right viral capsid protein. One of the applicable capsid proteins used in their research is from Cowpea Chlorotic Mottle Virus (CCMV), the simplest virus they work on. When the capsid protein from CCMV is combined with ssRNA under specific conditions, the contents spontaneously self-assemble into VLPs; CCMV VLPs thereby present a promising novel gene delivery system. However, plant-virus-derived VLPs without a lipid envelope

cannot enter mammalian cells without the help of transfection agents, which are unsuitable for *in vivo* applications.

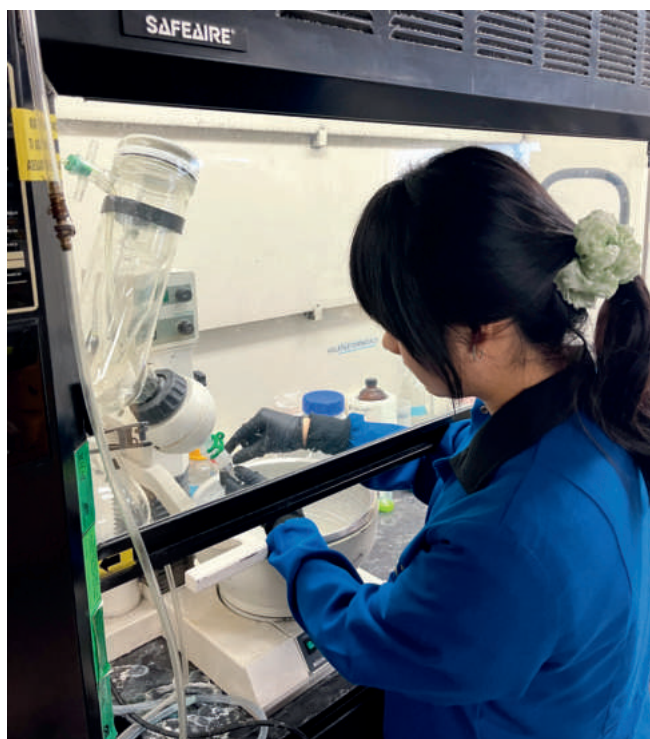
In the Gelbart Lab, Juang's project centers on the lipid-wrapping step, where viruses are wrapped in lipids to increase uptake in the body. A lipid outer layer is present in all mammalian viruses in addition to the protein capsid shell found in plant viruses. The lipid envelope allows for host cell targeting and reduces the chances of viruses triggering an immune response when entering cells, thereby facilitating uptake. Importantly, plant virus capsid proteins, including the ones from CCMV, do trigger immune responses when incorporated. In her research, Juang proposes that wrapping VLPs containing plant virus components with an outer lipid bilayer, could increase their uptake by baby hamster kidney cells (BHK-21)—since spontaneous uptake of CCMV VLPs is not seen in this cell line—without triggering an immune response.

This research focus was briefly addressed in the lab but was not explored deeply, so Selina wanted to pursue this novel question. By targeting lipid-wrapping techniques, she is addressing a key knowledge gap in the field. Current research systems for gene delivery lack lipid-based methods for wrapping virus-like particles, making existing mechanisms less efficient. Studying how lipid wrapping helps protect particles and efficiently deliver them to the body has become Selina's unique contribution to the lab and viral gene delivery research.

In her study, Juang creates Enveloped Virus Like Particles (EVLPs) by wrapping CCMV VLPs with a lipid envelope. Cationic lipids were used to encourage electrostatic interactions with CCMV capsid proteins, which are negatively charged at the physiological pH of 7. When forming the EVLPs, Juang first starts with multilayer vesicles which are then broken into bilayers via sonication. However, Juang discovered that sonication led to significant RNA degradation and implemented a freeze-thawing protocol as an alternative. Freeze-thawing is commonly used when creating lipid nanoparticles (LNPs)—a separate gene delivery system—and involves cycles of freezing and thawing to envelope genes with lipid particles.

Juang faced several challenges while optimizing this methodology. She noted that past research used multiple rounds of sonication and liquid nitrogen to wrap molecules in lipid nanoparticles, but this technique proved inefficient. To improve it, Juang devised a method that utilizes liquid nitrogen to freeze and warm water, enhancing lipid nanoparticle formation. Additionally, she refined the process for modifying the reporter gene length, leading to more effective gene delivery. Since Juang's work in the Gelbart Lab focuses on general mRNA, it has broad applications, helping advance her fellow researchers' gene delivery systems. In the future, she hopes to expand her research beyond hamster cells, testing human cells and even mouse models to assess this system's effectiveness across various biological environments. She believes that further research could contribute to advancements in pharmaceutical applications.

As her paper showcases, Juang's investigation into EVLPs is fruitful, demonstrating that her created EVLPs exhibit an increase in uptake by host cells, without the use of a toxic transfection



agent. In future research, Juang hopes that the VLP-wrapping protocol can be further refined to reduce RNA degradation, VLP-wrapping efficiency can increase, and the cellular uptake of EVLPs in other mammalian cell lines can be explored. Her work on EVLPs fits into the Gelbart Lab's broader goal to develop a novel gene delivery system that can work in a wide variety of human cell types to effectively address diseases.

Throughout her four years of research at UCLA and her experience working with USJ to publish her paper, Selina has learned the importance of effectively communicating research findings. She has developed skills in attention to detail, phrasing methods and conclusions clearly, and drawing diagrams to aid comprehension. Beyond writing, she has also honed her ability to critically read and analyze scientific papers, an essential skill for her future in medicine. This experience has reinforced her passion for research as she applies to medical school, aiming to integrate scientific inquiry into her future career. Reflecting on her journey in research, Selina explained that she came into college with minimal experience. Nevertheless, she emphasizes that PIs are very understanding and there to help. She encourages undergraduate students to ask questions, be willing to learn, pursue labs that interest them, and form strong relationships with their PIs and mentors.

Professor William Gelbart, Selina's mentor, is a distinguished Professor of Chemistry and Biochemistry at UCLA. Over a notable career of over 50 years, Gelbart's research interests have been diverse and multifaceted. After attending several prestigious institutions for his undergraduate, graduate, and postdoctoral training in theoretical physics—including Harvard University and UChicago—Gelbart served as an Associate Professor of Chemistry at UC Berkeley studying statistical mechanics of fluids, eventually moving his lab to UCLA in 1975.

In the late 1990s, Gelbart became intrigued by studying viruses as physical objects, transitioning his lab's focus once again to the biophysical theory of viruses. In his study of the statistical physics theory behind self-assembling charged-polymer systems, Gelbart realized the best studied charge polymer systems were biomolecules like proteins and nucleic acids. In discussions with colleagues and independent analysis, Gelbart began thinking of viruses from a solely "physical lens," treating them as physical bodies fundamentally defined by their arrangement of charged biomolecules.

Gelbart was able to effectively use his theoretical physics background to answer novel questions in biological systems, namely inquiring about the relationship between nucleic acid composition in the viral core and its resultant internal pressure. At the time, this question remained largely unexplored due to the non-overlapping interests of biological experimentalists, who did not apply physical interpretations to biological systems, and biophysicists, who did not study infectious diseases. To answer this question, Gelbart redefined his lab's focus to viruses as their self-assembling system of choice.

As the Gelbart lab became more familiar with viruses, their perspective of viruses transitioned from studying them as purely "physical objects" to biological agents with severe implications in gene therapy, evolution, and human health and disease. The Gelbart Lab took a renewed interest in how viruses deliver their genetic load and their role in larger biological systems: cells and organisms. Gelbart's research is integral for refining existing viral-mediated gene therapy and nucleic-acid delivery methods by studying viruses from a biophysical and evolutionary lens.

Gelbart's lab primarily utilizes two viral systems in this pursuit: Virus Like Particles (VLPs) and Enveloped Virus Like Particles (EVLPs). VLPs, derived from plant viruses, tend to be more immunogenic than EVLPs, which are insulated in a lipid bilayer shell. Current usage of VLPs in larger biological systems is complicated by potential immune events, while EVLP creation is resource-intensive and unreliable. The Gelbart Lab, through projects like Selina's, seeks to explore mechanisms to make VLPs more immune-friendly, devise protocols to increase the yield of VLPs and EVLPs they can produce, and increase their efficiency for tasks such as gene delivery.

Beyond viruses, gene therapy, and physics, Gelbart has also taken a prominent role as a mentor and teacher to budding undergraduate researchers. A winner of the 1996 University Distinguished Teaching Award, Gelbart has mentored many undergraduates over the course of his distinguished career. While Gelbart is intensely passionate about science and research, he also recognizes the importance of having people appreciate and trust science rather than be hostile or overwhelmed by it. Gelbart says he wants to do everything he can to train the next generation of scientists while ensuring that they play a role in encouraging public engagement and trust in science. Gelbart believes there are several pressing areas where new research is direly needed to alleviate suffering, such as pain research, and he wants to play a role in training the future researchers who will study these areas.

For current undergraduates curious in research, Gelbart has one piece of advice: "Figure out what you love doing, and do it." Gelbart

advises that only by finding the field that truly captivates you will success be found. As Gelbart adds "Life is so difficult, so its all the more important that you find something that makes you feel good about hard work." Gelbart encourages undergraduates interested in research not to focus on the job availability or funding available for a research field, but rather what interests them the most—ensuring maximal research contribution. Gelbart also encourages undergraduates to get involved in the research publication process by learning early on to write clearly and communicate one's results in a manner that allows for scientific consensus while also ensuring rigorous and constructive inspection.

From his work in statistical mechanics, to theoretical physics, to biophysical and viral mediated gene-delivery, Professor Gelbart background allows him to utilize a unique perspective to preeminent biological questions with the capacity to revolutionize the tools available for gene delivery, transfection, and self-assembling biomolecular constructs. His lab, through elevating hardworking, ambitious undergraduates such as Juang highlights the rigorous high-quality work undergraduates can pursue under close faculty supervision at UCLA, and the potential for undergraduates—as future scientists—to make impactful, intelligent contributions to scientific fields. The two separate, yet intertwined pathways of Professor Gelbart and Juang demonstrates the variety of flexible avenues available to get involved in high-quality, captivating research at UCLA.

Selina Juang & William Gelbart are authors of "In Vitro Reconstituted Enveloped Virus-Like Particles for Gene Delivery" on page 34.

Tipping the Scales: The Endeavor to Restore Brain Health Through Neuroprotective Research

By Karch Borsa, Priya Ravi, Sumedha Shastri, Paul Zhang, Sohan Talluri



Principal Investigator
Rajiv Ratan, MD, PhD
Department of Neurology and Neuroscience,
Weill Cornell Medicine, New York.



Student
Caterina Stoica
Department of Psychology,
University of California, Los Angeles.

Much like how a thermostat adjusts itself to keep a room at a comfortable temperature, our bodies constantly self-regulate metrics ranging from blood glucose to body temperature to cell division. Through this process of homeostasis, our bodies maintain the specific balance of conditions our cells, tissues, and organs need to survive and function. Disease states arise when this fine balance is disrupted.

One of the processes our bodies delicately balances is neuronal cell death. On one hand, neuronal cell death via apoptosis is an integral part of brain development, helping to prune neural connections and create functional neuronal networks. Nevertheless, neuronal apoptosis during development is a highly regulated process. Uncontrolled death of neurons in conditions such as strokes and Alzheimer's disease can lead to life-altering cognitive and physical disabilities. Although neuroprotective drugs that prevent abnormal neuron death could substantially benefit patients suffering from these conditions, few such drugs are currently available to physicians.

A major cause of abnormal neuronal death is oxidative stress from reactive oxygen species. These molecules, which include superoxide (O_2^-), hydroxyl radicals ($\cdot OH$), and hydrogen peroxide (H_2O_2), can form free radicals that severely damage cell membranes, proteins, and DNA. Reactive oxygen species are

produced in the mitochondria as a normal byproduct of cellular respiration, but kept in check through cellular antioxidants such as glutathione. In neurodegenerative diseases such as Alzheimer's disease and Parkinson's disease, oxidative stress has been found to play a key role.

One pathway for neuronal cell death resulting from oxidative stress is ferroptosis, which results from iron dyshomeostasis. Iron plays a crucial role in many physiological processes, including forming the hemoglobin that carries oxygen in our blood. However, iron can also convert reactive oxygen species into free radicals, which can cause catastrophic cell damage and cell death when present in excessive levels. Neurodegenerative diseases such as Parkinson's disease often present with abnormally high levels of iron in the brain. In these conditions, the balance between iron being physiologically necessary and cellularly disruptive is disturbed, leading to cell death. Iron chelators, which render free iron biologically inactive, offer a possible solution to slowing the progression of neurodegenerative diseases.

This possibility was investigated by Caterina Stoica, a 4th year undergraduate student majoring in psychobiology, during her summer internship at the Ratan lab. Conducting *in vitro* experiments on immortalized mouse hippocampal neurons, Stoica tested whether the Fe^{2+} -chelators dipyrpyridyl

(DP) and 1,10-phenanthroline (PHT) and the Fe^{3+} -chelators deferoxamine (DFO) and deferiprone (DFP) were effective in preventing cell death caused by erastin, a ferroptosis-inducing agent. Stoica found that DP, PHT, and DFO were all effective at preventing ferroptosis, while DFP was ineffective. By investigating the different pathways that each chelator acts on, she determined that chelating iron in its early intracellular or extracellular stages may be more successful than targeting it in its later stages.

While Stoica's results show potential for preventing and treating neurodegenerative disease, bringing iron chelators to the clinic is a complex process that cannot be rushed. To highlight the importance of thorough bench research in ensuring the safety of potential therapeutics, Stoica pointed to a 2022 clinical trial testing DFP in treating neurodegenerative diseases (1). This study tested oral DFP tablets on Parkinson's patients, expecting DFP to successfully chelate iron and thus improve cognitive function. However, similar to what Stoica's results imply, patients taking DFP experienced greater impairment than those taking the placebo, with some even developing life-threatening white blood cell disorders such as neutropenia and agranulocytosis. These results demonstrate the importance of thorough preclinical testing before moving any drug to the clinical stage.

As Stoica put it, "It's really important to take a step back, go back to the lab and investigate iron chelators before starting to implement them in clinical practice because some of them could be toxic; some of them could have other negative effects and not really target ferroptosis as well as we want them to, and so that was kind of my goal."

To ensure that the successful *in vitro* iron-chelating drugs would be safe and effective in humans, Stoica explained that the next step would be to test the drugs on primary cortical neurons, which mimic the physiological environment of the brain more closely than the immortalized mouse hippocampal line she worked with. Since she only tested four different chelating drugs, she also believes it's important to look at other iron chelators with similar properties to those she found successful to see which perform the best *in vitro*.

Though these next steps in ferroptosis research are exciting, Stoica is uncertain whether she'll be the one to carry them out. As a pre-medical student, she has to balance her passion for hands-on wet lab research with her desire to work with people face-to-face in a clinical setting. While she recognizes that her work on ferroptosis has real potential to translate to therapeutics, she also recognizes that it's still very much in its early stages, so it could take years before iron-chelation therapies move to the clinical stage. Since she wants to experience the next step of clinical research herself, she may have to change her research focus entirely. Regardless of what she ends up pursuing professionally, Stoica intends to stay updated on new developments in the Ratan lab and jump back into neurodegenerative disease research if the opportunity presents itself.

Mentoring Stoica is Dr. Rajiv Ratan, a seasoned neuroscientist and Chief Executive Officer of the Burke Neurological Institute at Weill Cornell Medicine. Dr. Ratan's neurological expertise is a great fit for Stoica, a researcher deeply curious about the brain. While ferroptosis is a cornerstone of the Ratan lab and is particularly relevant to Stoica's research, Dr. Ratan's work explores several other avenues of preventing neurodegenerative disease, including research into the cutting-edge molecules adaptaquin, selenoproteins, and 2-deoxyglucose.

Adaptaquin is what Dr. Ratan describes as a "next-generation" chelator. To understand this drug, it makes sense to think of it as Dr. Ratan does: a molecular switch-flipper. Whereas standard chelators directly bind to the target chemical and decrease its concentration in the body, adaptaquin utilizes a different approach. Within a cell, molecular sensors called hypoxia-inducible factor prolyl hydroxylases (HIF-PHDs) detect drops in oxygen levels and, if activated, advance the ferroptosis pathway. Excess iron in the blood can also activate these molecular switches, which is why iron chelation is effective in keeping these switches in the "off" position. But what makes this process so difficult to regulate is iron's centrality to numerous essential cellular processes. If too little iron is present due to over-chelation, the cell will die. On the other hand, too much iron will trip the switch, triggering ferroptosis.

Maintaining this balance is where adaptaquin excels. Adaptaquin is able to directly inhibit HIF-PHDs, mimicking the effect of a chelator and greatly decreasing the likelihood of triggering ferroptosis. What makes adaptaquin unique, however, is its ability to avoid interacting with iron or iron-related enzymes in the blood, allowing the metal to continue supporting vital cellular processes while intervening only where it needs to: at the switch itself. Dr. Ratan's work in using adaptaquin to maintain neuronal homeostasis has been incredibly successful, especially when it comes to its applications as a stroke prophylactic and treatment. The Ratan lab hopes to advance adaptaquin to clinical trials to get it one step closer to becoming among the first neuroprotectives in the global pharmaceutical toolbox.

Another focus of the Ratan lab is utilizing the nonmetal selenium and its antioxidant properties to combat oxidative stress. Because of its electron configuration, selenium can easily donate electrons to free radicals, effectively neutralizing what would otherwise be cytotoxic oxidative molecules. Sulfur, a component of the amino acids methionine and cysteine, also has the ability to reduce free radicals, but selenium is unique in its ability to resist the irreversible electron depletion to which sulfur-containing amino acids typically succumb. This means that the amino acids selenomethionine and selenocysteine—identical to typical methionine and cysteine but with selenium instead of sulfur—are much more effective antioxidants. These characteristics are what make selenoproteins so promising in neuroprotective applications.

The Ratan lab has made multiple promising discoveries within the realm of selenoproteins. Most excitingly, they measured

an uptick in cellular selenoprotein production while the cell is under oxidative stress, and that this response is much more robust if the cell is treated with selenium. Unfortunately, these results were difficult to reproduce *in vivo*. Selenium has a narrow therapeutic window since it can quickly upset homeostasis of the body's natural oxidative pathways at high concentrations, making selenium cytotoxic unless administered at low doses. To overcome this hurdle, Dr. Ratan's group found that by coupling a 10-amino-acid peptide to a selenoprotein responsible for shuttling the element into cells, selenium's dosage window shifts. Instead of needing to target a minuscule range of concentrations, selenium can be administered with greater leeway and at higher dosages. In light of this work, Dr. Ratan is confident that this application of selenoproteins can serve as a widely-applicable treatment for numerous ailments, indicating that the molecule will continue to be a central focus for his lab moving forward.

Beyond selenoproteins, Dr. Ratan has also focused on molecules that influence neuronal resilience, namely a glucose analog called 2-deoxyglucose (2-DG). Previous work has shown that low glucose levels improve cognition, but the pathways responsible for this effect remain unclear. Dr. Ratan and his lab have studied 2-DG in an effort to clarify this question.

When glucose stores are depleted during intermittent fasting, the subsequent decline in circulating glucose levels leads to the conversion of fatty acids into ketone bodies. These ketone bodies offer an alternative energy source for the body and have been shown to produce various signaling molecules that improve cognitive impairment in healthy aged mice and an elderly human population.

Dr. Ratan's lab specifically honed in on 2-DG as it competitively inhibits glucose metabolism, and can thus be used to study the effects of low glucose. Dr. Ratan's work showed that 2-DG upregulates genes involved in learning and memory by enhancing brain-derived neurotrophic factor expression via ketone-independent pathways *in vivo* and *in vitro* (2). 2-DG also contributes to long-term potentiation, which is correlated with improved learning and memory. In ischemic stroke patients, 2-DG has led to improved sensory and motor functional recovery (2). Just as Dr. Ratan's ferroptosis research studies neuronal death and how to mitigate the negative impacts of iron dyshomeostasis, his research on 2-DG aims to demystify how neuronal resilience can be achieved. These findings on the cognitive benefits of 2-DG offer insights for future clinical trials related to Alzheimer's and stroke patient populations.

In the cancer realm, 2-DG is already utilized clinically approved anticancer drug. At a dose that is 60 times lower than the one needed for cancer treatment, 2-DG administered to rodent neurons was shown to improve cognition in Dr. Ratan's lab. The drastically lower dose points to the clinical applicability of this administration and is a promising indication of 2-DG's potential in improving cognition. As this work is based in rodents, further testing is needed before 2-DG is utilized in clinical trials. Pilot

studies in Dr. Ratan's lab are now focusing on the ideal amount of 2-DG to promote the upregulation of these cognition genes. His lab is looking at the levels of certain markers in the blood to indicate optimal 2-DG dosage. A fine balance of 2-DG that promotes improved cognition must be found before it can be clinically applicable.

Adaptaquin, selenium, and 2-DG are testaments to the way that medical research is rooted in achieving balance. Balancing natural stress in the body to create resilience while eliminating the negative impacts that stress has on the body is a longstanding goal in medical research. In the ferroptosis realm, ensuring that enough iron exists to carry out its crucial processes while preventing iron saturation and ferroptosis remains a difficult but important endeavor. Through dedicated work by scientists like Dr. Ratan and the brave steps taken by emerging researchers like Stoica, achieving this necessary balance in the body is getting closer by the day.

Achieving a balance between building skills and producing concrete results as a new scientist is another difficult but crucial step to master. As Dr. Ratan notes, building skills early on in one's scientific career is very important to long-term success. Stoica's work with ferroptosis has introduced her to medical research—a field that is filled with trial and error, reading, and questions—and the many skills that come with it.

The goal of medical research is to provide solutions to longstanding diseases within society. Dr. Ratan has dedicated his career to doing this, and in the process, has helped tip the balance in our body's systems away from disease. As Dr. Ratan emphasized, disease is a failure of adaptation and it is our job as scientists—both experienced and new scientists alike—to facilitate our body's transition from disease back to homeostasis. Dr. Ratan's overarching goal in his career is to produce a clinically sound drug to help patients with Alzheimer's and stroke, an endeavour that will continue to be supported by new scientists like Stoica. These collaborations will help champion the discovery of drugs and medical approaches that support the body rather than work against it, thereby promoting human health.

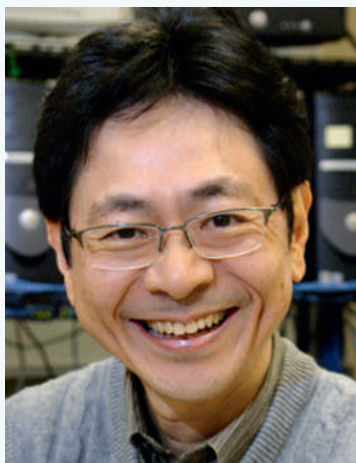
REFERENCES

1. D. Devos *et al.*, Trial of Deferiprone in Parkinson's Disease. *N. Engl. J. Med.* **387**, 2045–2055 (2022). doi: 10.1056/NEJMoa2209254
2. A. Kumar *et al.*, 2-Deoxyglucose drives plasticity via an adaptive ER stress-ATF4 pathway and elicits stroke recovery and Alzheimer's resilience. *Neuron* **111**, 2831–2846 (2023). doi: 10.1016/j.neuron.2023.06.013

Caterina Stoica & Rajiv Ratan are authors of "Differential Effects of Iron Chelation on Ferroptosis and Neuroprotection" on page 48.

Fluid Dynamics Reveal the Physics of Aneurysms: A Journey From Engineering to Medicine

By Vyas Koduvayur, Oliver Wang, Dashrit Pandher



Principal Investigator
Katsushi Arisaka, PhD

Department of Electrical and Computer Engineering,
University of California, Los Angeles.



Student
Ashwath Nayagadurai

Department of Physics and Astronomy,
University of California, Los Angeles.

Much can change in four years of college, and fourth-year biophysics major Ashwath Nayagadurai can attest to this all too well. He began his academic journey at UCLA four years ago with a clear goal: medical school. Eager to get involved, Nayagadurai sought out research opportunities early on to gain experiences that would support his journey, and he decided to join the Elegant Mind Club at UCLA—a biophysics group headed by Dr. Katsushi Arisaka. The group broadly aims to study the basic physics laws that define our universe, exploring the fundamental physics underlying our body's biological systems. With a diverse array of projects and an even wider range of student researchers, the Elegant Mind Club provided Nayagadurai with a space to engage in hands-on, cutting-edge work.

As a first-year student, however, Nayagadurai admits that he didn't know what to expect. "I didn't really know what was going on," he recalls. After working with a few different teams, he decided to focus on a microscopy project in hopes of sinking his teeth into biological research that aligned with his pre-medical goals. However, things didn't go as smoothly as he had initially hoped. "A lot of the skills that I had were skills that...they didn't really need," he explains. Rather than solely working on microbiological research as he had anticipated, Nayagadurai found himself in an engineering-heavy project that required knowledge of how to assemble microscopes and program in MATLAB.

Rather than being discouraged, however, he decided to take on the challenge with an open mind, recognizing it as an opportunity to develop new skills. He vividly remembers his graduate mentor sitting him down and saying, "We're going to learn how to code in MATLAB today." Nayagadurai worked hard, spending an entire quarter gradually growing confident in working with the language. But just as he grew proficient, however, the team decided to switch to Unity. Though initially frustrating, Nayagadurai now looks back and sees this as an invaluable learning experience, saying that if it weren't for that initial plunge, he never would have learned how to code. He lays it out in his philosophy: "Learning as much as you can is the point of research." Now proficient in three programming languages, Nayagadurai is confident that they will be incredibly valuable tools in whatever future career path he takes.

While building his technical experience, Nayagadurai took notice when Dr. Naoki Kaneko, a professor working at the Ronald Reagan UCLA Medical Center, approached the Elegant Mind Club with a new project idea. Dr. Kaneko was studying brain aneurysms and was particularly interested in identifying predictive factors for their formation and eventually finding ways to provide better treatment and care. Having heard of the microscopy work done by the group, Dr. Kaneko sought the expertise of a strong, interdisciplinary team of researchers.

Recognizing this as a golden opportunity to apply his skills to medical research, the now third-year Nayagadurai jumped at the chance to get involved. Aneurysms, he knew, were deadly, with mortality rates reaching 50%. By working towards achieving preventative care for aneurysms, countless lives could be saved.

Together, the team got to work. The project, at first glance, seemed simple: develop imaging techniques for aneurysms. However, Nayagadurai quickly realized that they would face significant technical hurdles. Imaging at the necessary high frequencies meant that they needed to build a new microscope completely from scratch. This daunting task would combine the skills Nayagadurai had learned in engineering and medical research, putting all of his abilities to the test. Over time, the team made remarkable progress, overcoming a plethora of troubleshooting issues. This experience, he says, marked the beginning of his deep dive into the new topic he has now been investigating for the past several months: stenosis—the narrowing of blood vessels—and its impact on blood flow dynamics.

When reflecting on his current research, Nayagadurai acknowledges the many challenges he has faced. One of the biggest hurdles was defining the parameters for the experiment. “How big do we make the stenosis, what material should we use, what microscope would be best?” he lists. His solution? “I read papers for days,” he laughs. As he spent hours scouring the literature, Nayagadurai encountered tomography, a method for creating cross-sectional images of objects using penetrating waves.

By facilitating noninvasive brain scans, tomography holds immense potential for detecting future aneurysms in the clinical setting. For the time being, however, Nayagadurai performed tests on relatively simple silicone models of brain blood vessels. He recounts applying mathematical tools for modeling purposes, including the Fast Fourier Transform—an algorithm that extracts frequency data and quantifies oscillations occurring within sample models.

Beyond the technical challenges, however, Nayagadurai admits that one of the most difficult parts of the project was actually writing his research paper for the Undergraduate Science Journal (USJ). “There were a lot of things that you don’t expect to be problems,” he reflects. Since this was his first serious foray into the world of scientific writing, he struggled with some aspects that were not necessarily well-taught in classrooms. Citations, he singles out, proved to be especially frustrating, as different courses he had taken required different styles. Despite these challenges, he successfully submitted a strong manuscript to USJ, marking a significant milestone in his research career.

When asked about the broader impacts of his work, Nayagadurai’s passion was evident. “The way they do [medicine] now, it’s all very reactive,” he explains. But with advancements in predictive medicine, he believes that early detection of aneurysms and other neurological diseases will become the norm. He hopes that his research at the intersection of physical engineering and biological medicine will contribute to this shift, paving the way for improved patient care moving forward.

As he looks back on his study, Nayagadurai doesn’t hesitate to admit that there are many things he would approach differently if given another chance. “I’d probably redo the whole project,” he says. Whether by replacing the water with a higher viscosity liquid, utilizing a different optical lens system to see higher resolution images, or using an alternative vessel model with varying lengths, he notes that there are countless ways to continue refining the experimental approach.

But to Nayagadurai, that’s the essence of research. “In retrospect, there are lots of things that I could have done, and I only see that now because I put in the effort to do it all in the first place,” he notes. While the final results matter, it’s the process of trial and error, making thoughtful decisions, and ultimately learning from the experience that truly fuels scientific progress.

Looking ahead, Nayagadurai believes that one of the next key steps for his project is to move beyond using water, which served as a substitute for blood in his experiment. He explains that while water is useful for preliminary trials, there are certain key properties that it doesn’t share with blood. For example, blood is significantly more viscous, more dense, and exerts higher shear stress compared to water. “It reacts differently,” he explains. He emphasizes that these differences could potentially have a significant impact on the outcome of the results, and plans on taking them into account for future experiments. “I think the next further experiment should use...something that mimics blood. That definitely could have influenced the results.”

With graduation quickly approaching, Nayagadurai’s four years at UCLA are soon coming to an end. As for what lies ahead, Nayagadurai is already preparing for the next big chapter: medical school. “After undergrad, my plans are four years of med school,” he says. “I applied to med schools last summer, and I’m doing interviews right now.”

Most applicants would agree that the next part is the hardest: the waiting game. “Now, I’m just waiting to hear back from the schools,” Nayagadurai says. He doesn’t need to elaborate—anyone who’s been through the application process knows exactly how agonizing the suspense can feel.

While Nayagadurai has given some thought to his specific path within medicine, he continues to keep his options open. “I’m not sure,” he admits when asked about a specific specialization. “I always have some idea, but what I like now was not what I liked six months ago, which was not what I liked six months before that. So, I do like keeping an open mind to what I do.”

Although he remains undecided, one area that’s caught his interest is surgery. Over the past few years, Nayagadurai has worked under a neurosurgeon in a clinical role. His mentor has given him valuable insight into the complexities of blood vessels—their structure and how they behave—and that exposure has reinforced his interest in microscopy and sparked another in neurosurgery. “But things change,” he reiterates. “Don’t quote me,” he adds with a smile.

As highlighted by Nayagadurai's work, research and medicine are deeply intertwined—scientific inquiry fuels medical advancements, and clinical practitioners translate these discoveries into innovative patient care. “I definitely plan on doing research in med school,” Nayagadurai says without hesitating, “especially because I have a lot of these specialized skills working with microscopes.” With his experience in microscopy and imaging techniques, he envisions himself joining a research lab as he pursues medicine, enabling him to further apply the technical skills that he has developed throughout his time at UCLA and in the Elegant Mind Club.

However, while research has been a fulfilling experience for Nayagadurai, he doesn't necessarily see it as a long-term career path. “Career-wise is a different story,” he admits. “I don't see myself doing research for a career.” Although he enjoyed working alongside his faculty advisors and loved the process of scientific inquiry, he ultimately envisions his future as a clinical practitioner. With that said, he remains open to continuing research during medical school and even into residency.

When it comes to what specifically he wants to research in medical school, Nayagadurai is keeping an open mind. “I'd probably just take it as it goes,” he says. His time in the Elegant Mind Club provided him with a strong foundation, but he acknowledges that the group's broad scope meant that attention and funding were divided. He notes that “the Elegant Mind Club was great as a stepping stone, but they worked on a lot of projects. And when I [say] a lot, I mean a lot.”

While there are benefits to having a broad variety of available projects to work on, resources could sometimes be spread thin,

which made it challenging to focus deeply on specific areas that interested Nayagadurai—like microscopy. In the future, he hopes to join a lab with a more specialized focus. “If I did work in another lab, I think I'd probably find a lab that only worked in microscopy—their skill set would be just as specialized as mine,” he explains. “I think that would be a good place to end up.”

For future undergraduates looking to get involved in research, Nayagadurai has one key piece of advice: embrace collaboration. “Get used to working in teams,” he emphasizes. Having worked in the same team for four years, he is aware that while it can be incredibly rewarding, teamwork has its own set of challenges. “You're gonna love each other sometimes, you're gonna hate each other sometimes,” he adds.

Nevertheless, Nayagadurai's teammates have become some of his closest friends, and he reiterates the importance of finding a compatible group of people to work with. “Find a team that you think you'll succeed in,” he advises. But teamwork isn't just about picking the right people—it's a skill that takes time to develop. He recalls, “When I came into undergrad, I don't think I was a great team player. I don't think that was something wrong with me, I just think that was a skill I had to learn.”

As Nayagadurai prepares for the next stage of his journey, he carries with him the lessons he's learned—both in research and in healthcare. Whether in the lab or the clinic, the ability to work with others, adapt, and learn constantly will be a defining aspect of his career. Although no one knows what the future entails, one thing is certain: Nayagadurai's curiosity and dedication to his work will continue to guide him forward.

Ashwath Nayagadurai & Katsushi Arisaka are authors of “Non-Invasive Analysis of Vessel Wall Vibrations During Blood Flow” on page 67.

From Curiosity to Cancer Research: Uncovering Metabolic Adaptations in Prostate Cancer

By Ken Woo, Joanna Rhim, Katherine Morrisette, Andrew Tsui, Malvika Iyer



Principal Investigator
Andrew Goldstein, PhD

Department of Molecular, Cell, and Developmental Biology,
University of California, Los Angeles.



Student
Kylie Heering

Department of Molecular, Cell, and Developmental Biology,
University of California, Los Angeles.

After cancer touched the lives of her family members, Kylie Heering knew that she wanted to take action and play a role in the search for a cure. At the age of 16, the high schooler from New Jersey began by conducting literature reviews on the topic, eventually stumbling upon an article about aging and prostate cancer from the Goldstein Lab at UCLA. Eager to learn more, she reached out, and eventually found herself moving across the country to spend eight weeks in Dr. Goldstein's Lab.

The eight weeks she spent working in the lab were transformative for her, and she credits this time with cultivating and catalyzing her growth as a budding scientist. She enjoyed every aspect of working in the laboratory, from running Western blots to thoughts of one day becoming a pioneer in cancer research.

After high school, Heering spent two years in the army before returning to UCLA as an undergraduate student. Upon committing to UCLA, she reached out to Dr. Goldstein, reconnected with him, and joined his lab—as an undergraduate researcher. More motivated than ever, Heering took on her own independent research project on prostate cancer. Dr. Goldstein recalled being impressed with how hard she had worked when she initially met him during her high school years, but this time, she asked him if she could do more research than before. This blend of personal

determination and academic curiosity not only set the stage for her research but also fueled her commitment to understanding the intricate challenges of prostate cancer.

Building on her personal research journey, Heering delved into the science behind prostate cancer by exploring how it disrupts the normal function of a key male organ. The prostate gland—a small, walnut-sized organ located just below the bladder—is essential for producing seminal fluid that nourishes and transports sperm. In prostate cancer, abnormal cells begin to proliferate within this gland, impairing its ability to contribute effectively to reproductive health. Although this type of cancer typically grows more slowly than other forms, early detection is critical, as treatments are often highly successful when the disease is caught in its initial stages.

The specific causes of prostate cancer have not yet been identified, however, the disease begins when cells within the prostate gland acquire mutations in their DNA. These changes lead these cells to grow and multiply at much higher rates than normal. If left untreated or if treatments are unsuccessful, the cells form large masses called tumors within the prostate gland and can spread throughout the body in a process known as metastasis. When the cancer has spread outside of the prostate

gland, it is regarded as metastatic prostate cancer and it becomes significantly more difficult to treat.

In order for these abnormal cancerous cells to continue proliferating, they must synthesize large amounts of energy, much more than a typical cell would require. Furthermore, these cells can adapt their rates of energy production in response to a variety of external factors, which can affect the success rates of different cancer treatments and therapies. Yet, the precise biochemical pathways that allow for this metabolic flexibility remain largely elusive. There is a significant lack of understanding in the biochemistry involved in this process, and Heering's project aims to fill this gap.

Heering's research, "Characterization of Mitochondrial Evolution in Prostate Cancer," explores how tumor cells in prostate cancer adapt their energy production under treatment stress, which is a critical mechanism in why some cancers become resistant to therapy. At its core, the study examines how tiny energy factories in cells, called mitochondria, change their shape and function when faced with drugs and genetic alterations.

In healthy cells, mitochondria constantly switch between splitting into smaller units (a process known as fission) and merging back into longer, connected networks (known as fusion). These processes are essential for balancing energy production and meeting the cell's demands. Kylie's study has identified a key player in all this: DRP1, a protein that acts like a pair of molecular scissors to cut mitochondria into smaller pieces, plays a central role. When DRP1 is active, mitochondria exist in their smaller units and perform a fast but less efficient form of energy production called glycolysis. However, when DRP1 activity is reduced, mitochondria fuse back into their elongated form, hinting that the cell might switch to a slower, more efficient energy production method known as oxidative phosphorylation.

To investigate these changes, Heering used a well-established model: the 16D prostate cancer cell line. In her experiments, she treated these cells with enzalutamide, a drug that blocks androgen receptors, which are proteins that typically help prostate cancer cells grow. By simulating this clinical treatment in the lab, she

could see how the cells' energy production and mitochondrial structure respond. A key observation was that enzalutamide treatment led to a significant drop in the activity of DRP1, which was measured by the reduced addition of a chemical group (phosphate) at a particular site on the protein (serine 616). In simple terms, this means the molecular "scissors" were less active, and as a result, the mitochondria were not breaking apart as they normally would.

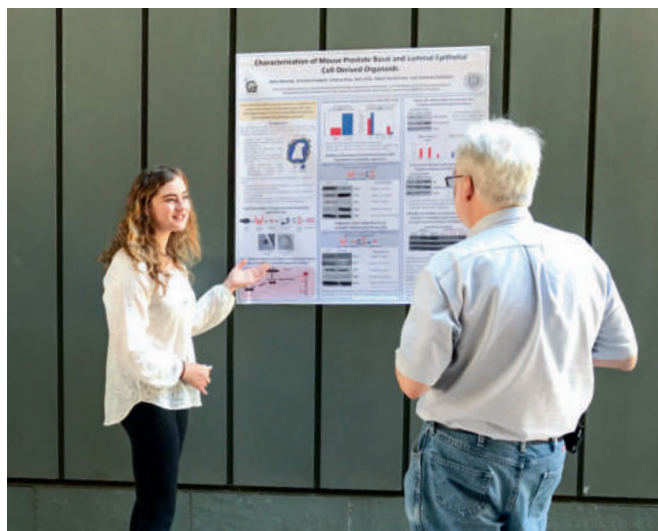
But Heering didn't stop at drug treatment. She also modified the cells' genetic makeup to explore how different genes affect mitochondrial behavior. In one set of experiments, she increased the levels of a gene associated with aggressive cancer behavior called N-MYC. With higher N-MYC, the cells managed to keep their mitochondria in a fragmented, or "normal," state even when treated with enzalutamide. This suggests that N-MYC might help cancer cells resist the effects of the drug by preserving their usual energy production method.

In a contrasting experiment, Heering deactivated the tumor suppressor gene RB1, a gene that normally helps control cell growth. Without RB1, the cells showed an even greater drop in DRP1 activity, leading to very elongated mitochondria. Additionally, there was a buildup of alpha-ketoglutarate, a key molecule in the cell's energy cycle known as the tricarboxylic acid cycle. In other words, the accumulation of alpha-ketoglutarate suggests that the cells are rerouting their energy production processes, perhaps as an adaptation to the stresses imposed by both the drug treatment and the genetic changes.

Throughout the study, Heering employed several methods to validate her findings. Western blot analyses, a technique that allows scientists to measure specific proteins, confirmed the changes in DRP1 activity and the levels of other important enzymes like hexokinase 2 and lactate dehydrogenase A, which are involved in glycolysis. Confocal microscopy provided visual evidence by capturing detailed images of the mitochondria, showing clearly how their shapes changed under different conditions. Meanwhile, metabolomic assays, which analyze the various chemicals produced by cells, revealed the shifts in metabolic intermediates like alpha-ketoglutarate. Together, these techniques paint a comprehensive picture: under the pressure of AR inhibition, prostate cancer cells modify their energy strategies by reshaping their mitochondria and altering their metabolism.

What makes Heering's study particularly significant is how it ties together the intricate interactions between cellular energy production and cancer cell survival. Instead of viewing metabolic changes as mere side effects of treatment, her work shows that these changes are fundamental adaptations that cancer cells use to cope with therapeutic stress. This research not only deepens our understanding of prostate cancer biology but also provides a window into how metabolism and cancer intersect. By revealing that genetic factors like N-MYC and RB1 can dramatically influence mitochondrial structure and, by extension, energy production, her findings suggest that targeting these metabolic shifts might be a promising approach to overcoming drug resistance.

In exploring this intersection, Heering's work hints at a broader principle: the way a cell produces energy is intimately linked



to its ability to survive under stress. For cancer cells, which are constantly battling against therapies, switching from a rapid, less efficient energy mode to a more sustainable one could be the key to enduring long enough to develop resistance. This insight opens up new perspectives for future research, suggesting that future treatments might need to target not just the cancer's growth signals, but also its underlying energy machinery.

Beyond Heering's interest in mitochondrial evolution within prostate cancer, Dr. Goldstein and his group are working to understand prostate epithelial cells. With advancing technologies such as multi-omics and single-cell RNA sequencing, he recognizes that these tools can help unravel the multifaceted complexity of prostate cancer. For example, single-cell RNA sequencing utilizes cellular heterogeneity in cost-effective and robust ways, making gene expression more accessible. Although Goldstein Lab is capable of executing many techniques, Dr. Goldstein emphasizes the importance of collaborative science in every research project. While their lab group focuses on the chromatin accessibility, other labs or industry partners may specialize in different techniques. Working with these groups is essential for reducing costs, accelerating research, and addressing complex scientific issues. Even at the doctoral level, individuals acknowledge the value of others' expertise, and leveraging their collective knowledge enhances research quality.

Besides frequent collaboration in research, Dr. Goldstein and his lab are exploring how pyruvate and lactate metabolism in prostate differentiation could potentially lead to therapeutic drug development. Many different cell types and tissues rely on pyruvate and lactate metabolism as a foundational process. Therefore, he emphasizes the importance of understanding the basic science before considering cancer treatment application. With further studies, their research aims to bridge the gap to clinical applications—particularly in identifying tumor features in patients with varying levels of pyruvate oxidation. Some patients are more sensitive to treatment, while others show more resistance. Dr. Goldstein suggests that a promising direction is reversing these metabolic processes in order to better understand therapeutic resistance, as patients may experience different treatment outcomes.

Another area of focus is the use of preclinical models, which allow experiments to be conducted in simplified systems. However, simplifying these systems comes with inherent limitations. Translating data to human applications involves additional processes beyond analyzing phenotypes in cells, tumors, and mice. Nevertheless, gaining better understanding of phenotypes and cellular outcomes increases confidence in clinical testing, even though it can be described as a “best guess at biology” based on predictive models. Dr. Goldstein has found that many concepts relevant to cancer research have the potential to evolve into clinically based projects that can make a lasting impact.

One of the most valuable aspects of Dr. Goldstein's lab is its broad applicability across different types of cancer and how perspectives can shift from one area to another. Some researchers investigate prostate cancer through molecular pathways or signaling molecules, but these insights can also be applied to



other contexts—such as mammary glands, which are hormonally regulated tissues. There are notable similarities between treatment-resistant prostate and lung cancer, as they share common phenotypic traits across tissues. Research in one area can often be translated to others. In terms of metabolism, relatively little is known about transcription factors or signaling pathways. However, in the context of lactate metabolism, some tissues have shown a strong treatment response linked to tumor aggressiveness. Although metabolism is not yet a prominent field within cancer research, there is significant overlap between different study areas within the field.

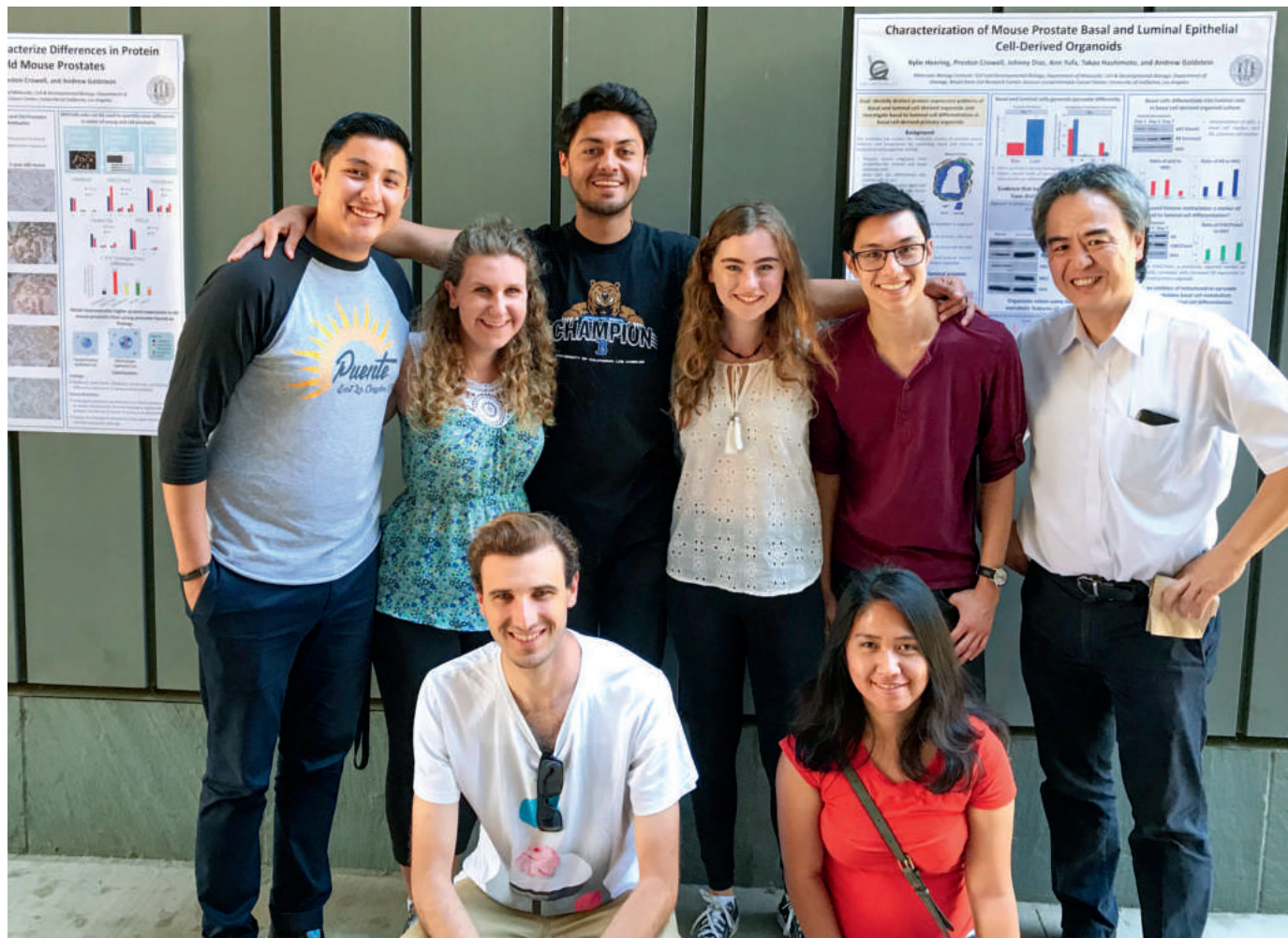
As efforts to fully elucidate the pathology of prostate cancer continue, Dr. Goldstein and his team have identified the causes for carcinogenesis and the progressive evolution of tumor cells as immediate areas of interest for future investigation. Although risk factors such as age, inherited mutations, and chronic inflammation have already been identified, little is known about how these factors impact healthy cells and cause their transformation into cancerous cells. Dr. Goldstein noted that research of these processes will help to reveal the foundational causes for the disease, which in turn can lead to significant advancements in disease prevention. Additionally, the reliance of tumors on certain metabolic pathways for their sustenance and growth makes research on their metabolism, including Heering's work, crucial in developing approaches to interfere with specific metabolic pathways and thus inhibit cancer proliferation.

The journey to publication was not trivial for Heering. Throughout the writing process, she had to carefully consider the most effective means for scientifically communicating her findings. Heering encourages future student researchers to write with consideration to a broader general audience who may not possess the same technical background, ensuring that concepts are conveyed communicably without an overreliance on scientific jargon. She also encourages future student researchers to emphasize the implications of the findings, which will demonstrate the significance of the field and to inspire others to pursue research.

Heering also encourages prospective undergraduate student researchers to take advantage of the plethora of research

opportunities at UCLA. She personally found the MCDB 196 courses to be extremely helpful for scientific communication, and she also alluded to the Biomedical Research Minor as another helpful pathway for research guidance. Heering also pointed to her own unorthodox research journey as a source of encouragement for prospective student researchers seeking opportunities. Although her attempts to contact PIs were shut down or ignored many times, she believes that her persistence is what led her to the amazing mentorship she has now in Goldstein Lab. While Heering acknowledges that it may be intimidating as an undergraduate, she believes that this is in fact the opposite, noting that undergraduate researchers are too making their own important contributions.

Similarly, on the topic of undergraduate student researchers, Dr. Goldstein expressed his admiration for undergraduates involved in professional research in addition to their classes and other extracurriculars. Furthermore, he believes that students coming in with different goals and interests prevents a lab monoculture, instead fostering a multi-perspective environment within the lab. Dr. Goldstein encourages students to be meticulous in their work, take good notes, and pay close attention to detail, stating that the students who get the most rewarding research experiences are almost always those who put the most in. While poster presentations and publication authorships are not guaranteed, he emphasizes that the experience gained is far more valuable.



Kylie Heering & Andrew Goldstein are authors of "Investigating Mitochondrial Evolution in Advanced Prostate Cancer" on page 58.

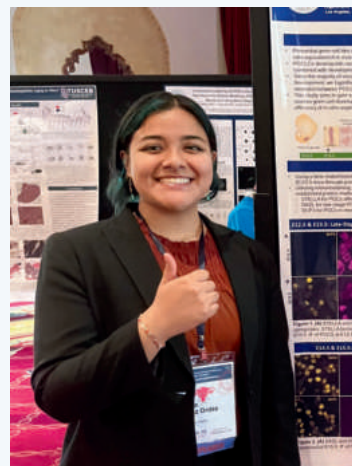
From Embryos to Ethics: Mapping the Future of Reproductive Biology

By Chahak Gupta, Melody Jiang, Phillip Tang, Archi Patel



Principal Investigator
Amander T. Clark, PhD

Department of Molecular, Cell, and Developmental Biology,
University of California, Los Angeles.



Student
Azra J. Cruz

Department of Molecular, Cell, and Developmental Biology,
University of California, Los Angeles.

The blueprint of lifelong health is often written long before birth, in the earliest stages of development. Driven by a fascination with how the body's organs take shape, Professor Amander Clark, Director of the UCLA Center for Reproductive Science, Health, and Education, embarked on a journey into the world of stem-cell biology. "At my heart, I'm a developmental biologist, and I'm really interested in how organs and cells in the body form because if the organs are not built correctly, then it's hard to imagine how they will...function for a long, healthy lifespan," says Dr. Clark. She expressed her passion for studying the developmental origins of disease, which involves investigating defects during development that result in negative health outcomes later in life. She notes that "by working in this space of developmental biology and developmental origins of disease, it helps us to try and think about how we could prevent disease before it even happens."

While pursuing her PhD at the University of Melbourne, Dr. Clark studied the formation of the kidney, with a special interest in transforming growth factor beta (TGF- β), a crucial cytokine involved in cell growth and differentiation in renal tissues. Investigating the role of the TGF- β superfamily in developmental and reproductive biology led her to a postdoctoral fellowship at the Baylor College of Medicine in Texas. She remarked that the intersectional development of many molecular tools, including embryonic stem cells and their genetic modification through homologous recombination, drew her to research in

a new country. Since then, Dr. Clark has utilized these novel technologies as they have increased in precision. "We've really leveraged and taken advantage of new technologies as they have been built by collaborators in the field or by the field in general," she says. Embryo models have provided researchers the ability to study early human development and advanced the field toward solutions for infertility and reproductive diseases. The Clark lab will continue to explore these models and technologies to progress their mission to treat illnesses and improve reproductive health.

When formulating and choosing which scientific questions to investigate, Dr. Clark places collaboration at the forefront. "It's really important to meet with and talk with other scientists and learn from different disciplines because there can be clues in other fields of research that can help inform the work that we do in the lab. Going to conferences, going to seminars, attending poster sessions, and having people come to your posters and ask you questions about your research can be so insightful," she notes. Additionally, Dr. Clark emphasized the importance of letting the results of active projects guide new experiments.

Research in the Clark lab is driven by the continual work of the lab's many passionate scientists, including 4th-year Molecular, Cell, and Developmental Biology major and author of "Immunofluorescence of Mouse Fetal Ovary Reveals Timing of Meiotic Progression," Azra Cruz. Cruz was first introduced to biology through forensic science and pathology. Television shows

like *CSI: Crime Scene Investigation* and *Dexter* sparked their interest in forensics, and their initial career goal was to become a medical examiner. In their first year at UCLA, however, Cruz discovered their interest in research through a *Yeast, Genetics, and Molecular Biology* research class (MCDB 30H) taught by Tracy Johnson, UCLA's current Dean of Life Sciences. When Cruz later enrolled in MCDB 50, a stem cell biology course taught by Dr. Clark, their interest was streamlined to developmental biology research and regenerative medicine. Cruz recalls, "The first few times I met her, [Dr. Clark] was extremely kind, and I talked to her about some of the research interests that I had in the future." Cruz later joined the Clark lab and along with conducting their own research, they had the opportunity to network with other scientists via conferences such as USC's California Institute for Regenerative Medicine Trainee Network Conference. Their experiences in the Clark lab and at multiple research symposia inspired them to pursue a PhD, and Dr. Clark has supported Cruz's passions and helped them advance toward their goals through her mentorship.

Cruz's ability to be directly involved in everything from designing their own project to providing candid insight on data is what drew them to Dr. Clark's lab. "There's been so much trust given to me, and that has allowed me to really flourish and feel independent in the lab and feel like I can really rely on myself and how I'm thinking of the data as well. Ultimately, what makes successful mentorship is being able to trust the person that you're mentoring, and have that trust between each other, that you can rely on each other," Cruz remarks. In addition to being mentored by Dr. Clark, Cruz was trained in lab techniques by graduate student Isaias Roberson before working independently on their project. As a result of this support and trust, Cruz was quickly able to find their place within the Clark lab as they became proficient in the complex workings of a wet-lab environment.

Cruz's research examines the dynamic expression of two key proteins—STELLA, a marker for germ-cell competency, and synaptonemal complex protein 3 (SCP3), a marker for meiosis—in a mouse model at various embryonic stages. They use immunofluorescence to quantify protein expression levels, building a novel timeline to examine key developmental points in the mouse developmental germline. This work has significant implications for improving infertility treatments, particularly through the use of the reconstituted ovary (rOvary)—a lab-made model that mimics a natural ovary to support oocyte development.

Even after the thorough planning and thought that went into their project, from the experimentation to drafting their publication, Cruz still faced challenges. One of their most memorable challenges was reconciling the conflicts in prior literature. "We've come to find that the literature can say something and though they're not technically wrong, they're not entirely specific, and so sometimes, we would be doing these stains...and we would also see other things that weren't covered in the literature," Cruz notes. Another challenge Cruz faced was "the timing of the mice, [as] they can [breed] at any time," even when Cruz is not in the lab, but their results can only be based on what they directly observe. Nevertheless, these difficulties allowed them to better understand the experimental design process and how to mitigate unforeseen challenges.

Both Cruz and Dr. Clark share a passion for this project and what it means for the future of the queer community. Cruz says, "I'm really interested in doing future research specifically on trans and queer communities, and I think we [Cruz and Dr. Clark] connected on that level just because the *in vitro* gametogenesis project also fights to include the queer community." For both researchers, their scientific impact is also deeply personal—it's about creating inclusive technologies that affirm and support diverse identities. By advancing reproductive research in this direction, they hope to challenge longstanding exclusions within biomedical science and offer meaningful representation for LGBTQ+ individuals in fertility discussions.

When working in the field of reproductive research and *in vitro* gametogenesis, ethical concerns are paramount. Thus, both Cruz and Dr. Clark emphasize the importance of collaborating with scientific professionals and engaging with the general public concerning these sensitive topics. To address ethical concerns, Dr. Clark collaborates with researchers such as Dr. Hannah Landecker and Dr. Anne Le Goff, who explore public opinion on *in vitro* gametogenesis. Dr. Landecker and Dr. Le Goff's work provides insight into how different communities perceive the implications of reproductive technologies and helps guide research to align with societal values. By incorporating these perspectives from the start, Cruz and Dr. Clark aim to avoid the common bioethical pitfall of developing technologies in isolation from the people they are meant to serve.

Despite advances, gaps remain in our understanding of early reproduction. Research on key developmental proteins and experimental models like the rOvary is crucial in understanding the science behind gametogenesis, making Cruz's work a foundational step towards developing future reproductive technologies. The rOvary model, in particular, offers a promising avenue for investigating the earliest stages of oocyte formation in a controlled, observable environment. By shedding light on these previously inaccessible processes, Cruz's contributions will help pave the way for future interventions in fertility medicine, regenerative biology, and inclusive reproductive care.

Azra J. Cruz & Amander T. Clark are authors of "Immunofluorescence of Mouse Fetal Ovary Reveals Timing of Meiotic Progression" on page 43.

Various Fruit Consumption Forms and Their Health Outcomes

Shubhreet Bhullar¹

¹Department of Psychology, University of California, Los Angeles.

ABSTRACT

Fruit consumption plays a vital role in influencing a wide range of health outcomes. This review examines the effects of different forms of fruit consumption—whole fruits, fruit juices, and fruit smoothies—on cardiovascular health, diabetes/blood sugar, musculoskeletal health, and mental health. A comprehensive review of cross-sectional studies, clinical trials, and meta-analyses was conducted to offer a holistic understanding of these relationships. In general, the findings suggest that consuming whole fruits is consistently associated with better triglyceride management and reduced cardiovascular disease and stroke risk. Additionally, fruit consumption positively influences blood sugar regulation, enhances insulin sensitivity, and lowers diabetes risk. Musculoskeletal health benefits include reduced chronic pain, increased muscle strength, and improved bone mineral density. In terms of mental health, regular fruit intake is linked to a reduced risk of depression, anxiety, and psychological distress, with varying effects between men and women. While the benefits of whole fruits are well-documented, the effects of fruit juices and smoothies are more nuanced, varying based on factors such as fiber content and processing methods. Overall, this review underscores the importance of fruit consumption as part of a balanced diet for maintaining and enhancing health. Further research should explore the differential effects of various fruit consumption forms and broaden the range of health outcomes examined to include the interplay between multiple health outcomes and comorbidities.

INTRODUCTION

Although some studies have found no correlation between apple consumption and reduced reliance upon medical interventions for chronic diseases, the overall benefits of consuming fruits should not be negated (1). Diet plays a critical role in overall health by influencing growth and development. A healthy diet is associated with reduced risk of non-communicable diseases such as cancer, cardiovascular conditions, and lifestyle diseases (2). Moreover, a healthy diet fosters the development of healthy gut microbiota, which helps decrease inflammation, increase metabolic function, and decrease the risk of chronic diseases (3). Although some aspects of diet (vegetable, sugar, fat, oil, and meat consumption) have been extensively studied, fruit consumption lacks sufficient and nuanced research compared to other constituents of diet in regards to intake amount and intake form. Since most studies lump fruits with vegetables, there is also limited research exploring the relationship between health outcomes and fruit consumption (4). For example, fruit and vegetable intake have been shown to alleviate joint and bone pain; however, there remains a need for isolating the correlation of fruit and musculoskeletal pain (5).

An umbrella review found that consuming an additional daily serving of fruit could decrease the risk of cardiovascular disease, stroke, congenital heart disease, and oral cancer, with the most dramatic reduction observed in risk of oral cancer (6). However, this study did not differentiate between different forms of fruits and considered juices, smoothies, and solid fruits to be equally effective. Meanwhile, a systematic review study observed a 31% increase in

the risk of developing cancer when increasing daily consumption of 100% fruit juice by 250 mL (7). Alternatively, a different study found that 100% fruit juice consumption was associated with decreased hypertension, arterial stiffness, and organ damage, and increased immune function due to the presence of various bioactive compounds within the juice (8). These findings reveal the contrasting conclusions regarding the healthiness of fruit juices, as well as the lack of a comprehensive study examining the influence of fruit juices on a wide variety of health outcomes, ranging from cardiovascular and diabetic health to mental and musculoskeletal health.

While fruit smoothies have been shown to alleviate psychological distress in individuals receiving opioid agonist therapy (9), there is no research conducted on the relationship between fruit smoothies and overall health. Public health campaigns often fail to highlight the public misconceptions about fruit juices being healthy despite their potential to contribute to higher calorie and sugar intake, leading consumers to overconsume processed forms of fruit. Current dietary guidelines emphasize the importance of fruits but often treat all forms of fruit consumption as equivalent, despite evidence that processing (e.g., blending or juicing) can alter nutrient composition and glycemic response (10). This lack of differentiation may lead to suboptimal dietary advice, as some scientists have hypothesized that fruit juices and smoothies lose fiber during processing, resulting in their higher sugar content and lower fiber levels compared to whole fruits (11).

This review paper provides nuanced insights that could inform dietary guidelines to recommend specific forms of fruit consumption for optimal health benefits. For example, while researchers know

that fruit consumption is correlated with physical fitness (as measured by decreased oxidative stress and inflammation), they might be able to further improve musculoskeletal health by utilizing a specific form of fruit consumption (12). This study postulates that distinct types of fruit consumption (solid fruits, fruit juices, and fruit smoothies) will have distinct impacts on various health outcomes, such as chronic diseases, mental health, and musculoskeletal health. Solid fruits (fruits in solid form, whether whole or sliced), for example, retain fiber and a wide range of vitamins, which may contribute to better cardiovascular health by modulating blood sugar and cholesterol levels. In contrast, fruit juices (consisting only of juiced fruits) lack fiber and absorb sugar more quickly, resulting in them having a higher glycemic index and potentially adverse effects on cardiovascular and diabetic health (11). Although fruit smoothies (consisting of only blended fruits) are also theorized to have these adverse effects due to their blended nature, the variety of fruit included in smoothies might offer a balanced nutritional profile that supports both physical and mental health (11). A systematic review design was implemented to analyze the effects of various fruit consumption forms on a wide range of health factors, including physical and mental health outcomes. Previous research often focused on one or two outcomes (e.g., cardiovascular diseases or body mass index (BMI)), overlooking the interplay between fruit consumption and a holistic range of health factors. Identifying specific health outcomes linked to different forms of fruit consumption could guide more targeted health interventions.

ANALYSIS

Cardiovascular Health

Many studies have clearly depicted an improvement of cardiovascular health associated with healthy dietary patterns (13). Particularly, the proper ingestion of nutrients, vitamins, bioactive compounds, and dietary antioxidants found in fruits and vegetables are most beneficial (14). As previously mentioned, there is a limited number of studies that focus solely on the effects of fruit consumption on cardiovascular health. However, some studies suggest that whole fruit intake provides cardiovascular benefits due to its fiber and antioxidant content (15) and others raise concern about the impact of fruit juices and smoothies on blood sugar and lipid levels (16).

A meta-analysis research study conducted by Kodama *et al.* (2018) examined the effects of fruit intake on hypertriglyceridemia to explore the notion that fruits elevate blood triglyceride levels due to their high fructose concentrations. The researchers ensured that the studies they evaluated isolated fruit consumption and did not focus on one specific type of fruit (e.g. citrus fruits), but rather various types of fruit—so long as they were whole fruits. Their findings revealed that an incremental increase of fruit intake by 1 serving/day had an odds ratio (OR) of 0.91 (95% CI of 0.84–0.98) (17). This implies that there was an inverse relationship between fruit intake and incidence of hypertriglyceridemia.

Scheffers *et al.* (2018) conducted a correlational study that categorized fruit and fruit juice consumption into quintiles and examined their relationship with health outcomes, where fruit consumption included all forms of fruit consumption (whole fruits, fruit juices, fruit smoothies) and fruit juice consumption included only pure (100%) fruit juice. Moderate pure fruit juice consumption was associated with a 20–24% lower risk of

stroke, and up to 7 glasses/week was linked to a 12–15% lower risk of cardiovascular diseases (CVD) and a 14–17% lower risk of congenital heart disease, though no dose-dependent relationship was found, except for the ≥ 8 glasses/week group, which showed similar risks to non-drinkers. Additionally, fruit intake was linked to a 12–13% decrease in CVD risk, but again, not in a dose-dependent manner. The difference between the amount of fruit consumption is not statistically significant, as long as pure fruit juice consumption does not exceed 7 glasses/week (18).

While Kodama *et al.* (2018) focused solely on the relationship between whole fruit consumption and hypertriglyceridemia (17), Scheffers *et al.* (2018) examined both whole fruits and fruit juices across various cardiovascular conditions. Although both studies suggest that higher fruit consumption is linked to better cardiovascular health, Scheffers *et al.* (2018) also found that low to moderate fruit juice intake might reduce cardiovascular risk, though not in a dose-dependent manner (18). However, Kodama *et al.* (2018) focused on hypertriglyceridemia limits their findings, as they did not assess other cardiovascular markers such as blood pressure, arterial stiffness, cholesterol, or inflammation (17). Furthermore, researchers only considered whole fruits and ignored all other forms (namely fruit juices and fruit smoothies). While Scheffers *et al.* does consider fruit juice, it grouped all fruit types together and has limited external validity, as it was based on a Dutch cohort from only three towns (18). This comparison underscored the need for further research on various forms of fruit intake, particularly fruit smoothies, which are underrepresented in scientific literature. All studies either focused on smoothies containing one specific kind of fruit (e.g., acai) (19) or smoothies containing both fruits and vegetables (20).

Type 2 Diabetes and Blood Sugar

Studies have shown that eating whole fruits generally has a smaller impact on blood sugar levels and is associated with a lower risk of diabetes compared to consuming fruit juices (21). Since the juicing process removes most of the fiber, which slows down the absorption of sugar into the bloodstream, fruit juices contribute to a faster and more significant spike in blood sugar than whole fruits. This means that fruit juices have a higher glycemic index (GI) (measure of how quickly a carbohydrate-containing food raises blood sugar levels) than whole fruits. However, due to the lack of studies regarding fruit smoothies, scientists are unsure of the interactions between this fruit consumption method and blood sugar regulation. Some scientists postulate that fruit smoothies have high glycemic indexes like fruit juices, while others argue that the fiber retention of fruit smoothies aligns their glycemic impact more closely with whole fruits. Moreover, some scientists reason that the blending of fruits may break down the fruits' cellular structures (in a manner potentially different than juicing), resulting in an unknown effect upon the glycemic index of fruit smoothies, revealing a need for future research (22).

As depicted in Figure 1, risk of type 2 diabetes might be mitigated by fruit intake due to its composition of dietary fiber, phytochemicals (flavonoids), and fructose, as well as the process of mastication. These researchers postulate that fiber content reduces the GI of fruit and promotes a healthy intestinal microbiota (23). Fiber acts as a prebiotic for healthy bacteria in the large intestine, which helps create a diverse balance of healthy and unhealthy bacteria, resulting in improved digestion,

a stronger immune system, and reduced inflammation. This, in turn, reduces the likelihood of developing a chronic disease like type 2 diabetes (24). While fructose can increase the glycemic index of fruits, it also increases the feeling of satiety by increasing GLP-1 (glucagon-like peptide) and FGF21 (fibroblast growth factor-21) secretion, which results in increased insulin sensitivity. Mastication also enhances GLP-1 secretion, which directly stimulates pancreatic beta cells to release insulin, thereby improving insulin sensitivity (23). Flavonoids activate the PI3K/Akt (phosphatidylinositol 3-kinase/protein kinase B) pathway glucose transporter (24), resulting in increased insulin sensitivity. Insulin sensitivity allows for insulin to be released effectively and efficiently, such that blood glucose levels do not rise too high, decreasing the risk of developing insulin resistance, a key factor in type 2 diabetes (23).

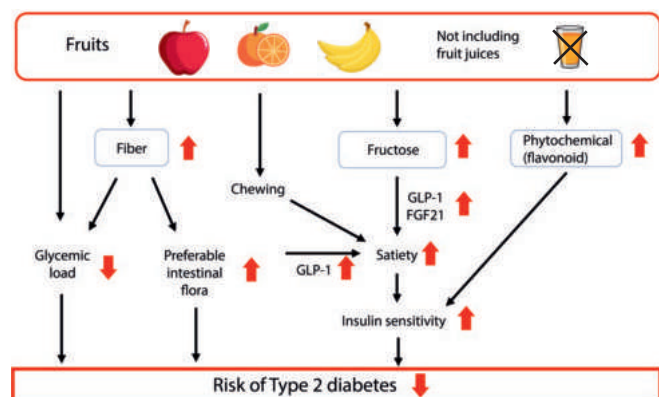


Figure 1: Pathways from fruit consumption to type 2 diabetes.

The various pathways by which solid fruit consumption can result in a decrease in the risk of developing type 2 diabetes are depicted.

Li *et al.* (2014) found a non-linear relationship between overall fruit intake and type 2 diabetes in their meta-analysis, with a threshold of 200 grams of fruit per day linked to a 13% reduction in diabetes risk. Studies lasting over a decade showed more significant results than those shorter than ten years (25). Bondonno *et al.* (2021) conducted a population-based survey in Australia to examine the correlations between whole fruit and fruit juice ingestion and various diabetes-related measures. They found a nonlinear negative correlation between whole fruit intake and type 2 diabetes risk, with a 36% reduction at 200–300 grams per day, while fruit juice consumption was associated with a 10% higher risk per serving. Higher whole fruit intake was linked to lower plasma glucose, serum insulin, and better insulin sensitivity (26). The study also found that consuming 3 servings per week of certain fruits (berries, grapes, apples, pears, and bananas) reduced diabetes risk, while cantaloupe intake increased diabetes risk, likely due to its higher sugar and lower fiber content (26, 27). Overall, the study highlighted the benefits of whole fruit consumption and the harmful effects of fruit juices on diabetes risk (26).

While previous studies have shown that fruit juices might increase the risk of diabetes, we cannot generalize these findings to fruit smoothies, as they retain more fiber. However, an experiment conducted by Crummett and Grosso (2022) demonstrated that fruit smoothies without added sugars or foods yielded a lower postprandial glycemic response than consuming the same serving

size of whole fruits. It is postulated that the blending process breaks the cell walls, allowing the nutrients to be more efficiently absorbed by the body (11). This increased nutrient bioavailability of fruit smoothies compared to whole fruits could contribute to a decrease in diabetes risk. After conducting a secondary analysis of an experiment, Jenkins *et al.* (2010) found that consuming fruit with low glycemic indexes as part of a low glycemic index diet was associated with lower risk and better management of type 2 diabetes, as well as lower HbA_{1c} (average blood glucose over the past 2–3 months) and blood pressure (28). Since fruit smoothies have lower glycemic indexes (GI) and lower GI fruits are linked to reduced type 2 diabetes risk, it follows that fruit smoothie intake may lower type 2 diabetes risk.

Redfern *et al.* (2017) conducted a within-subjects factorial design (crossover design), such that participants served as their own controls. The study had two arms: the mixed fruit arm (with 25g banana, 25g mango, 50g passion fruit, 50g pineapple, 50g kiwi, and 50g raspberries) and the mango arm (181g mango). Each arm tested whole fruit (frozen) and nutrient extracted fruit (blended into smoothies and then frozen) compared to glucose control meals (25g glucose in 125 mL water). Participants fasted for 12 hours before testing, refrained from alcohol, caffeine, and exercise for 24 hours, and had a minimum 3-day washout period between meals (29). Blending mango did not alter its glycemic index, but blended (nutrient-extracted) mixed fruits had a much lower GI (32.7 ± 8.5) than whole mixed fruits (66.2 ± 8.2). This study found a causal link between blended mixed fruits and a lower GI, which is correlated with improved diabetic management and decreased risk of developing diabetes type 2 (29).

While Li *et al.* (2014) found a negative correlation between fruit intake and diabetes type 2 risk (25), Bondonno *et al.* (2021) found a similar correlation for whole fruit, in addition to a positive correlation between fruit juice consumption and type 2 diabetes risk (26). The difference in findings may be attributed to the decreased fiber and increased sugar content of fruit juices, which can cause a rapid spike in blood sugar and are positively correlated with diabetes risk (22). However, Bondonno *et al.*'s (2021) findings are limited by the fact that those who responded to the survey were likely of a higher socioeconomic status and those who were lost to follow-up (i.e., did not attend follow-up research sessions) tended to be less healthy (26). Furthermore, neither study considered fruit smoothies, an important yet under-researched form of fruit intake. Redfern *et al.* (2017) addressed this gap, showing that frozen blended fruit had a lower GI than frozen whole fruit, suggesting a potential benefit of smoothies in diabetes prevention. However, the generalizability of these results is limited due to the fact that the experiment tested whole fruits and smoothies (blended fruits) in their frozen form (29). Mastication of the frozen blended fruit might have affected the GI of the fruit such that it would be different from the GI of a smoothie consumed in liquid form. The precise process by which nutrition extraction decreases the postprandial glycemic response is, however, not yet ascertained and is currently undergoing research (23). One key consideration when interpreting these findings is the accuracy of biological markers, such as postprandial glycemic response, which may be systematically overestimated by glucometers. However, since the same measurement tools were used across all participant groups, any potential error would likely be consistent, meaning the relative differences in glycemic response between groups would remain unaffected.

Musculoskeletal Health

A diet low in proinflammatory foods and rich in unsaturated fats, fruits, and vegetables is associated with reduced chronic pain (30), suggesting that dietary patterns can play a significant role in managing musculoskeletal discomfort. Additionally, fruit and vegetable intake has been linked to higher physical activity levels in older adults, which may further contribute to better musculoskeletal health and overall well-being (31). The positive effects of fruit and vegetable consumption extend beyond physical activity, with evidence showing correlations with reduced risk of sarcopenia (32), increased muscle strength (33), and lower risk of bone fractures in postmenopausal women (34). These findings indicate that dietary choices may help mitigate age-related declines in muscle and bone health. However, there is limited research specifically examining the effects of fruit consumption alone on musculoskeletal health, particularly in terms of pain relief. The mixed findings from studies, such as one on a fruit-based concoction for muscle recovery (35), underscore the need for further investigation into the broader benefits of fruit consumption for musculoskeletal health.

Liu *et al.* (2015) conducted a population-based cross-sectional survey of elderly Chinese men and women to examine bone mineral density via dual-energy X-ray absorptiometry. On average, bone mineral density was respectively 4.5% and 6.4% greater in the whole body for men and women when fruit intake was increased by 100 g/kcal per day (36). This increase in bone mineral density (which is correlated with higher fruit intake) is correlated to increased bone strength, particularly in supporting muscles and preventing injury (37).

A multivariable analysis by Huang and Xie (2024) looked at low back pain in patients from databases from the IEU Open GWAS project and the FinnGen project. After adjusting for the covariates of fresh fruit intake, BMI, current tobacco smoking, alcohol intake frequency, total body bone mineral density, serum 25-hydroxyvitamin D levels, and vigorous physical activity, the study found a link between dried fruit consumption and decreased low back pain (38).

Daud *et al.* (2023) completed a review of various pure fruit juices and their effects on both muscle recovery and sports performance. The polyphenols in the fruit juices were hypothesized to protect muscle cells from the effects of reactive oxygen species (ROS) produced during exercise. Sports performance was measured by VO_2 max, running/cycling speed, or heart rate/blood pressure, and muscle recovery was assessed using biomarkers such as creatine kinase, myoglobin, and interleukin-6. Daud *et al.* (2023) found a positive correlation between the consumption of various fruit juices (beetroot, grape, pomegranate, cherry, and mixed fruits) and sports performance/muscle recovery (39).

Medonca *et al.* (2020) performed an integrative review to analyze the interactions between various dietary components and musculoskeletal pain. Consumption of passion fruit peel extract, strawberries, and blueberries were found to each be independently correlated with decreased levels of various inflammatory markers, namely interleukin-6, interleukin-1 β , and tumor necrosis factor- α (40). Decreased levels of these inflammatory markers are correlated with increased muscle mass, muscle strength, and decreased musculoskeletal pain, which often arises due to inflammation (41).

Although Liu *et al.* (2015) found a correlation between fruit consumption and increased bone strength, the external validity of this finding is limited by the study's inclusion of only elderly

Chinese adults (36). While Medonca *et al.* (2020) also found a relation between fruit consumption and decreased musculoskeletal pain, their external validity was also limited due to their use of only three specific types of fruits (40). Huang and Xie (2024) identified a correlation between dried fruit consumption and decreased back pain, even though they had to account for a multitude of covariates. They were, however, unable to access individual medication use and were therefore unable to adjust for the pain-relieving functions of certain medications. Furthermore, all of the participants were of European descent, limiting the generalizability of the findings (38). While Liu *et al.* (2015) only focused on fruit consumption as a whole without considering different forms of consumption (36), Huang and Xie (2024) only examined dried fruit intake, which has a higher fiber and lower sugar content than solid fruits (38). While Daud *et al.* (2023) only examined fruit juices, they found that they were correlated with better sports performance and muscle recovery. However, the difference in the operational definitions of the dependent variables across the different studies analyzed in their review paper might weaken the internal validity of these results (39).

Mental Health

Dietary patterns influence mental health outcomes, such as depression and anxiety, by affecting neurotransmitter production through nutrient intake (42). Diets rich in fruits, vegetables, whole grains, and omega-3 fatty acids are generally linked to improved mental well-being, whereas high consumption of processed foods and sugars is associated with negative mood states and an increased risk of mental health issues (43). Whole orange and orange juice intake can prevent folate deficiency, which is associated with neurological disorders such as depression and cognitive impairment (44). The chlorogenic acid found in prunes enhances oxidative protection, which is hypothesized to reduce the severity of and effectively treat anxiety disorders (45). Chlorogenic acid has been shown to reduce anxiety in mice, supposedly through the activation of benzodiazepine receptors (46). The combination of nutraceutical fruits, which provide certain health benefits and disease prevention/management (e.g. berries, citrus fruits, prunes fruits), with omega-3 fatty acids has been shown to be associated with decreased incidence of a wide range of mental disorders, such as attention-deficit disorder, dementia, depression, bipolar disorder, and schizophrenia (47). However, there is a limited number of studies discussing the effects of various types of fruit consumption on various mental health conditions.

Saghafian *et al.* (2018) utilized a cross-sectional study to find that women who regularly consumed fruits had significantly lower odds of having depression, anxiety, and psychological distress, while there was no difference in mental conditions in men despite differences in fruit consumption (48). Yan *et al.* (2023) analyzed National Health and Nutrition Examination Survey (NHANES) data, finding that those who consumed more than 1.49 cups of fruits per day have a decreased risk of neuroticism traits related to depression (loneliness, miserableness, feeling fed-up, irritability, and neuroticism) as compared to those who consumed less than 0.12 cups of fruits per day (49).

Agarwal *et al.* (2022) analyzed NHANES data to assess a wide variety of neurocognitive measures (cognitive function, dementia, anxiety, and depression) in those who consumed 100% juice (more than 2 oz per day) and those who did not (consumed less than 2 oz per day). Researchers found that the fruit juice group spent 16.3%

less days of the month feeling anxious compared to the no fruit juice group. Unfortunately, no correlations were found between 100% fruit juice consumption and any other neurocognitive measures assessed in this study (50).

Currently, the only study detailing the effects of fruit smoothies on psychological conditions is an experiment formulated by Fadnes *et al.* (2022) on patients receiving opioid agonist therapy. The outcome variable of psychological distress was measured by using the ten-item version of the Hopkins Symptom Checklist (HSC-10) at baseline and completion of the study. The respective differences between the baseline and completion psychological distress scores for the control and intervention group of -0.05 and -0.07 were found to not be significant (51).

While Saghafian *et al.* (2018) found decreased depression, anxiety, and psychological distress in fruit-consuming women, these findings did not carry over to men and were limited by the inclusion of only Iranian adults (48). Yan *et al.* (2013) found that whole fruit consumption is negatively correlated with neuroticism and depression (49), while Agarwal *et al.* (2022) found fruit juice consumption to be negatively correlated with anxiety (50). Fadnes *et al.* (2022) found no effect of fruit smoothies on psychological distress, but this study focused on a specific population (patients receiving opioid agonist therapy) and lacked a placebo-controlled, double-blind experimental design (51). While Saghafian *et al.* (2018) focused on fruit consumption as a whole instead of considering different types of fruit consumption, all of the other studies focused on only one specific form of fruit consumption, resulting in a decrease in the generalizability of these findings. Furthermore, these studies only examined a few specific mental health outcomes instead of a wide range, further limiting their external validities. Notably, the contradictory findings between these studies could be due to differences in sample populations, study designs, or the specific types and quantities of fruit consumed. Given that dietary patterns take a long time to influence health outcomes, the use of cross-sectional studies as opposed to longitudinal studies might be seen as a limitation; however, the researchers in all the aforementioned studies mitigated this by inquiring about fruit consumption over an extended period of time.

DISCUSSION

The relationship between fruit consumption and health outcomes is complex and multifaceted, varying significantly depending on the form of fruit consumed—whole fruits, fruit juices, or fruit smoothies. This review aimed to provide a comprehensive analysis of existing literature on the effects of fruit consumption on cardiovascular health, diabetes and blood sugar regulation, musculoskeletal health, and mental health. By exploring the differential impacts of various forms of fruit consumption, this paper sought to clarify inconsistencies in current findings and identify gaps in research that warrant further investigation.

Understanding the nuanced effects of fruit consumption is crucial for informing dietary guidelines, public health strategies, and clinical practices. As dietary habits continue to evolve, particularly with the increasing popularity of fruit juices and smoothies, it is imperative to distinguish their health impacts from those of whole fruits. This review not only synthesized existing evidence but also aimed to provide direction for future research to better understand the role of fruit consumption in promoting overall health and preventing chronic diseases.

As seen in Figure 2, the findings highlight both the potential benefits and limitations associated with each form of fruit consumption, revealing complexities that warrant further exploration. Consistent evidence supports a correlation between increased overall fruit consumption and decreased risk of cardiovascular diseases, decreased risk of diabetes type 2, increased bone mineral density, and decreased incidence of psychological distress, anxiety, and depression. Solid fruit consumption is associated with decreased hypertriglyceridemia, decreased risk of diabetes type 2, decreased blood sugar, decreased postprandial glycemic response, increased insulin sensitivity, decreased inflammatory markers, decreased neuroticism, and decreased depression. As dried fruit intake was inversely correlated with incidence and severity of low back pain, there is potential for fruit composition to impact musculoskeletal health. Fruit juice intake tends to decrease the incidence of stroke, cardiovascular diseases, congenital heart disease, and anxiety. Fruit juice intake also tends to increase sports performance, muscle recovery, and diabetes type 2. Consumption of fruit smoothies has been shown to negatively correlate with plasma glucose levels, risk of developing diabetes type 2, and severity of diabetes type 2. Overall, this review demonstrates that whole fruits consistently show the most beneficial health outcomes across all categories studied, whereas fruit juices and smoothies yield more variable results—albeit likely due to limited research into the effectiveness of these fruit consumption types.

Fruit Consumption Forms and their Associated Health Outcomes

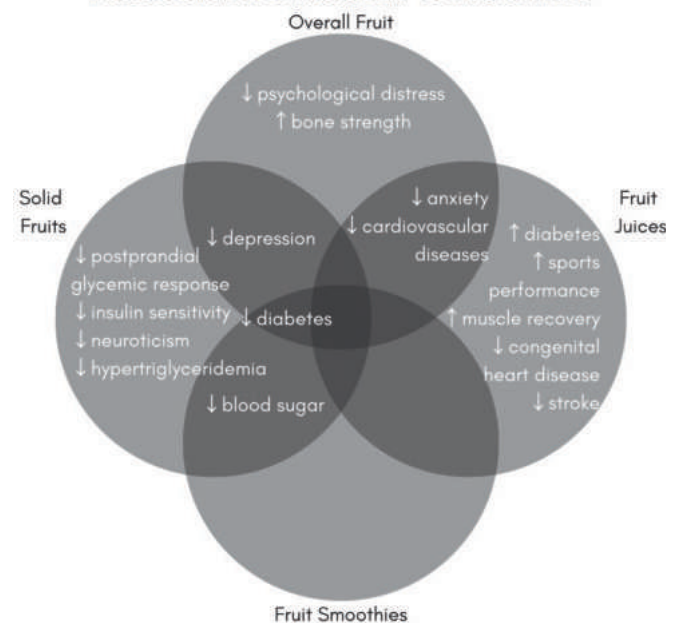


Figure 2: Fruit consumption forms and their associated health outcomes.

The various fruit consumption forms examined in this review study (overall fruit, solid fruit, fruit juice, and fruit smoothie consumption) are charted with their respective impacts on a wide variety of health outcomes. This format is intended to simplify the benefits and limitations of each fruit consumption form.

The consistent evidence supporting whole fruit consumption as beneficial for cardiovascular health, diabetes prevention, musculoskeletal integrity, and mental health underscores the need to emphasize whole fruits over processed forms in dietary recommendations. Currently, dietary recommendations do not distinguish between the different fruit consumption forms and consider them all equally beneficial (52), likely due to the sparse number of studies regarding a specific form of fruit consumption (i.e., whole fruits) as compared to the overwhelming quantity of studies discussing overall fruit consumption (53). Separating whole fruits, fruit juices, and fruit smoothies in dietary databases and nutrition research would enhance the accuracy of dietary assessments and improve the reliability of epidemiological studies, enabling more targeted research and more effective public health strategies.

Furthermore, the findings from this review have important implications for clinical practice, especially in the management of chronic conditions such as cardiovascular disease, diabetes, and mental health disorders. Personalized nutrition interventions could be designed to incorporate whole fruits as a key component of therapeutic diets due to their high fiber content, low glycemic index, and rich antioxidant profile, which collectively contribute to improved health outcomes. However, it is important for clinicians to exercise caution when recommending fruit juices, given the potential for adverse effects such as increased diabetes risk and inconsistent benefits in cardiovascular health. In addition, the mental health benefits associated with polyphenol-rich fruits may offer a complementary approach to psychological treatments, potentially providing patients with an integrated strategy for managing anxiety, depression, and stress. The limited research on fruit smoothies coupled with their rising popularity as a convenient dietary option indicates a need for clearer guidance regarding their nutritional value. While incorporating fruits into dietary regimens has great promise, clinicians should consider the broader context of individual health needs and be aware of the varying impacts of different forms of fruit consumption on overall well-being.

Although this study produced valuable knowledge, it still possesses a few limitations. The reliance upon correlational studies, such as cross-sectional, longitudinal, and observational studies, limits the ability to establish causal relationships. Various confounding variables, such as other lifestyle factors, overall diet quality, physical activity, and socioeconomic status, can not be fully controlled for. Some studies only assessed fruit consumption at the baseline and did not account for change in dietary intake over time, resulting in a lack of consideration of changing dietary patterns and long-term impacts of fruit consumption on health outcomes. Additionally, the use of self-reported dietary intake in many of the studies might result in recall bias and misreporting, potentially impacting the validity of the findings. Another limitation is the inconsistent operational definitions of fruit consumption across the studies, with some focusing on whole fruits while others grouped various forms of fruit consumption together. Furthermore, some studies focused particularly on just a few specific types of fruits, limiting the generalizability of their findings. This variation complicates direct comparisons and may obscure the unique health effects of each form. Moreover, the limited number of studies examining fruit smoothies prevents robust conclusions about their health impacts. In addition, most studies did not account for potential variations in nutrient composition among different fruit types or the effects of food processing on nutrient bioavailability

and glycemic index. Some research studies were limited by their focus on a specific group (selected by medical history, ethnicity, or gender), accentuating the need for a large and diverse participant pool to accurately represent the population.

Future research should focus on addressing the limitations identified in this review to provide a more comprehensive understanding of fruit consumption on various health outcomes (e.g. cardiovascular health, blood sugar regulation, musculoskeletal functionality, and mental health). First, longitudinal studies and randomized controlled trials are needed to establish causal relationships between fruit consumption and these health outcomes in order to verify whether the correlations observed are a result of fruit intake or some other confounding factor (e.g., overall dietary patterns or lifestyle behaviors). Researchers should ensure standardization of operational definitions for health outcomes in order to avoid the limitations of Daud *et al.*'s (2023) study (39). In addition, conducting research in diverse populations—incorporating participants of various ages, cultural backgrounds, and health statuses—would improve the generalizability of findings and enhance our understanding of how fruit consumption impacts different demographic groups and society as a whole. Researchers should also explore the long-term effects of fruit intake on chronic health conditions and assess whether the timing and frequency of fruit consumption influences health outcomes. A deeper understanding of the distinctions between the long-term effects of each fruit consumption form can help individuals make more informed choices and contribute to more targeted public health recommendations in the future.

Additionally, future studies should consistently define and differentiate between various forms of fruit consumption within the same study design, allowing for more accurate comparisons of their distinct health effects. It is also essential to examine a wider range of fruit types and consider the impact of fruit processing on nutrient bioavailability and glycemic index. Investigating how specific nutrients or phytochemicals in different fruits influence health outcomes could provide insights into the mechanisms underlying the observed associations. Furthermore, the impact of fruit smoothies on health outcomes is severely understudied despite scientific debate regarding their healthiness (54, 55). While it is known that blending fruits may alter glycemic response (11), further research is needed to assess how mastication influences postprandial glycemic response and insulin sensitivity (23). Given the known role of dietary fiber in gut microbiome health, future studies should investigate how consuming fruit in smoothie form as opposed to other forms affects microbial composition and its subsequent impact on diabetes risk (24).

Current research is severely limited not only in terms of the inclusion of various forms of fruit consumption but also in the variety of health outcomes examined. There is a scarcity of research on the independent effects of fruit intake on different aspects of a single health domain (e.g., cardiovascular or musculoskeletal health), let alone across multiple health domains. Most studies focus solely on one area of health and, even then, typically consider only a few specific health outcomes. Expanding the range of health outcomes assessed could address these knowledge gaps and provide valuable insights for future dietary recommendations regarding fruit consumption. By addressing these gaps, future research can contribute to more effective dietary guidelines and public health strategies aimed at improving overall health through fruit consumption.

ACKNOWLEDGMENTS

No funding was associated with this research study. The author formulated study methodology and research design. The author conducted literature research and analysis. There were no other author or non-author contributions. The author does not have conflicts of interest.

REFERENCES

1. M. A. Davis, J. P. W. Bynum, B. E. Sirovich, Association between apple consumption and physician visits: Appealing the conventional wisdom that an apple a day keeps the doctor away. *JAMA Intern. Med.* **175**, 777–783 (2015). doi: 10.1001/jamainternmed.2014.5466
2. H. Cena, P. C. Calder, Defining a healthy diet: Evidence for the role of contemporary dietary patterns in health and disease. *Nutrients* **12**, 334 (2020). doi: 10.3390/nu12020334
3. F. C. Ross *et al.*, The interplay between diet and the gut microbiome: Implications for health and disease. *Nat. Rev. Microbiol.* **22**, 671–686 (2024). doi: 10.1038/s41579-024-01068-4
4. C. Devirgiliis, E. Guberti, L. Mistura, A. Raffo, Effect of fruit and vegetable consumption on human health: An update of the literature. *Foods* **13**, 3149 (2024). doi: 10.3390/foods13193149
5. H. S. Han, C. B. Chang, D. C. Lee, J. C. Lee, Relationship between total fruit and vegetable intake and self reported knee pain in older adults. *J. Nutr. Health Aging* **21**, 750–758 (2017). doi: 10.1007/s12603-016-0842-7
6. L. Sun *et al.*, Fruit consumption and multiple health outcomes: An umbrella review. *Trends Food Sci. Technol.* **118**, 505–518 (2021). doi: 10.1016/j.tifs.2021.09.023
7. B. Pan *et al.*, Association of soft drinks and 100% fruit juice consumption with risk of cancer: A systematic review and dose–response meta-analysis of prospective cohort studies. *Int. J. Behav. Nutr. Phys. Act.* **20**, (2023). doi: 10.1186/s12966-023-01459-5
8. E. L. Beckett *et al.*, Health effects of drinking 100% juice: An umbrella review of systematic reviews with meta-analyses. *Nutr. Rev.* **83**, (2024). doi: 10.1093/nutrit/nuae036
9. E. J. Arjmand *et al.*, Update of statistical analysis plan for: Effect of fruit smoothie supplementation on psychological distress among people with substance use disorders receiving opioid agonist therapy: Protocol for a randomised controlled trial (FruktBAR). Research Square [Preprint] (2024). doi: 10.21203/rs.3.rs-4748489/v1
10. P. Silva *et al.*, Nutrition and food literacy: Framing the challenges to health communication. *Nutrients* **15**, 4708 (2023). doi: 10.3390/nu15224708
11. L. T. Crummett, R. J. Grosso, Postprandial glycemic response to whole fruit versus blended fruit in healthy, young adults. *Nutrients* **14**, 4565 (2022). doi: 10.3390/nu14214565
12. B. Schrage *et al.*, Evaluating the health benefits of fruits for physical fitness: A research platform. *J. Berry Res.* **1**, 35–44 (2010). doi: 10.3233/br-2010-004
13. R. M. Taylor, *et al.*, Diet quality and cardiovascular outcomes: A systematic review and meta-analysis of cohort studies. *Nutr. Diet.* **81**, 35–50 (2023). doi: 10.1111/1747-0080.12860
14. R. Casas *et al.*, Nutrition and cardiovascular health. *Int. J. Mol. Sci.* **19**, 3988 (2018). doi: 10.3390/ijms19123988
15. P. Buil-Cosiales *et al.*, Consumption of fruit or fiber-fruit decreases the risk of cardiovascular disease in a mediterranean young cohort. *Nutrients* **9**, 295 (2017). doi: 10.3390/nu9030295
16. C. H. Ruxton, M. Myers, Fruit juices: Are they helpful or harmful? An evidence review. *Nutrients* **13**, 1815 (2021). doi: 10.3390/nu13061815
17. S. Kodama *et al.*, Relationship between intake of fruit separately from vegetables and triglycerides - a meta-analysis. *Clin. Nutr. ESPEN* **27**, 53–58 (2018). doi: 10.1016/j.clnesp.2018.07.001
18. F. R. Scheffers *et al.*, Pure fruit juice and fruit consumption and the risk of CVD: The European prospective investigation into cancer and nutrition–Netherlands (EPIC NL) Study. *Br. J. Nutr.* **121**, 351–359 (2018). doi: 10.1017/S0007114518003380
19. R. M. Alqurashi *et al.*, Consumption of a flavonoid-rich açai meal is associated with acute improvements in vascular function and a reduction in total oxidative status in healthy overweight men. *AJCN.* **104**, 1227–1235 (2016). doi: 10.3945/ajcn.115.128728
20. E. Maeda, The effects of green smoothie consumption on blood pressure and health-related quality of life: A randomized controlled trial. (2000). doi: 10.15760/etd.974
21. L. Li *et al.*, Whole fresh fruit intake and risk of incident diabetes in different glycemic stages: A nationwide prospective cohort investigation. *Eur. J. Nutr.* (2022). doi: 10.1007/s00394-022-02998-6
22. C. Visuthranukul *et al.*, Glycemic index and glycemic load of common fruit juices in Thailand.” *J. Health Pop. Nutr.* **41**, (2022). doi: 10.1186/s41043-022-00284-z
23. Y. Seino *et al.*, Eating whole fruit, not drinking fruit juice, may reduce the risk of type 2 diabetes mellitus.” *J. Diabetes Investig.* **12**, 759–1761 (2021). doi: 10.1111/jdi.13639
24. J. Fu *et al.*, Dietary fiber intake and gut microbiota in human health. *Microorganisms* **10**, 2507 (2022). doi: 10.3390/microorganisms10122507
25. S. Li *et al.*, Fruit intake decreases risk of incident type 2 diabetes: An updated meta-analysis.” *Endocrine* **48**, 454–460 (2014). doi: 10.1007/s12020-014-0351-6
26. N. P. Bondonno *et al.*, Associations between Fruit Intake and Risk of Diabetes in the Ausdiab Cohort. *J. Clin. Endocrinol. Metab.* **106**, (2021). doi: 10.1210/clinem/dgab335
27. I. Muraki *et al.*, Fruit Consumption and risk of type 2 diabetes: Results from three prospective longitudinal cohort studies. *BMJ.* **347** (2013). doi: 10.1136/bmj.f5001
28. D. J. Jenkins *et al.*, The Relation of Low Glycaemic Index Fruit Consumption to Glycaemic Control and Risk Factors for Coronary Heart Disease in Type 2 Diabetes. *Diabetologia* **54**, 271–279 (2010). doi: 10.1007/s00125-010-1927-1
29. K. M. Redfern *et al.*, Nutrient-extraction blender preparation reduces postprandial glucose responses from fruit juice consumption. *Nutr. Diabetes.* **7**, (2017). doi: 10.1038/nutd.2017.36
30. S. Dragan *et al.*, Dietary patterns and interventions to alleviate chronic pain. *Nutrients* **12**, 2510 (2020). doi: 10.3390/nu12092510
31. C. M. T. Van der Avoort *et al.*, Higher levels of physical activity are associated with greater fruit and vegetable intake in older adults. *J. Nutr. Health Aging* **25**, 230–241 (2021). doi: 10.1007/s12603-020-1520-3
32. S. Hong, Y. Bae, Association of dietary vegetable and fruit consumption with sarcopenia: A systematic review and meta-analysis. *Nutrients* **16**, 1707 (2024). doi: 10.3390/nu16111707
33. C. E. Neville *et al.*, Effect of increased fruit and vegetable consumption on physical function and muscle strength in older adults. *AGE.* **35**, 2409–2422 (2013). doi: 10.1007/s11357-013-9530-2
34. L. Blekkenhorst *et al.*, Vegetable and fruit intake and fracture-related hospitalisations: A prospective study of older women. *Nutrients* **9**, 511 (2017). doi: 10.3390/nu9050511
35. M. H. Pinheiro *et al.*, Effect of a fruit and vegetable drink on muscle recovery after resistance exercise. *HSJ.* **12**, 57–65 (2022). doi: 10.21876/resch.v12i4.1325
36. Z. Liu *et al.*, Greater fruit intake was associated with better bone mineral status among Chinese elderly men and women: Results of Hong Kong Mr. Os and Ms. Os studies. *J. Am. Med. Dir. Assoc.* **16**, 309–315 (2015). doi: 10.1016/j.jamda.2014.11.001
37. K. N. Haseltine *et al.*, Bone mineral density: Clinical relevance and quantitative assessment. *J. Nuc. Med.* **62**, 446–454 (2020). doi: 10.2967/jnumed.120.256180
38. J. Huang, X. Zheng-Fu Xie, Dried fruit intake causally protects against low back pain: A Mendelian randomization study. *Front. Nutr.* **10**, (2023). doi: 10.3389/fnut.2023.1027481
39. M. Daud *et al.*, Pure juice supplementation: Its effect on muscle recovery and sports performance. *Malay. J. Med. Sci.* **30**, 31–48 (2023). doi: 10.21315/mjms2023.30.1.4
40. C. Mendonça *et al.*, Effects of nutritional interventions in the control of musculoskeletal pain: An integrative review. *Nutrients* **12**, 3075 (2020). doi: 10.3390/nu12103075
41. C. S. L. Tuttle *et al.*, Markers of inflammation and their association with muscle strength and mass: A systematic review and meta-analysis. *Ageing Res. Rev.* **64**, 101185 (2020). doi: 10.1016/j.arr.2020.101185
42. R. Selvaraj *et al.*, Association between dietary habits and depression: A systematic review. *Cureus* (2022). doi: 10.7759/cureus.32359
43. R. Zhang *et al.*, Associations of dietary patterns with brain health from behavioral, neuroimaging, biochemical and genetic analyses. *Nature Mental Health.* **2**, 535–552 (2024). doi: 10.1038/s44220-024-00226-0
44. R. K. Keservani *et al.*, Medicinal effect of nutraceutical fruits for the cognition and brain health. *Scientifica* **2016**, 1–10 (2016). doi: 10.1155/2016/3109254

45. J. Bouayed *et al.*, Oxidative stress and anxiety: Relationship and cellular pathways. *Oxid. Med. Cell. Longev.* **2**, 63–67 (2009). doi: 10.4161/oxim.2.2.7944
46. J. Bouayed *et al.*, Chlorogenic Acid, a polyphenol from *Prunus domestica* (Mirabelle), with coupled anxiolytic and antioxidant effects. *J. Neurol. Sci.* **262**, 77–84 (2007). doi: 10.1016/j.jns.2007.06.028
47. D. Bagchi, H.G. Preuss, A. Swaroop, Eds., *Nutraceuticals and Functional Foods in Human Health and Disease Prevention* (CRC Press, ed. 1, 2015).
48. F. Saghaian *et al.*, Consumption of fruit and vegetables in relation with psychological disorders in Iranian adults. *Eur. J. Nutr.* **57**, 2295–2306 (2018). doi: 10.1007/s00394-018-1652-y
49. Z. Yan *et al.*, Increased fruit intake is associated with reduced risk of depression: Evidence from cross-sectional and Mendelian randomization analyses. *Front. Public Health* **11**, (2023). doi: 10.3389/fpubh.2023.1276326
50. S. Agarwal *et al.*, Association of 100% fruit juice consumption with cognitive measures, anxiety, and depression in U.S. adults. *Nutrients* **14**, 4827 (2022). doi: 10.3390/nu14224827
51. L. T. Fadnes *et al.*, Effect of fruit smoothie supplementation on psychological distress among people with substance use disorders receiving opioid agonist therapy: Protocol for a randomised controlled trial (FruktBAR). *BMC Nutr.* **8**, (2022). doi: 10.1186/s40795-022-00582-z
52. H. G. Stewart *et al.*, Adherence to Federal dietary recommendations for total fruit consumption and the intake of underconsumed nutrients: Findings from the National Health and Nutrition Examination Survey, 2015 to 2018. *J. Nutr.* **153**, 1476–1482 (2023). doi: 10.1016/j.tjnut.2023.03.018
53. T. C. Wallace *et al.*, Fruits, vegetables, and health: A comprehensive narrative, umbrella review of the science and recommendations for enhanced public policy to improve intake. *Crit. Rev. Food Sci. Nutr.* **60**, 2174–2211 (2019). doi: 10.1080/10408398.2019.1632258
54. D. McCartney *et al.*, Smoothies: Exploring the attitudes, beliefs and behaviours of consumers and non-consumers. *Curr. Res. Nutr. Food Sci. J.* **6**, 425–436 (2018). doi: 10.12944/crnfsj.6.2.17
55. D. McCartney *et al.*, Perceived health benefits of smoothie consumption: Investigating consumers' attitudes, beliefs and behaviours. *JNIM.* **8**, 74–75 (2017). doi: 10.1016/j.jnim.2017.04.052

In Vitro Reconstituted Enveloped Virus-Like Particles for Gene Delivery

Selina Juang¹, William M. Gelbart²

¹Department of Molecular, Cell, and Developmental Biology, University of California, Los Angeles. ²Department of Chemistry and Biochemistry, University of California, Los Angeles.

ABSTRACT

In vitro reconstituted virus-like particles (VLPs) are promising gene delivery platforms for mammalian cell gene therapy, with many advantages over lentiviral vectors, adenoviral vectors, and lipid nanoparticles due to their pure composition—consisting solely of capsid proteins and RNA—and precise stoichiometry. However, their being made of viral components raises the possibility of heightened immune responses to the particles when administered for therapeutic purposes. This study aims to lower the immunogenicity of *in vitro* reconstituted VLPs by the addition of lipid envelopes, creating enveloped virus-like particles (EVLPs) that are spontaneously taken up by specific mammalian cells *in vivo* and can be easily functionalized with the addition of targeting ligands. This encapsulation of VLPs in lipids is optimized by varying the mass ratio of VLPs to lipids, pH and composition of the buffer, and wrapping method. Electron microscopy was used to verify the formation of EVLPs, and their uptake efficiency into baby hamster kidney cells at varying concentrations was analyzed and compared to that of VLPs. The EVLPs without lipofectamine were found to have a slightly higher uptake efficiency than that of VLPs without lipofectamine. Additionally, RNA extracted from EVLPs produced by drying-sonication methods show degradation, suggesting that RNA has increased susceptibility to degradation during sonication and prompting the need to explore alternative VLP-wrapping methods, such as freeze-thawing. In this study, two different VLP-wrapping protocols—drying-sonication and freeze-thawing—are compared and the use of shorter reporter genes for more consistent particle size and stability are explored, as shorter RNA sequences demonstrated better success in EVLP formation. Further studies using these wrapping methods could refine the VLP-wrapping process, thereby optimizing EVLP stability and gene delivery efficiency. Together, these findings can help develop safer and more effective gene delivery systems for downstream therapeutic applications, treating diseases such as cancer and genetic disorders.

INTRODUCTION

Gene therapy continues to be a promising field of study, with implications for treating diseases at the molecular level. Recent efforts have focused on developing gene delivery systems to correct disease-causing mutations or express therapeutic genes, treating a wide variety of diseases including cancer (1), acquired immunodeficiency syndrome (AIDS) (2), infectious diseases (3), cardiovascular diseases (4), and genetic disorders, such as X-linked severe combined immunodeficiency (5). However, DNA delivery into human cells poses a risk of insertional mutagenesis, a process in which the cellular genome is unintentionally altered by transgene integration (6). The use of RNA to express transgenes is a viable alternative approach; it has proven to be effective in treating several diseases. For example, the transfection of human T lymphocytes with messenger RNA (mRNA) encoding a chimeric immune receptor against the surface antigen CD19 has been shown to induce strong T cell cytotoxicity against CD19+ malignant cells, demonstrating therapeutic potential for leukemia and lymphoma (7). Several studies have also explored the therapeutic application of small regulatory RNAs like small interfering RNAs (siRNAs) or microRNAs (miRNAs) for RNA interference (8).

A challenge with gene therapy is the development of safe and targeted gene delivery platforms that can overcome biological barriers. An effective gene delivery method should protect its transgene from degradation by nucleases in both the extracellular and intracellular matrices (9) and facilitate its transport across the plasma membrane of target cells to their nuclei, where it can be expressed (10). Viruses have the natural ability to enter specific cells and utilize host cell machinery to replicate their genetic material and are therefore a key tool for gene therapy. However, using naturally occurring viruses for gene therapy carries significant risks as it can lead to uncontrolled viral growth and pose threats to patients (11). Accordingly, significant effort has been devoted to creating stoichiometrically-precise virus-like particles (VLPs), which are noninfectious forms of viruses reconstituted *in vitro* and have a similar structure but without the associated risks. One example of this type of particle uses capsid protein from the cowpea chlorotic mottle virus (CCMV), which is a plant virus. Past studies have shown that when the capsid protein of CCMV is mixed *in vitro* with single-stranded RNA (ssRNA) under specific pH and ionic strength conditions (Figure 1), the contents will spontaneously self-assemble into VLPs. These self-assembled VLPs have a uniform spherical capsid with 180 proteins and a diameter of approximately 28 nm (12).

The advantages of using VLPs in therapeutic applications as opposed to other commonly used particles, like lipid nanoparticles, include stoichiometric and structural uniformity, as well as increased stability. VLPs also offer the advantage of being synthesized *in vitro* without the associated risks that cell and viral-derived vectors pose, such as unintentional encapsulation of cytoplasmic RNA in host cells. There are only a few viruses that can self-assemble *in vitro* with heterologous RNA, CCMV being one of them (13). Thus, by replacing the viral RNA with non-viral RNA, CCMV VLPs present a promising platform for gene delivery applications.

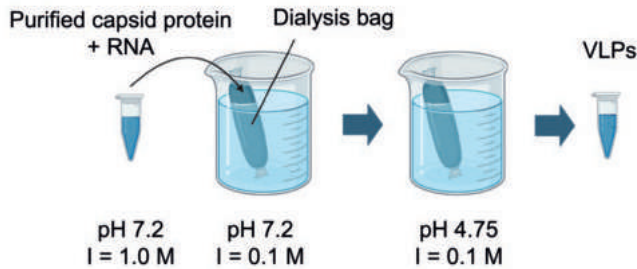


Figure 1: Schematic representation of Virus-Like Particle (VLP) assembly protocol.

The purified capsid protein of the plant virus cowpea chlorotic mottle virus (CCMV) is mixed with single-stranded RNA (ssRNA) and placed into different solutions. This protocol initiates changes in pH and ionic strength that enable the spontaneous self-assembly of capsid protein and ssRNA into VLPs. The mixture of capsid protein and ssRNA is contained within a dialysis bag, which is made of a semipermeable membrane that allows for fluid and ion exchange with the surrounding solution. The solution is then transferred to a test tube for storage. The VLPs produced by this protocol consist of 180 capsid proteins encapsulating 1 RNA molecule, forming spherical structures with a diameter of around 28 nm.

Despite these advantages, most unenveloped plant-virus-derived VLPs can only enter mammalian cells with the aid of electroporation or transfection agents like lipofectamine (14). While effective for *in cellulo* VLP studies, these methods are unsuitable for *in vivo* applications, as electroporation can only be performed on cells *in vitro* and lipofectamine has cytotoxic effects on mammalian cells, limiting the therapeutic potential of VLPs (15). Some studies have shown that CCMV VLPs can be spontaneously taken up by mammalian cell lines such as human embryonic kidney immortalized (HEK-293) cells and human epithelial adenocarcinoma (HeLa) cells without the aid of lipofectamine (16). However, spontaneous uptake of CCMV VLPs is not seen with baby hamster kidney cells (BHK-21) (14). To ensure consistent vector particle uptake by all potential target cells for a broader range of therapeutic applications—including those from animal models like mice and hamsters for *in vivo* studies—this study investigates VLP uptake by BHK-21 cells.

A notable difference between mammalian viruses and plant viruses is the presence of an outer lipid layer in mammalian viruses in addition to a protein capsid shell. This additional lipid envelope enables two distinct modes of host cell entry. The first mode of entry consists of membrane fusion, where the viral envelope is brought into close proximity with the host cell membrane and the two are merged, bringing the capsid into the cytoplasm. The second is endocytosis, in which the virus mediates the formation of a vesicle around itself, allowing it to be internalized and later released by

rupturing out of the endosome (17). The lipid envelope, along with its associated glycoproteins, helps evade immune detection and suppress innate immune responses (18), thereby reducing immunogenicity. In contrast, plant virus capsid proteins, like the ones from CCMV, are inherently immunogenic, making plant-virus-derived VLPs susceptible to opsonization and immune recognition (19). It was proposed that encapsulating VLPs made of plant virus components with a lipid bilayer—thus mimicking the structure of mammalian viruses—could enhance their uptake by mammalian cells while evading the host immune system.

In this study, enveloped virus-like particles (EVLPs) were created by wrapping CCMV VLPs in lipids. The isoelectric point of CCMV capsid protein is pH 4.8; thus, at around the physiological pH of 7, the CCMV surface charge is negative (20). Cationic lipids were used to form EVLPs, as electrostatic interactions between the anionic capsid proteins and cationic lipids drive wrapping of particles (Figure 2). This study hypothesizes that the lipid bilayer will serve as an additional layer of protection and stability due to the electrostatic interactions with the protein, which reduces the likelihood of RNA degradation. It can also enable functionalization for cell targeting, as lipids conjugatable to certain proteins can be added to the lipid mix.

Initial attempts to form EVLPs started with multilayer vesicles, which were first disrupted into bilayers by sonication, facilitating encapsulation of VLPs (Figure 3A). However, this approach led to significant RNA degradation, raising concerns regarding the stability of these particles. Therefore, a freeze-thawing protocol (Figure 3B) was investigated as an alternative.

The more translational aspect of this study is to investigate whether the cellular intake of EVLPs without the use of lipofectamine or electroporation is possible. VLPs were assembled to contain a replicon—mRNA that self-replicates in host cells—that encodes both Enhanced Yellow Fluorescent Protein (EYFP) and RNA-dependent RNA polymerase (RdRp) from the Nodamura insect virus, one of the shortest RdRps at 3200 nucleotides (nt) (Figure 4). After assembly, VLPs were then wrapped with a lipid mixture similar to the lipid composition of mammalian cells. The lipid mixture used in this study has a low cytotoxicity (21), consisting predominantly of a neutral lipid 1,2-Dimyristoyl-sn-glycero-3-phosphocholine (DMPC), with smaller amounts of cholesterol and the cationic lipid 1,2-Dioleoyl-3-Trimethylammonium-propane (DOTAP), in order to optimize fusion with mammalian cell membranes. The EVLPs were overlaid on BHK cells, which fluoresce

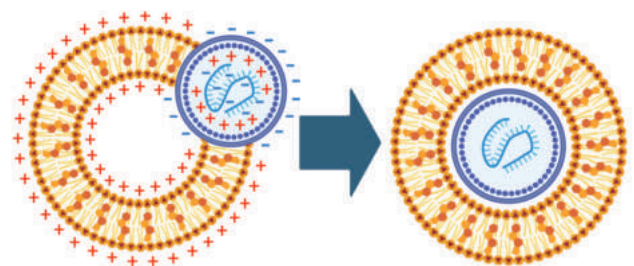


Figure 2: Schematic of Virus-Like Particle (VLP) wrapping.

At a pH of 7, similar to physiological pH, the charge of the VLP's outer surface is negative, allowing the VLP to electrostatically interact with the positive charge of the lipid mix (left), forming Enveloped Virus-Like Particles (right).

only if EVLPs have successfully entered the cells, disassembled, and released the reporter gene without lipofectamine. Fluorescence in the cells that have been overlaid with EVLPs without lipofectamine indicated that the lipid bilayer surrounding EVLPs can facilitate the uptake of particles by BHK cells, suggesting a promising use of these particles for *in vivo* gene therapy.

However, RNA degradation and particle size inconsistencies—due to the replicon form of the reporter gene being too long to be packaged exclusively into single, ribonuclease-protected, capsids (22)—prompted a shift toward using the reporter gene HiBiT (33 nt), as it is much shorter than the EYFP gene (720 nt). The HiBiT gene encodes for the HiBiT protein, an 11 amino acid peptide that has a high affinity ($KD = 0.7$ nM) for a larger subunit called Large BiT (LgBiT). In the presence of furimazine substrate, the HiBiT-LgBiT complex produces bioluminescence, serving as a sensitive method for detecting gene expression in cells. HiBiT's relatively short length makes it an ideal candidate for efficient packaging in replicon form within VLPs and EVLPs, minimizing the risk of RNA degradation during VLP wrapping.

Given the advantages of lower immunogenicity, increased modalities of entry into target cells, and more robust RNA protection, adding a lipid envelope around VLPs is hypothesized to provide a safer and more effective method of gene delivery. This study aims to refine the EVLP formation process and assess its potential for gene delivery in mammalian cells. Findings from

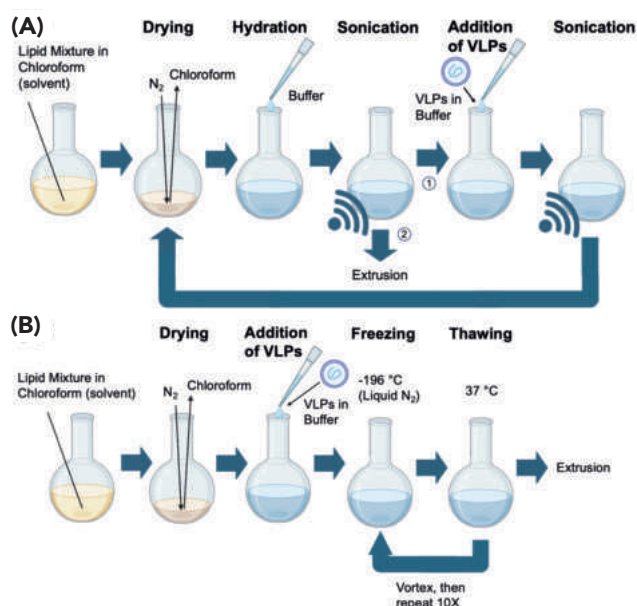


Figure 3: Schematics of the two methods for wrapping Virus-Like Particles (VLPs).

Lipid mixtures are dissolved in chloroform, and VLPs are pre-dissolved in Tris buffer (pH 7.0). A VLP to lipid mass ratio of 1:8 optimizes wrapping. **(A)** Drying-sonication method. The lipid mixture is added to a round bottom flask and dried with nitrogen gas using a Rotovap to form a dry lipid film. Tris buffer is added to the flask, sonicated, then dried again. The VLP mixture is added, and the solution is vortexed, sonicated, and dried. Tris buffer is then added for rehydration, and the solution is sonicated and filtered using an extruder. **(B)** Freeze-thawing method. The lipid mixture is added to a round-bottom flask and dried with nitrogen gas using a Rotovap to form a dry lipid film. The VLP mixture is added, and flasks are freeze-thawed repeatedly (10 times) in liquid nitrogen and a water bath at $37^\circ C$, with ten seconds of vortexing between each cycle. The solution was filtered with an extruder.

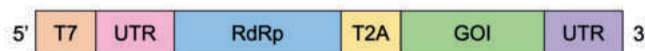


Figure 4: Schematic of replicon gene construct used in Virus-Like Particles (VLPs).

Nodamura insect virus (NoV) is a positive-sense RNA virus with a bipartite genome (29), in which its first RNA molecule (RNA1, ≈ 3200 nt) encodes the RNA-dependent RNA polymerase (RdRp). RNA1 is demonstrated to have strong amplification of itself and downstream genes in mammalian cells (23, 30). In the replicon gene construct used in VLPs, there are two untranslated regions (UTRs) flanking the 5' and 3' ends of NoV RNA1 and the gene of interest (GOI). T7 is the transcriptional promoter, and T2A is *Thosea asigna* virus 2A self-cleaving peptide, which enables the separation of the RdRp and GOI proteins after translation into a RdRp-GOI polyprotein (24). The GOIs used in this study were the Enhanced Yellow Fluorescent Protein (EYFP) gene and the HiBiT gene. The GOI can be replaced by a therapeutic gene in future studies.

this study could contribute to the development of EVLPs as a platform for RNA-based disease therapies.

MATERIALS AND METHODS

Materials

RNA Assembly Buffer (RAB) was prepared from 50 mM NaCl, 10 mM KCl, 5 mM $MgCl_2$, 1 mM dithiothreitol (DTT), and 50 mM Tris-HCl pH 7.2. Virus Extraction Buffer (VSB) was prepared from 50 mM sodium acetate, and 8 mM magnesium acetate pH 4.75. The protein buffer (Buffer B) was made from 1 M NaCl, 20 mM Tris-HCl pH 7.2, 1 mM EDTA, 1 mM DTT, and 1 mM phenylmethylsulfonyl fluoride (PMSF). The plasmid construct consisting of the Enhanced Yellow Fluorescent Protein fused with RdRp from the Nodamura insect virus (pNod-EYFP)—in which the EYFP gene is separated from the RdRp by a *Thosea asigna* virus 2A (T2A) ribosome skipping sequence that mediates self-cleavage during translation—was provided by Dr. Raul Andino (University of California, San Francisco) and was synthesized using a cloning protocol with the Simian Virus 40 (SV40) promoter and trailed by a Hepatitis Delta Virus (HDV) ribozyme (23). Upon transcription, the plasmid generates a replicon that can be translated upon cellular uptake (24), with EYFP serving as a reporter of gene delivery and expression. CCMV capsid proteins were obtained from stocks from the Gelbart Lab (University of California, Los Angeles), which were obtained from an *Escherichia coli* (E. coli) bacterial expression system and purified by running the cell lysate over using a $7\times$ histidine tag (25). Tris Buffer 75 mM was made to have a pH of 7.0, the pH determined to be optimal for wrapping by past Gelbart Lab experiments. The lipids DMPC, DOTAP, and cholesterol were obtained from Avanti Polar Lipids, Alabaster, AL and were dissolved in chloroform. BHK-21 cells were obtained from cell culture stocks from the Gelbart Lab. The HiBiT sequence was obtained from the Nano-Glo HiBiT Lytic Detection System kit (Promega, Madison, WI).

Cloning of Nod-HiBiT Replicon Construct

Due to concerns about the long length of the EYFP gene (720 nt), the HiBiT gene (33 nt) was explored as an alternative reporter gene to be encapsulated in VLPs. HiBiT is part of the Nano-Glo HiBiT Lytic Detection System kit (Promega, Madison, WI), which is derived from the NanoLuc Binary Technology (Promega, Madison, WI), a binary complementation system based on

NanoLuc luciferase. The HiBiT assay's ultra-sensitivity and highly quantitative properties make it more effective than fluorophore-based assays like EYFP, increasing its suitability as a reporter gene. The plasmid construct pNod-HiBiT was obtained using the Promega molecular cloning protocol (Promega, Madison, WI), in which the plasmid pNod-EYFP was first cut at the AgeI and NdeI restriction sites, which flank the EYFP gene. The sample was then run on an agarose gel, after which the gene fragment containing the Nodamura replicon was extracted and the HiBiT gene was inserted using a T4 DNA ligase. The recombinant plasmid containing HiBiT was then introduced into chemically competent cells of the *E. coli* strain and transformed colonies with ampicillin resistance were selected for plasmid extraction. To verify the proper cloning of pNod-HiBiT, constructs were sent in for whole plasmid sequencing by Plasmidsaurus (Plasmidsaurus, Arcadia, CA) using Oxford Nanopore Technology with custom analysis and annotation.

In Vitro Transcription of mRNA

Plasmid constructs of pNod-EYFP and pNod-HiBiT were linearized by single digestion with XbaI and purified using QIAquick polymerase chain reaction (PCR) purification columns from Qiagen (Valencia, CA, USA) to prepare for transcription. Linearized DNA was transcribed using a MEGAscript™ T7 Transcription Kit (Thermo Fisher Scientific, Waltham, MA) and purified using the RNeasy Mini Kit (Qiagen, Valencia, CA). A 7-methylguanylate cap structure was then added to the 5' end of the RNA using a vaccinia virus capping system (New England Biolabs, Ipswich, MA) in order to ensure downstream translation, and purified a second time using the RNeasy Mini Kit.

VLP Assembly

A mixture of either Nod-EYFP or Nod-HiBiT RNA, along with CCMV capsid protein (at a protein to RNA ratio of 4.2:1) and Buffer B was added to a dialysis bag, sealed, and placed into a beaker of RAB. After 16 hours, the dialysis bag was transferred to a beaker containing VSB for 8 hours. After the second dialysis, the solution was transferred into a tube for storage. This protocol is commonly used by the Gelbart Lab to create CCMV VLPs (24). Initial attempts for EVLP wrapping utilized VLPs containing Nod-EYFP RNA; however, previous studies have shown multiple CCMV capsids packaging around a single ssRNA when the RNA length exceeds 3500 nt (26), leading to less robust RNA protection due to exposure of RNA threaded between the capsids. Therefore, VLPs containing Nod-HiBiT RNA, a shorter reporter gene, were assembled *in vitro*.

EVLP Assembly Through Drying-Sonication

The VLPs were wrapped with lipids at a mass ratio of 1 VLP to 8 lipids, with a lipid composition of 60% neutral lipids, 30% cationic lipids, and 10% cholesterol, a ratio found to be the most efficient for wrapping VLPs in past experiments by the Gelbart Lab. To achieve this, a 200 µL mixture of DMPC (a neutral lipid), DOTAP (a cationic lipid), cholesterol, and chloroform were added in a 50 mL round-bottom flask. The flask was attached to a rotary evaporator (Rotovap, BUCHI, Flawil, Switzerland) and the solvent was evaporated by a continuous flow of nitrogen gas until a thin and dry film remained on the flask surface. The VLPs and Tris buffer were then added to the round flask and placed in a bath sonicator (Thermo Fisher Scientific, Waltham, MA) for 1

hour to facilitate interactions between lipid layers and capsids. After sonication, the Rotovap was used to dry the contents. Once dry, Tris buffer was added to rehydrate the contents before sonicating them again for one hour. The solution was extracted from the flask and extruded through polycarbonate membrane filters with 200 nm pores using a Mini-Extruder (Avanti Polar Lipids, Alabaster, AL); 200 nm is the smallest pore size shown to be effective in filtering out lipid aggregates, as previous attempts with 100 nm filters yielded fewer particles.

Transfection of EVLPs into BHK Cell Lines

BHK-21 cells, which are anchorage-dependent, were grown as monolayers in 100 µL of Dulbecco's Modified Eagle Medium (DMEM, Thermo Fisher Scientific, Waltham, MA) with 10% (v/v%) fetal bovine serum (FBS, Thermo Fisher Scientific, Waltham, MA) and 1% (w/v%) penicillin/streptomycin (Thermo Fisher Scientific, Waltham, MA) on a 96-well plate at 37°C in a CO₂ incubator for 24 hours. BHK-21 monolayers were grown to 70–90% confluence with approximately 10,000 cells per well. The RNA, VLPs, and EVLPs were diluted to yield either 60, 120, or 300 ng of RNA per well (see experimental conditions below) with Opti-MEM reduced-serum medium (Thermo Fisher Scientific, Waltham, MA) to a total volume of 50 µL and each sample was overlaid on cells grown in triplicates. The first experimental condition was treatment only with Lipofectamine transfection agent (Thermo Fisher Scientific, Waltham, MA). The second experimental condition was treatment only with RNA and lipofectamine. The third and fourth experimental conditions were treatments with VLPs with and without lipofectamine, respectively, both with 60 ng of RNA per well in VLP form. The fifth and sixth experimental conditions were with EVLPs with and without lipofectamine, respectively, with 60 ng RNA per well in EVLP form. The seventh and eighth experimental conditions were treatments with EVLPs containing 120 ng and 150 ng of RNA, respectively. Transfection for samples containing lipofectamine was done following a well-established protocol (14), where samples of naked RNA, VLPs, or EVLPs were first incubated with Lipofectamine-2000 (Thermo Fisher Scientific, Waltham, MA) before being overlaid on cells. Samples without lipofectamine were overlaid on cells after dilution to 50 µL with Opti-MEM. The cells were collected after 24 hours and their fluorescence in arbitrary units (A.U.) was measured with a fluorescent microplate reader (Infinite M Plex Tecan instrument, Männedorf, ZH) to quantify the amounts of EYFP reporter expression.

RNA Extraction and Gel Electrophoresis

Prior to RNA extraction, assembled VLPs were either treated with RNaseA (Thermo Fisher Scientific, Waltham, MA) at a mass ratio of 0.11 RNaseA to 1 RNA at 37°C for 30 minutes and purified with a 100 kDa Amicon spin column (Millipore Sigma, St. Louis, MO) or not RNaseA-treated. RNA was extracted from wild-type CCMV, VLPs, and EVLPs using the QIAGEN Viral RNA Mini Kit, following the protocol from the manufacturer (QIAGEN, Aarhus, Denmark). The RNA extracted from CCMV VLPs and EVLPs containing EYFP was run in electrophoresis buffer (1 x Tris Acetate-EDTA (TAE) buffer, pH 8.0) on a 0.8% (w/v%) agarose gel at 100 V for 1.5 hours. To investigate RNA degradation further, more samples of RNA were extracted, including RNA samples from wild-type CCMV, and run on an agarose gel with a higher w/v% of 1.2%. This gel was run at 100 V for 2 hours, which, in tandem, with the increased

w/v%, provides a better molecular separation than a 0.8% agarose gel run for 1.5 hours. RNA was also extracted from CCMV containing HiBiT in order to verify the correct length of the reporter gene. All gels were run alongside an Invitrogen Millennium RNA Marker (Thermo Fisher Scientific, Waltham, MA), and RNA was visualized by prestaining with 2 μ L 200X GelRed (Biotium, Fremont, CA).

EVLP Assembly Through Freeze-Thawing

Due to concerns raised by the RNA extraction experiments regarding the integrity of RNA being encapsulated by the EVLPs, an alternative VLP-wrapping method was explored as a potential solution for more effective EVLP formation. Freeze-thawing is a method commonly used for creating lipid nanoparticles (LNPs), involving cycles of freezing and thawing, which disrupts the liposomal bilayer to allow for RNA molecule diffusion through lipids (27) and allows for encapsulation of genes in lipid particles (22). The freeze-thawing protocol used in Dr. Irene Chen's Lab (University of California, Los Angeles) for the preparation of phospholipid vesicles (22) was adapted for this study to wrap VLPs instead of naked RNA—RNA not enclosed within capsid proteins or lipids—aiming to avoid RNA degradation that occurs during sonication methods. Similar to the sonication method, the VLPs were wrapped in lipids at a mass ratio of 1 VLP to 8 lipids with a composition of 60% neutral lipids (DMPC), 30% cationic lipids (DOTAP), and 10% cholesterol. These components were added in a small round bottom flask, attached to the Rotovap, and spun with low nitrogen gas flow until dry. After the lipids were dried and the VLPs and Tris buffer were added, the flasks were freeze-thawed 10 times repeatedly in liquid nitrogen and a water bath at 37°C with 10 seconds of vortexing between each cycle. The solution was extracted from the flask and extruded through polycarbonate membrane filters with 200 nm pores as described above.

Electron Microscopy Characterization of VLPs and EVLPs

The characterization of the VLPs and EVLPs was determined by transmission electron microscopy (TEM), where VLP or EVLP samples were first diluted to 0.2 mg/mL and deposited on glow-discharged carbon-coated copper (200-mesh) PELCO Pinpointer grids (Ted Pella, USA), which were stained with 2% w/v uranyl acetate (6 μ L). Micrographs were then obtained using a Tecnai G2 TF20 High-resolution electron microscope (FEI, Hillsboro, OR) (27).

Statistical Analysis

A one-way analysis of variance (ANOVA) was used to determine whether there were significant differences in EYFP fluorescence in BHK-21 cells among group means, comparing RNA delivery via VLPs or EVLPs with or without lipofectamine. If the ANOVA test indicated a significant effect ($p < 0.05$), a Tukey's Multiple Comparisons test was used to identify which specific group comparisons were statistically significant.

RESULTS

EVLP Samples Contain Lipid Aggregates

Electron microscopy images of Nod-EYFP VLPs show uniformly sized and shaped particles with diameters around 28 nm (Figure 5). Electron microscopy images of Nod-EYFP EVLPs that have

undergone the drying-sonication process show presence of unwrapped particles about 28 nm in diameter and wrapped particles about 40 nm in diameter (Figure 6). The larger structures formed from excess lipids are lipid aggregates, which vary in size, ranging from around 100 nm to 200 nm in diameter.

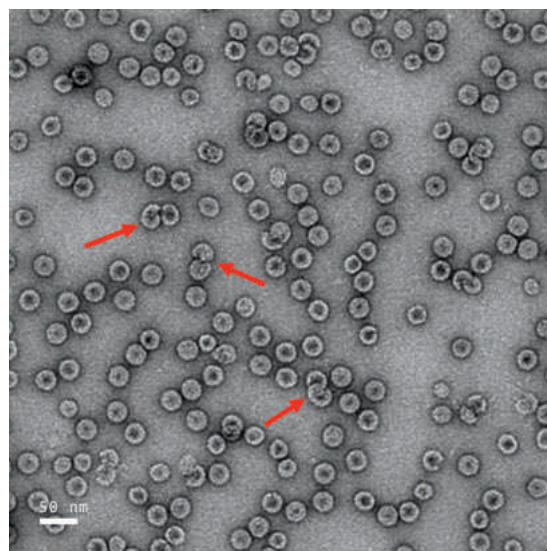


Figure 5: Electron microscopy image of Virus-Like Particles (VLPs) containing Enhanced Yellow Fluorescent Protein Nodamura Replicon (Nod-EYFP).

Images show uniform spherical VLPs of around 28 nm in diameter. Some pairs of VLPs (indicated with red arrows) are linked together through their sharing of a common RNA molecule. Scale bar: 50 nm.

Fluorescence Indicates Cellular Uptake of EVLPs Without Lipofectamine

BHK-21 cells were overlaid with naked RNA, RNA-containing VLPs, or RNA-containing EVLPs, either with or without the lipofectamine transfection agent. Fluorescence levels were measured using a plate reader (Figure 7). All RNA-containing samples at 1x concentration involved equal amounts of RNA molecules (60 ng). The highest fluorescence intensity when comparing samples with 60 ng of RNA was when naked RNA was transfected along with lipofectamine, with EVLPs and VLPs at the same concentration showing around 15000 A.U. lower fluorescence. There was no significant difference in fluorescence between cells treated with VLPs with lipofectamine and cells treated with EVLPs, both with and without lipofectamine. Compared to fluorescence from cells treated with VLPs and lipofectamine, EVLPs at RNA concentrations of 2x (120 ng/well) and 2.5x (150 ng/well) produced significantly higher fluorescence (Figure 7).

Drying-Sonication Method Shows Significant RNA Degradation

Since the fluorescence of EVLPs without the lipofectamine transfection agent was not significantly stronger than that of VLPs (Figure 7), it was hypothesized that the RNA encapsulated in EVLPs may not be fully intact. RNA was therefore extracted from Nod-EYFP VLPs and Nod-EYFP EVLPs for comparison. A 0.8% agarose gel shows clear bands at around 4000 nt containing Nod-EYFP RNA in lane 2 and RNA extracted from Nod-EYFP VLPs in lane 3 (Figure 8A). There is no clear band at 4000 nt or at any

other location in lane 4, which contains the RNA extracted from Nod-EYFP EVLPs, the only sample that had undergone sonication. To investigate RNA degradation further, more samples of RNA were extracted—including RNA samples from wild-type CCMV—and run on a 1.2% agarose gel. Given that brome mosaic virus RNA1 (B1 RNA) is approximately the same length as wild-type CCMV RNA (around 3200 nt), it was used as a reference for the extracted wild-type CCMV RNA. There are distinct bands at 3200 nt for B1 RNA in lane 2 and at 4200 nt for Nod-EYFP RNA in lane 5 (Figure 8B). No distinct bands were observed in the lanes containing RNA extracted from samples that were sonicated. This includes lanes 3, 4, 6, and 7, which represent RNA extracted from wild-type CCMV without lipids, wild-type CCMV with lipids, Nod-EYFP VLPs without lipids, and Nod-EYFP EVLPs with lipids, respectively.

Shorter Reporter Gene Form Single VLPs (Singlets) that are RNase Protected

Electron microscopy images of Nod-HiBiT VLPs (Figure 9) show that the particles are around 28 nm in diameter. There are no connected pairs of capsids in the image, unlike in the images of Nod-EYFP VLPs. RNA extraction showed no RNA degradation from ribonuclease (RNase) in Nod-HiBiT VLPs (Figure 10), as gels indicate similar bands for RNA extracted from both RNase-treated and non-RNase-treated HiBiT-VLPs.

EVLP Assembly Through Freeze-Thawing as an Alternative VLP-Wrapping Method

Electron microscopy images (Figure 11) show the formation of EVLPs with diameters of around 50 nm. VLP particles of around 28 nm can be seen through visual inspection within the EVLPs, similar to what is seen in EVLP images from the drying sonication methods.

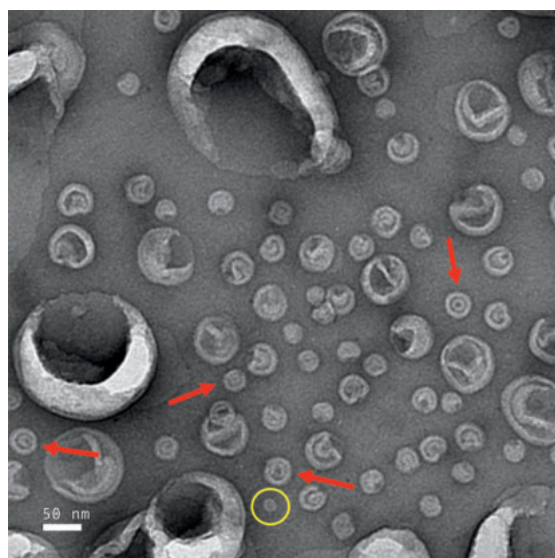


Figure 6: Electron microscopy images of Enveloped Virus-Like Particles (EVLPs) containing Enhanced Yellow Fluorescent Protein Nodamura Replicon (Nod-EYFP).

Images show naked, free VLPs (yellow circle, around 28 nm in diameter) and VLPs within larger particles (red arrows, around 40 nm in diameter). VLPs found within the larger 40 nm diameter particles are wrapped VLPs. Larger lipid aggregates are seen throughout the image, varying in sizes and shapes. Scale bar: 50 nm.

DISCUSSION

Virus-like particles are increasingly recognized for their therapeutic potential as a gene delivery platform. This study explores the wrapping of VLPs in lipids to create EVLPs, hypothesizing that an additional lipid bilayer reduces immunogenicity, facilitates entry into target cells, and strengthens the protection of RNA against degradation. The self-assembly of Nod-EYFP into CCMV VLPs creates uniform particles with a diameter of around 28 nm (Figure 5) and is consistent with previous studies on VLP self-assembly (12). Following the lipid-wrapping process, it was observed that only some of the VLPs were wrapped (Figure 6), which indicates that the wrapping efficiency of VLPs to form EVLPs is low. Electron microscopy images indicate the presence of lipid bilayers surrounding multiple VLPs, not just singly-wrapped particles. Since the bending rigidity of the lipid bilayer increases with lipid length (28), it can be inferred that the flexibility of the lipid bilayer to curve into a small (~40 nm-diameter) spherical structure is limited and that bilayers form more easily around larger groups of particles.

In the experiments involving the overlay of RNA or particles (VLPs or EVLPs) onto BHK-21 cells (Figure 7), the highest fluorescence intensity in a 24 hour period, when comparing samples with equal amounts of RNA, was observed in samples when lipofectamine was added to naked RNA. This aligns with the role of lipofectamine in enhancing cellular uptake of RNA and thereby increasing fluorescence intensity. EVLPs and VLPs showed lower fluorescence, indicating reduced translation of EYFP by cells and, consequently, reduced delivery efficiency *in vitro*. However, naked RNA is challenging to administer *in vivo*, as it is highly prone to degradation without the protection of a capsid and lacks the ability to be targeted to specific cells. Therefore, efforts to increase delivery efficiency should focus on optimizing EVLP formations to enhance RNA stability and cellular uptake. Results also show EVLPs requiring higher RNA concentrations (at 2 and 2.5 times more concentrated) to achieve significant fluorescence. Notably, the fluorescence produced by transfecting VLPs with and without lipofectamine is not significantly different from baseline fluorescence when only lipofectamine is administered, which could indicate the degradation of RNA in VLP form. RNA degradation in VLPs could be attributed to the presence of multiplerts (multiple capsids encapsulating a single RNA), which do not provide full RNA protection. It is important for EVLPs to consistently produce higher fluorescence than VLPs in order for them to be established as a superior gene delivery method over VLPs. Since EVLPs containing a total of 60 ng RNA exhibited a statistically non-significant level of fluorescence as VLPs containing 60 ng RNA, EVLPs must be further optimized to enhance RNA delivery and translation efficiency. EVLPs with 120 ng RNA produced higher fluorescence intensity than VLPs and EVLPs with 60 ng RNA, and EVLPs containing a total of 150 ng RNA exhibited the highest fluorescence intensity among all three EVLP samples. This is expected, as a higher concentration of particles contains higher amounts of RNA, correlating with higher expression of EYFP by cells.

RNA integrity was evaluated by extracting RNA from EVLPs and results indicate degradation of RNA in EVLPs, while no degradation is seen in RNA from VLPs (Figure 8A). This was initially hypothesized to be due to the length of Nod-EYFP RNA, as it is too long to be packaged into a single 28 nm capsid. Instead, it is shared by two VLP capsids, making it more prone

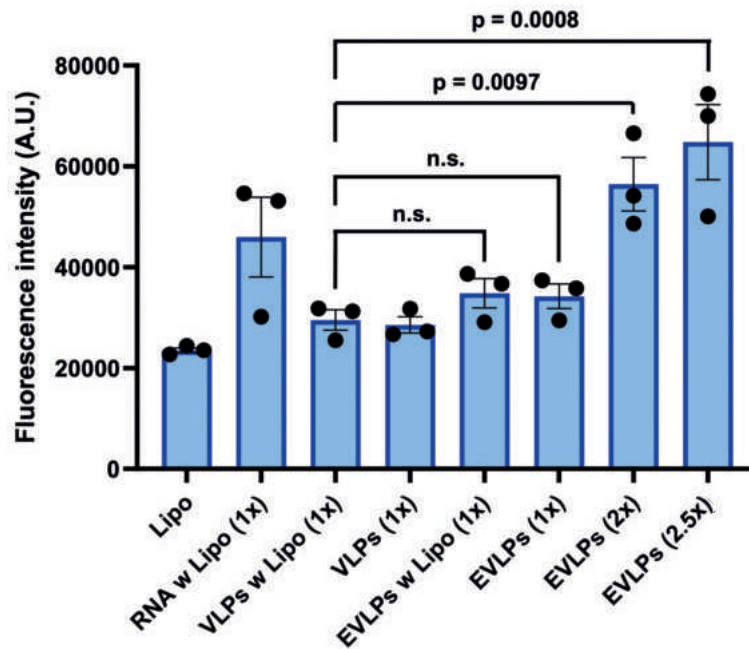


Figure 7: Enhanced Fluorescent Yellow Protein (EYFP) fluorescence in Baby Hamster Kidney cells.

Each sample of either RNA, VLPs, or EVLPs, was overlaid on cells grown in triplicates. The fluorescence intensity in arbitrary units (A.U.) at 24 hours was averaged for each sample and data was plotted in a bar graph. Standard errors of mean for biological triplicates (black dots, $n = 3$) are represented with error bars. The cells treated with lipofectamine (lipo) or lipids alone produced around 22500 A.U. (bar 1). Cells treated with RNA and lipo showed approximately 45000 A.U. (bar 2). Cells treated with VLPs and lipo showed fluorescence with a peak at 30000 A.U. (bar 3), as did cells given VLPs without lipo (bar 4). EVLPs at the same RNA concentration as the VLPs (1x) produced around 35000 A.U. fluorescence, both with and without lipo (bars 5 and 6). EVLPs at 2x concentration produced around 57500 A.U. fluorescence (bar 7), and EVLPs at 2.5x concentration produced around 65000 A.U. fluorescence (bar 8). Significance: n.s. = not significant; $\alpha = 0.05$.

to degradation during sonication compared to RNA packaged in a single capsid. To further investigate the causes of RNA degradation, another RNA extraction was performed from wild-type CCMV, VLPs, and EVLPs (Figure 8B). This condition compared RNA from particles encapsulating RNA in singlets versus multiplets, as well as those that underwent sonication versus those that did not. Since wild-type CCMV encapsulates RNA in singlets, not multiplets, its RNA served as a control to assess the integrity of fully encapsulated RNA within a capsid. The agarose gel indicates that the RNA from particles that have undergone the wrapping protocol (sonication, drying, extrusion), with or without the presence of lipids in the mixture, was not intact (Figure 8B). Since the wild-type CCMV RNA was also not present in the gel, this could suggest that the wrapping protocol degrades RNA even when encapsulated by singlets.

Although RNA degradation may be primarily caused by the sonication process, it is still important to increase the robustness and uniformity of EVLPs for downstream therapeutic purposes. Thus, the HiBiT reporter gene (33 nt), a shorter gene than EYFP (720 nt), was used to produce VLPs so that all of the assembled VLPs are essentially in singlets. This would also eliminate the possibility of RNA being degraded due to being encapsulated by multiple capsids. Electron microscopy images show that the Nod-HiBiT VLPs are uniform and self-assembled into particles measuring around 28 nm in diameter (Figure 9), which is similar to EYFP-containing VLPs (Figure 5). However, unlike the EYFP VLPs, the HiBiT VLP samples show no presence of multiplets, with all RNA encapsulated in single capsids. Furthermore,

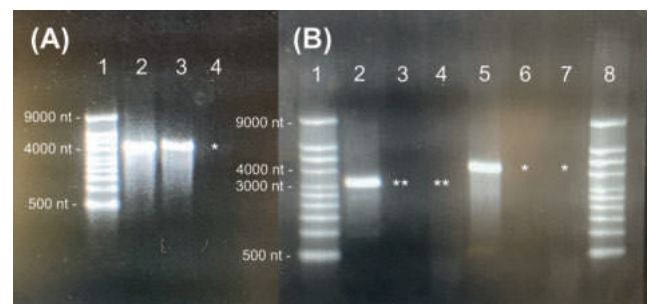


Figure 8: Extraction of Enhanced Yellow Fluorescent Protein (EYFP) RNA from Virus-Like Particles (VLPs) shows RNA degradation after drying-sonication.

EYFP RNA in Nodamura replicon form (Nod-EYFP) was extracted from VLPs and EVLPs, and run on an agarose gel. **(A)** Extracted RNA in 0.8% agarose gel. Lane 1: Millennium RNA Marker. Lane 2: Nod-EYFP RNA. Lane 3: RNA extracted from Nod-EYFP VLPs without sonication. Lane 4: RNA extracted from Nod-EYFP EVLPs formed by drying-sonication. The * shows absence of an RNA band at around 4199 nt, the full length of Nod-EYFP RNA. **(B)** Extracted RNA in 1.2% agarose gel. Lane 1: Millennium RNA Marker. Lane 2: B1 RNA (Brome mosaic virus RNA1). Lane 3: RNA extracted from wild-type CCMV that has undergone sonication without lipids. Lane 4: RNA extracted from wild-type CCMV that has undergone sonication with lipids. Lane 5: Nod-EYFP RNA. Lane 6: RNA extracted from Nod-EYFP VLPs that have undergone sonication without lipids. Lane 7: RNA extracted from Nod-EYFP EVLPs that have undergone sonication with lipids. Lane 8: Millennium RNA Marker. The * shows absence of an RNA band at around 4199 nt, the full length of Nod-EYFP RNA. The ** shows absence of an RNA band at around 3200 nt, the full length of wild-type CCMV RNA1.

RNase treatment of Nod-HiBiT VLPs (Figure 10) shows no degradation, suggesting that RNA is protected within the VLPs and that RNA degradation may be less likely to occur when the RNA is encapsulated within a single capsid. With improved RNA protection, the stability and therapeutic potential of the particles is significantly enhanced. The absence of multipliants also suggests that the use of the HiBiT reporter gene can help maintain the consistency and uniformity of the VLPs, making the gene delivery system more reliable for applications.

The freeze-thawing method, adapted from LNP formation, was also explored for EVLP production. Electron microscopy images show presence of EVLPs (Figure 11), around 50 nm in size, with some fused capsids and larger lipid aggregates along with naked VLPs. This method for EVLP formation has potential for development of a more effective gene delivery system, as it avoids the use of sonication, which we show may be linked to RNA degradation through RNA extraction experiments. However, more modifications to the protocol are needed to optimize VLP-wrapping and minimize the formation of large lipid aggregates. A more comprehensive comparison between EVLPs formed by drying-sonication versus freeze-thawing is also needed to evaluate differences in RNA stability and gene delivery efficiency. This will help determine whether freeze-thawing is a more advantageous alternative method for EVLP production.

Given the aforementioned limitations, future work can focus on refining the VLP-wrapping protocol to reduce RNA degradation, increase VLP-wrapping efficiency, and explore cellular uptake of EVLPs in other mammalian cell lines. More experiments with the freeze-thawing method can be conducted involving RNA extraction from EVLPs for further evaluation of RNA degradation. In this study, the relatively long lipids DPMC and DOTAP, both consisting of 18-carbon chains, were used. The effects of shorter lipids could be investigated through the use of 12-carbon chain lipids, which may lower the bending rigidity of lipid layers and

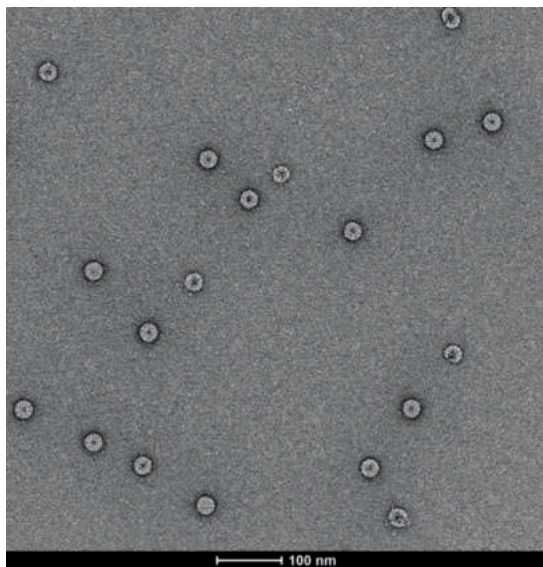


Figure 9: Electron microscopy image of Virus-Like Particles (VLPs) containing HiBiT Nodamura Replicon (Nod-HiBiT).

Image shows uniform spherical VLPs of about 28 nm in diameter. There are no pairs of capsids present, which are seen in images of VLPs containing Enhanced Yellow Fluorescent Protein. Scale bar: 100 nm.

increase wrapping efficiency. To obtain a cleaner sample of EVLPs and remove the presence of lipid aggregates (Figure 6), extruders with smaller pores may be beneficial. However, it is important to note that extruders with smaller pores may also reduce the overall yield of EVLPs, as fewer particles will be able to pass through.

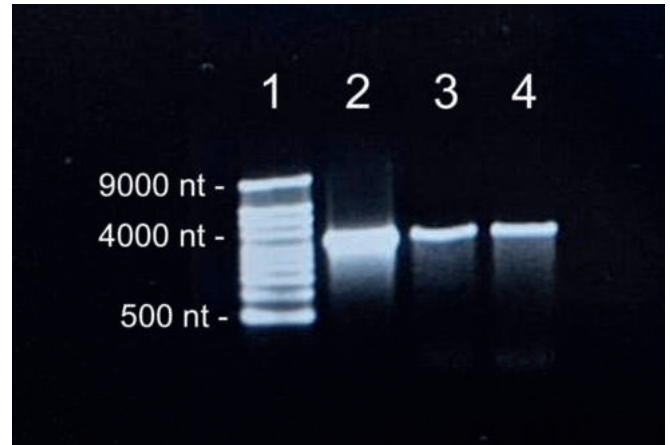


Figure 10: RNA extraction from Virus-Like Particles (VLPs) containing HiBiT Nodamura Replicon (Nod-HiBiT) shows RNase protection when run on agarose gel.

RNA was extracted from Nod-HiBiT VLPs and run on a 0.8% agarose gel. Protection from RNase treatment was inferred from the presence of full-length RNA at around 3233 nt. Lane 1: Millennium RNA Marker. Lane 2: Nod-HiBiT RNA. Lane 3: RNA extracted from Nod-HiBiT VLPs without RNase treatment. Lane 4: RNA extracted from Nod-HiBiT VLPs with RNase treatment.

Together, these results demonstrate the potential of encapsulating VLPs in lipids as an alternative to traditional gene delivery methods that rely on cytotoxic reagents like lipofectamine. The use of EVLPs shows cellular uptake without using lipofectamine, providing a safer approach for *in vivo* applications by eliminating dependency on the toxic lipofectamine reagent for administration of particles to mammalian cells. Investigations into RNA stability and integrity showed degradation from the drying-sonication process, possibly attributed to the protocol itself or the presence of multipliants due to overlong RNA. The use of shorter RNA constructs, like the HiBiT reporter gene, may be effective in minimizing RNA degradation and ensuring the formation of more uniform, single-capsid VLPs and EVLPs. Additionally, the freeze-thawing method can be explored as an alternative for EVLP formation, offering the advantage of avoiding sonication. These findings provide insight into the development of more robust EVLPs, proposing a novel and safer platform for RNA delivery to mammalian cells. This method has the potential to be applied to a wide range of RNA types, including microRNA, mRNA, and other RNA-based therapeutics. With further refinements to the EVLP formation process, EVLPs could offer a more effective and secure approach for targeted gene therapy in treating diseases such as cancer, genetic disorders, and other conditions requiring precise genetic interventions.

ACKNOWLEDGMENTS

I would like to thank William Gelbart, Ana Luisa Durán Meza, and David Moreno Gutiérrez for their continued support and mentorship throughout this project. I would also like to thank Charles Knobler, Ruben Cadena-Nava, and Jaime Ruíz-García

for helpful discussion and encouragement, and the Biomedical Research Minor, Department of Biological Chemistry, and financial support from the U.S. National Science Foundation (MCB 2103700). There are no conflicts of interest to report for this study.

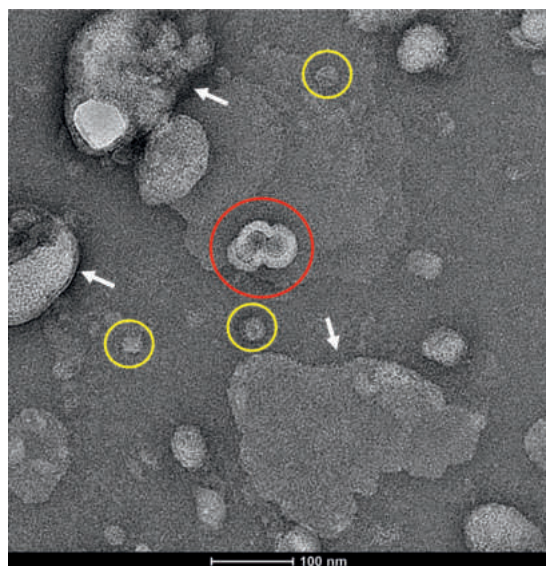


Figure 11: Electron microscopy image of Enveloped Virus-Like Particles (EVLPs) containing Nodamura replicon with HiBiT reporter gene (Nod-HiBiT) prepared by freeze-thawing method.

Image shows presence of limited EVLPs (red circle), around 50 nm in size. Multiple EVLPs are fused together. There are larger lipid aggregates present (white arrows), as well as naked Virus-Like Particles (VLPs) (yellow circles) that are around 28 nm in size. Scale bar: 100 nm.

REFERENCES

- C. F. Rochlitz, Gene therapy of cancer. *Swiss Med. Wkly.* **131**, 4–9 (2001). doi: 10.4414/smw.2001.09649
- M. Yu, E. Poeschla, F. Wong-Staal, Progress towards gene therapy for HIV infection. *Gene Ther.* **1**, 13–26 (1994).
- B. A. Bunnell, R. A. Morgan, Gene therapy for infectious diseases. *Clin. Microbiol. Rev.* **11**, 42–56 (1998). doi: 10.1128/CMR.11.1.42
- K. L. Dishart, L. M. Work, L. Denby, A. H. Baker, Gene therapy for cardiovascular disease. *J. Biomed. Biotechnol.* **2003**, 492073 (2003). doi: 10.1155/S1110724303209086
- D. B. Kohn, M. Sadelain, J. C. Glorioso, Occurrence of leukaemia following gene therapy of X-linked SCID. *Nat. Rev. Cancer.* **3**, 477–488 (2003). doi: 10.1038/nrc1122
- P. B. Hackett, D. A. Largaespada, K. C. Switzer, L. J. N. Cooper, Evaluating Risks of insertional mutagenesis by DNA transposons in gene therapy. *Transl. Res.* **161**, 265–283 (2013). doi: 10.1016/j.trsl.2012.12.005
- P. M. Rabinovich *et al.*, Synthetic messenger RNA as a tool for gene therapy. *Hum. Gene Ther.* **17**, 1027–1035 (2006). doi: 10.1089/hum.2006.17.1027
- M. B. Mowa, C. Crowther, A. Ely, P. Arbuthnot, Inhibition of hepatitis B virus replication by helper dependent adenoviral vectors expressing artificial anti-HBV pri-miRs from a liver-specific promoter. *Biomed. Res. Int.* **2014**, 718743 (2014). doi: 10.1155/2014/718743
- H. Zhang, J. Vandesompele, K. Braeckmans, S. C. D. Smedt, K. Remaut, Nucleic acid degradation as barrier to gene delivery: A guide to understand and overcome nuclease activity. *Chem. Soc. Rev.* **53**, 317–360 (2024). doi: 10.1039/d3cs00194f
- X. Gao, K.-S. Kim, D. Liu, Nonviral gene delivery: What we know and what is next. *AAPS J.* **9**, 9 (2007). doi: 10.1208/aapsj0901009
- A. Baldo, E. van den Akker, H. E. Bergmans, F. Lim, K. Pauwels, General considerations on the biosafety of virus-derived vectors used in gene therapy and vaccination. *Curr. Gene Ther.* **13**, 385–394 (2013). doi: 10.2174/15665232113136660005
- M. Comas-Garcia, R. D. Cadena-Nava, A. L. N. Rao, C. M. Knobler, W. M. Gelbart, *In vitro* quantification of the relative packaging efficiencies of single-stranded RNA molecules by viral capsid protein. *J. Virol.* **86**, 12271–12282 (2012). doi: 10.1128/JVI.01695-12
- J. B. Bancroft, E. Hiebert, C. E. Bracker, The effects of various polyanions on shell formation of some spherical viruses. *Virology* **39**, 924–930 (1969). doi: 10.1016/0042-6822(69)90029-4
- O. Azizgolshani, R. F. Garmann, R. Cadena-Nava, C. M. Knobler, W. M. Gelbart, Reconstituted plant viral capsids can release genes to mammalian cells. *Virology* **441**, 12–17 (2013). doi: 10.1016/j.virol.2013.03.001
- T. Wang, L. M. Larcher, L. Ma, R. N. Veedu, Systematic screening of commonly used commercial transfection reagents towards efficient transfection of single-stranded oligonucleotides. *Molecules* **23**, 2564 (2018). doi: 10.3390/molecules23102564
- M. V. Villagrana-Escareño *et al.*, VLPs derived from the CCMV plant virus can directly transfect and deliver heterologous genes for translation into mammalian cells. *Biomed. Res. Int.* **2019**, 4630891 (2019). doi: 10.1155/2019/4630891
- A. E. Smith, A. Helenius, How viruses enter animal cells. *Science* **304**, 237–242 (2004). doi: 10.1126/science.1094823
- S. Bhattacharyya *et al.*, Enveloped viruses disable innate immune responses in dendritic cells by direct activation of TAM receptors. *Cell Host Microbe.* **14**, 136–147 (2013). doi: 10.1016/j.chom.2013.07.005
- N. M. Gulati, A. S. Pitek, A. E. Czapar, P. L. Stewart, N. F. Steinmetz, The *in vivo* fates of plant viral nanoparticles camouflaged using self-proteins: Overcoming immune recognition. *J. Mater. Chem. B.* **6**, 2204–2216 (2018). doi: 10.1039/C7TB03106H
- J. R. Vega-Acosta, R. D. Cadena-Nava, W. M. Gelbart, C. M. Knobler, J. Ruiz-Garcia, Electrophoretic mobilities of a viral capsid, its capsid protein, and their relation to viral assembly. *J. Phys. Chem. B.* **118**, 1984–1989 (2014). doi: 10.1021/jp407379t
- S. Y. Kim, S. J. Lee, J. K. Kim, H. G. Choi, S. J. Lim, Optimization and physicochemical characterization of a cationic lipid-phosphatidylcholine mixed emulsion formulated as a highly efficient vehicle that facilitates adenoviral gene transfer. *Int. J. Nanomed.* **12**, 7323–7335 (2017). doi: 10.2147/IJN.S146785
- R. Saha, S. Verbanic, I. A. Chen, Lipid vesicles chaperone an encapsulated RNA aptamer. *Nat. Commun.* **9**, 2313 (2018). doi: 10.1038/s41467-018-04783-8
- L. Gitlin, T. Hagai, A. LaBarbera, M. Solovey, R. Andino, Rapid evolution of virus sequences in intrinsically disordered protein regions. *PLoS Pathog.* **10**, e1004529 (2014). doi: 10.1371/journal.ppat.1004529
- A. Biddlecome *et al.*, Delivery of self-amplifying RNA vaccines in *in vitro* reconstituted virus-like particles. *PLoS One* **14**, e0215031 (2019). doi: 10.1371/journal.pone.0215031
- S. Karan *et al.*, *In vivo* delivery of spherical and cylindrical *in vitro* reconstituted virus-like particles containing the same self-amplifying mRNA. *Mol. Pharm.* **21**, 2727–2739 (2024). doi: 10.1021/acs.molpharmaceut.3c01105
- R. D. Cadena-Nava *et al.*, Self-assembly of viral capsid protein and RNA molecules of different sizes: Requirement for a specific high protein/RNA mass ratio. *J. Virol.* **86**, 3318–3326 (2012). doi: 10.1128/JVI.06566-11
- A. P. Costa, X. Xu, D. J. Burgess, Freeze-anneal-thaw cycling of unilamellar liposomes: Effect on encapsulation efficiency. *Pharm. Res.* **31**, 97–103 (2014). doi: 10.1007/s11095-013-1135-z
- M. A. Sayem Karal, M. Masum Billah, M. Ahmed, M. Kabir Ahamed, A review on the measurement of the bending rigidity of lipid membranes. *Soft Matter* **19**, 8285–8304 (2023). doi: 10.1039/D3SM00882G
- K. L. Johnson, B. D. Price, L. A. Ball, Recovery of infectivity from cDNA clones of Nodamura virus and identification of small nonstructural proteins. *Virology* **305**, 436–451 (2003). doi: 10.1006/viro.2002.1769
- K. L. Johnson, B. D. Price, L. D. Eckerle, L. A. Ball, Nodamura virus nonstructural protein B2 can enhance viral RNA accumulation in both mammalian and insect cells. *J. Virol.* **78**, 6698–6704 (2004). doi: 10.1128/JVI.78.12.6698-6704.2004

Immunofluorescence of Mouse Fetal Ovary Reveals Timing of Meiotic Progression

Azra J. Cruz¹, Isaias Roberson¹, Amander T. Clark¹

¹Department of Molecular, Cell, and Developmental Biology, University of California, Los Angeles.

ABSTRACT

Infertility affects around 17.5% of the global population, and current existing clinical treatments fail to treat infertility at a germ cell level, leading to the importance of producing oocytes, or eggs, as a form of regenerative medicine. The reconstituted ovary (rOvary) is an *in vitro* mouse model capable of creating oocytes; however, the process remains inefficient as an assisted reproductive technology (ART) due to the inability for *in vitro* oocytes to reach the blastocyst stage after fertilization. To begin improving the rOvary, it is essential to closely understand the development of primordial germ cells (PGCs), the precursors to oocytes, *in vivo*. A timeline was created to closely examine the development of *in vivo* PGCs by studying the protein expression of key germ cell markers, including STELLA, a marker for PGCs, DAZL, a marker of meiotic competency, and SCP3, a marker of meiosis. This timeline highlights key developmental hallmarks for oogenesis, showcasing the dynamic expression of STELLA and SCP3. The timeline emphasizes three key developmental stages: at embryonic day 12.5 (E12.5), primordial germ cells (PGCs) express STELLA and DAZL and have gained the competence to enter meiosis; by embryonic day 15.5 (E15.5), most, if not all, PGCs are undergoing meiosis, as shown by the expression of SCP3 and DAZL; and by postnatal day 1 (P1), PGCs have transitioned into becoming oocytes. The timeline additionally emphasizes prophase I of meiosis as a paramount process to the formation of an oocyte, as seen by the long-lasting expression of SCP3 from E13.5 to P1. Studying the development of mouse ovarian germ cells is crucial to advancing *in vitro* oogenesis as an effective ART.

INTRODUCTION

Infertility is defined as the failure to conceive after 12 months or more despite unprotected sexual intercourse or insemination by a donor (1). It is estimated that 1 in 6 individuals are impacted by infertility worldwide due to complications within the reproductive system, which can result from varying causes, including age, genetic predisposition, lifestyle choices, or side effects from medical treatments (2, 3). *In vitro* fertilization (IVF), hormone therapy, and surrogacy exist as current options for infertility (3). However, these treatments do not resolve infertility that results from unfit or absent germ cells. Consequently, producing germ cells as a method of regenerative medicine is of significant interest to treat infertility (4).

In vitro oogenesis (IVO) offers a promising solution to infertility at a gametic level. IVO is a stem cell-based technology that attempts to recapitulate major developmental events that cells undergo *in vivo* to produce eggs, or oocytes, capable of fertilization utilizing a reconstituted ovary (rOvary), an *in vitro* mouse model (5, 6). This technology is inefficient in early embryonic development as about 20% of *in vitro* embryos reach the blastocyst stage compared to around 80% of *in vivo* embryos. In addition, IVO is inefficient in full-term development as there is about a 93% loss of *in vitro* embryos compared to about a 40% loss of *in vivo* embryos (5). Before the rOvary can be extended to humans as a form of regenerative medicine, it is critical to improve the efficiency of IVO in early embryonic and full-term development. To optimize the rOvary, it is crucial to closely understand the *in vivo* mouse ovarian and germ cell development.

In mice, germline development begins at embryonic day 6.25 (E6.25) with the specification of primordial germ cells (PGCs), the precursors to oocytes, which migrate through the developing hindgut around E7.5, where they express STELLA, also known as DPPA3 or PGC7, an essential marker for germ cell identity (7). Around E10.5, PGCs colonize the genital ridge (8) and begin to express DAZL, an RNA-binding protein required for gametogenesis and meiotic competency, sometime between E10.5 and E11.5 (9). PGCs proliferate for one to two days (10) before around E13.5, retinoic acid induces meiosis from anterior to posterior of the ovary as indicated by the expression of SCP3 (11, 12). Meiosis assists in the formation of oocytes and is the process of diploid cells becoming haploid (13). From E13.5 and forward, germ cells progress through prophase I of meiosis, which begins with the leptotene stage, where a programmed double-strand break occurs to initiate homologous recombination. The synaptonemal complex, a structure between homologous chromosomes, begins to form at this time. Next is the zygotene stage where the homologous chromosomes pair through synapsis and begin to condense. Next is the pachytene stage, the longest stage in prophase I, where the homologous chromosomes have finished synapsing, and the chromosomes continue to condense. Lastly is the diplotene stage, where the homologous chromosomes separate, and germ cell development arrests (13).

To better understand how to develop competent oocytes utilizing the rOvary, it is essential to analyze key developmental milestones that precede the formation of an oocyte. While maturation of the ovarian germline is well characterized, no resources have

carefully dictated key developmental time points that determine the formation of a healthy oocyte capable of fertilization and can undergo embryogenesis.

Here, a timeline was developed showcasing *in vivo* germline development utilizing STELLA, DAZL, and SCP3 to create a resource highlighting key developmental hallmarks important for the formation of an oocyte. Using a time-mated breeding strategy, we collected ovaries from E12.5 mice through postnatal day 1 (P1) pups. Utilizing immunostaining, PGCs were studied as they developed into oocytes via STELLA, DAZL, and SCP3 expression. Observing mouse ovarian germ cells as they develop is crucial as it can provide insight into the changing identity of germ cells and, ultimately, help improve IVO as an assisted reproductive technology.

METHODS

Mouse Embryo Tissue

Embryo tissues were retrieved from pregnant CD1 mice (Charles River, strain code: 022) at E12.5, E13.5, E14.5, E15.5, E18.5, and postnatal day 1 (P1) with IACUC approval (ARC 2008-070).

Paraffin Processing and Immunofluorescence (IF) of Tissue

Embryo tissue samples were fixed with 4% paraformaldehyde (Sigma-Aldrich, catalog no. 252549) for 24 hours. Samples were washed twice with phosphate-buffered saline (PBS; 1x; Fisher Bioreagents, catalog no. BP3994) at room temperature for 5 minutes before being processed in paraffin (Leica Biosystems, catalog no. 39603002). To prepare tissue samples for IF staining, 5µm slides were deparaffinized and rehydrated with PBS (1x). For antigen retrieval, samples were submerged in sodium citrate (Sigma-Aldrich, catalog no. S1804) at 95°C for 40 minutes. Samples were left to cool for 20 minutes at room temperature and were then washed with PBS (1x) for 5 minutes. Samples were washed with PBST (PBS and 0.2% Tween; MP Biomedicals, catalog no. TWEEN201). Samples were placed in a permeabilization buffer (PBS and 0.5% Triton X-100; MP Biomedicals, catalog no. 194854) for 20 minutes and then washed with PBST three times for 5 minutes. Blocking was done at room temperature with 10% normal donkey serum (NDS; Jackson ImmunoResearch, catalog no. 017-000-121) in PBST for 30 minutes. Primary antibodies, goat polyclonal anti-STELLA (R&D Systems, catalog no. AF2566), rabbit monoclonal anti-DAZL (Abcam, catalog no. ab215718), and mouse monoclonal anti-SCP3 (Abcam, catalog no. ab97672), were diluted, 1:200, 1:200, and 1:1000, respectively, in a 2.5% NDS in PBST solution and left on slides to incubate overnight at 4°C. The following day, samples were washed with PBST three times for 5 minutes. Secondary antibody fluorophores, AF594-conjugated donkey anti-goat (Jackson ImmunoResearch, catalog no. 705-586-147), AF488-conjugated donkey anti-rabbit (Jackson ImmunoResearch, catalog no. 711-545-152), and AF647-conjugated donkey anti-mouse (Jackson ImmunoResearch, catalog no. 715-605-151), were incubated for 2 hours at room temperature. Following incubation, samples were washed twice with PBST for 5 minutes each, first with 4',6-diamidino-2-phenylindole (DAPI) (Fisher Scientific, catalog no. D1306), then with PBST. A ProLong Gold antifade mountant (Invitrogen, catalog no. P36934) was added to the samples to mount them before a coverslip was applied (Eprelia, catalog no. 152460). Coverslips were sealed on the slides with nail polish (Sally Hansen, catalog no. 30070018001) and left to cure overnight at room temperature.

Confocal Microscopy

Images of tissue sample slides were taken using a confocal laser scanning microscope, LSM880 (Carl Zeiss), using a Plan-Apochromat 40x/1.3 NA water immersion objective. Confocal images were processed using Fiji ImageJ software to merge channels, add scale bars, and create representative images of the germ cells (15).

Germ Cell Quantification

Imaris 9.2.1 (Bitplane) software was used along with the Spots Property included in the software to quantify the germ cells. The Spots Property was used to count germ cells and manually track counts. Germ cell types were determined and categorized into two populations based on protein expression: STELLA+DAZL+ or SCP3+DAZL+. The average protein expression of each germ cell population and the overall germ cell population was determined from the manual counts taken from Imaris. A Welch's t-test was performed at E12.5, E13.5, E14.5, and E15.5 to determine the significance between the two germ cell populations.

RESULTS

PGCs Enter Meiosis at E13.5

PGC immunofluorescent staining at E12.5 displays that germ cells express STELLA protein, shown in magenta, and DAZL protein, shown in cyan; however, there is no expression of SCP3 protein (Figure 1A). At E12.5, 95.79% of germ cells are STELLA+DAZL+, and 0% are SCP3+DAZL+ (Figure 1B). At E13.5, PGC immunofluorescent staining shows that germ cells express either STELLA and DAZL or SCP3 and DAZL. SCP3 protein, shown in yellow, is expressed as a bright puncta in the germ cells. At this timepoint, the expression of STELLA begins to downregulate, and the expression of SCP3 begins to upregulate (Figure 1C). A significantly higher percentage of PGCs expressed SCP3 and DAZL (62.04%) compared to STELLA and DAZL (37.40%) (Figure 1D).

A High Number of PGCs Are in Meiosis by E15.5

At E14.5, STELLA continues to downregulate while SCP3 continues to upregulate. PGC immunofluorescence staining shows that germ cells express SCP3 and DAZL. SCP3 expression remains punctate, with some chromosomes beginning to condense (Figure 2A). At E14.5, 6.37% are STELLA+DAZL+, and 93.31% are SCP3+DAZL+ (Figure 2B). PGC immunofluorescent staining at E15.5 shows that germ cells start to gain a more uniform identity where they express SCP3 and DAZL. SCP3 expression remains punctate. However, some germ cells have complete chromosome condensation (Figure 2C). At E15.5, 98.76% of germ cells are SCP3+DAZL+, and 0% are STELLA+DAZL+ (Figure 2D).

PGCs Transition to Become Oocytes at P1

At E18.5, PGC immunofluorescent staining shows that germ cells are SCP3+DAZL+ (Figure 3A). At this timepoint, 100% of germ cells are SCP3+DAZL+, and 0% are STELLA+DAZL+ (Figure 3B). At P1, STELLA expression begins to upregulate, and DAZL expression begins to downregulate. Germ cells that do not express STELLA have chromosome condensation of SCP3, and oocytes that express STELLA have bright puncta of SCP3 (Figure 3C).

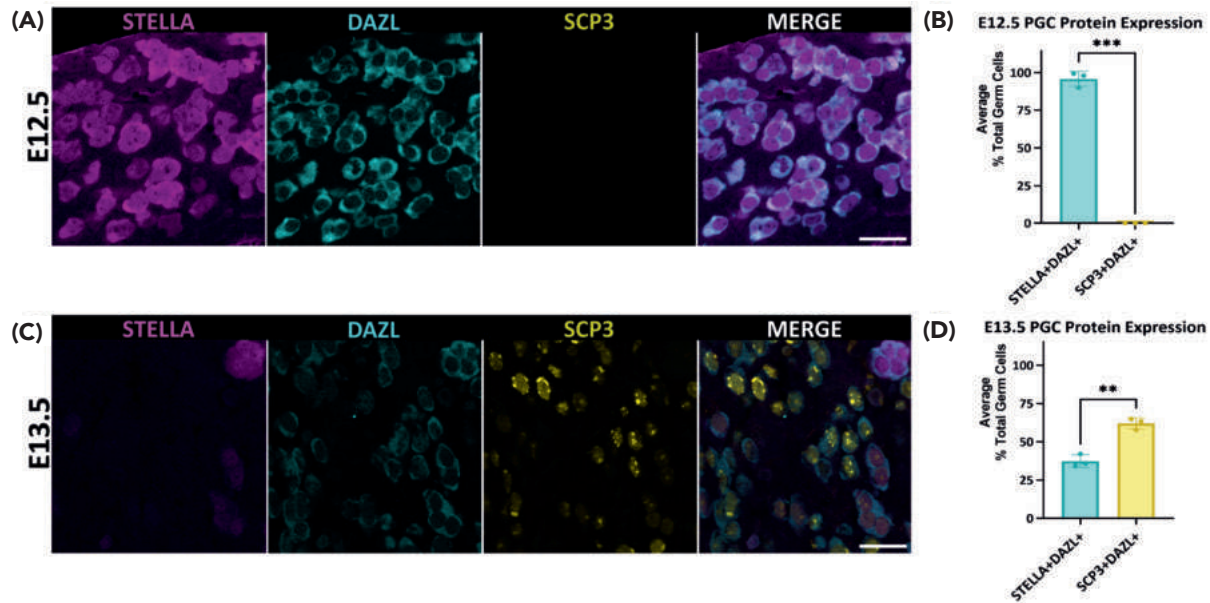


Figure 1: Primordial germ cells are pre-meiotic at E12.5 and enter meiosis at E13.5.

(A) Representative immunofluorescence (IF) image of CD1 mouse germ cells at E12.5. Scale bar = 20µm. (B) Bar graphs display the average percentage of germ cells expressing STELLA and DAZL, 95.79%, or SCP3 and DAZL, 0%, at E12.5. A Welch's t-test was conducted to determine significance: p-value = 0.0009 and SEM = 2.908. n = 3 biological replicates. (C) Representative IF image of CD1 mouse germ cells at E13.5. Scale bar = 20µm. (D) Bar graphs display the average percentage of germ cells expressing STELLA and DAZL, 37.40%, or SCP3 and DAZL, 62.04%, at E13.5. A Welch's t-test was conducted to determine significance: p-value = 0.0017 and SEM = 3.218. n = 3 biological replicates.

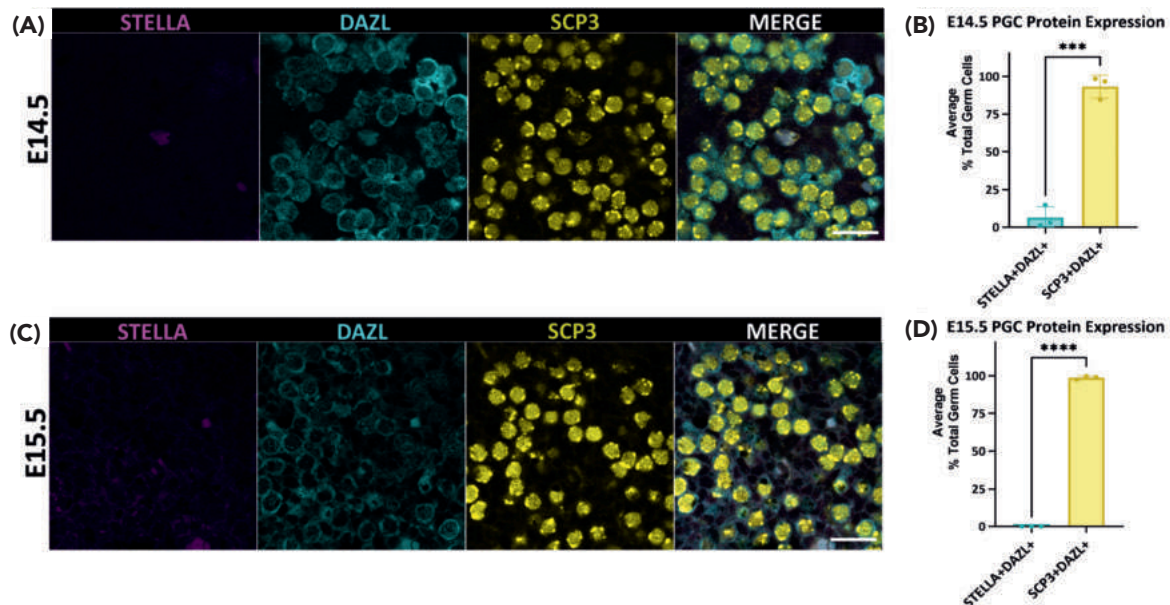


Figure 2: Primordial germ cells continue to undergo meiosis at E14.5 and E15.5.

(A) Representative immunofluorescence (IF) image of CD1 mouse germ cells at E14.5. Scale bar = 20µm. (B) Bar graphs display the average percentage of germ cells expressing STELLA and DAZL, 6.37%, or SCP3 and DAZL, 93.31%, at E14.5. A Welch's t-test was conducted to determine significance: p-value = 0.0001 and SEM = 6.078. n = 3 biological replicates. (C) Representative IF image of CD1 mouse germ cells at E15.5. Scale bar = 20µm. (D) Bar graphs display the average percentage of germ cells expressing STELLA and DAZL, 0%, or SCP3 and DAZL, 98.76%, at E15.5. A Welch's t-test was conducted to determine significance: p-value ≤ 0.0001 and SEM = 0.7070. n = 3 biological replicates.

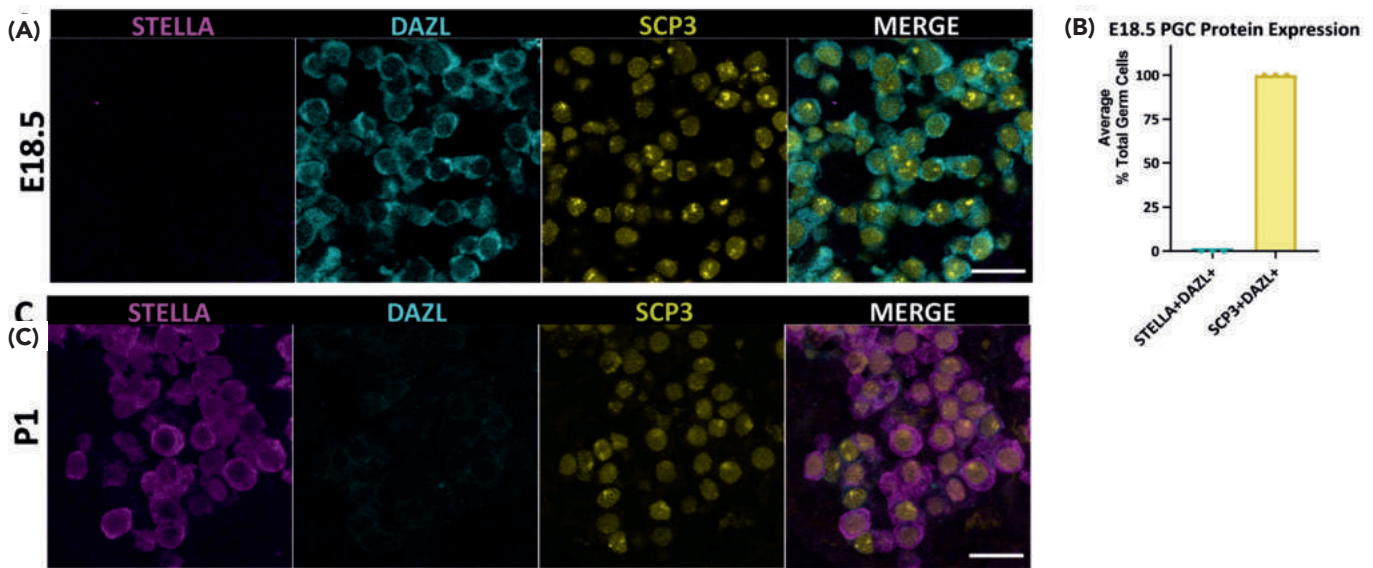


Figure 3: Primordial germ cells at E18.5 transition into becoming oocytes at P1.

(A) Representative immunofluorescence (IF) image of CD1 mouse germ cells at embryonic day 18.5 (E18.5). Scale bar = 20 μ m. (B) Bar graphs showing the average percentage of germ cells expressing STELLA and DAZL, or SCP3 and DAZL, at E18.5. n = 3 biological replicates. (C) Representative IF image of CD1 mouse germ cells and oocytes at P1. Scale bar = 20 μ m.

DISCUSSION

The rOvary is a potential solution to infertility that is being developed and modeled in mice; however, it remains inefficient due to the high occurrence of embryo loss in early and full-term development (5). Therefore, it is important to improve IVO before it can be used to help infertility in humans. Here, we created a resource that closely examines the protein expressions of STELLA, DAZL, and SCP3 from E12.5 to P1 to highlight key developmental hallmarks essential for the formation of a competent oocyte. This timeline indicates three critical timepoints important for oogenesis.

The first timepoint is E12.5, when germ cells are sexually differentiated based on the fetal gonad and somatic niche they enter, and all germ cells are localized within the ovaries (8, 9). At this time point, germ cells express STELLA and DAZL but do not express SCP3, meaning they are competent for meiosis; however, they are not currently undergoing meiosis (Figure 1A). DAZL is a key protein expressed in both mouse ovarian and testicular germ cells and expressed when a germ cell is competent for meiosis. It is then the concentration of retinoic acid present in the gonad that guides PGCs down either spermatogenesis or oogenesis. A high concentration of retinoic acid guides germ cells down the oogenesis pathway, leading PGCs to progress through meiotic prophase I with the localization of SCP3 (11, 12). If an ovarian mouse PGC does not express DAZL, PGCs cannot undergo meiosis. At E13.5, germ cells have finished proliferating and are entering prophase I of meiosis, as shown by the expression of SCP3 (12). Meiosis begins at the leptotene stage when chromosomes have not yet condensed and is characterized by bright puncta of SCP3 at E13.5 (Figures 1C, 4).

At E14.5, germ cells progress through meiosis and enter the zygotene stage of prophase I of meiosis, characterized by a mixture of bright puncta and chromosome condensation of SCP3 (Figure 4). The second critical time point is E15.5, when 98.76% of germ cells undergo meiosis and enter the pachytene stage of prophase

I of meiosis, characterized by chromosome condensation of SCP3 (Figure 2C). This stage highlights the importance of prophase I of meiosis for oogenesis (13, 14).

At E18.5, germ cells continue to progress through the pachytene stage of prophase I of meiosis. At this time point, germ cells are preparing to enter the final stage of prophase I, diplotene, and become arrested. The last critical time point is P1, when germ cells begin to resolve their pachytene stage to arrest at the diplotene stage and transition into becoming oocytes (16). As germ cells transition to oocytes, STELLA protein upregulates, and the expression of SCP3 changes from chromosome condensation to bright puncta.

The immunofluorescent timeline created for this study emphasizes prophase I of meiosis as an indispensable process of oogenesis, as it takes about 7 to 8 days to prepare chromosomes for segregation and prepare PGCs for their transition into becoming oocytes. Throughout prophase I of meiosis, programmed strand breaks must occur to commence homologous recombination; however, it must be done in a way that is free of error to prevent chromosomal abnormalities. In addition, the synaptonemal complex and cohesion elements must form and be maintained to ensure sister chromatids are connected to guarantee proper synapsis (16). If prophase I of meiosis goes awry, then chromosomal abnormalities are likely to occur, leading to genetic syndromes or aneuploidy, which can affect successful reproduction (17). Many factors cause infertility, including how the ovarian reserve begins to diminish and the quality of oocytes falters as women approach their late thirties (18). Therefore, infertility also becomes more prevalent in older women, likely due to the loss of cohesion, which affects the successful progression of prophase I of meiosis (17). Understanding the proper progression of meiosis prophase I allows for future research to prevent incorrect meiosis progression Figure 4 and counter infertility.

One limitation of this study is that only three proteins were utilized to investigate the development of germ cells when other

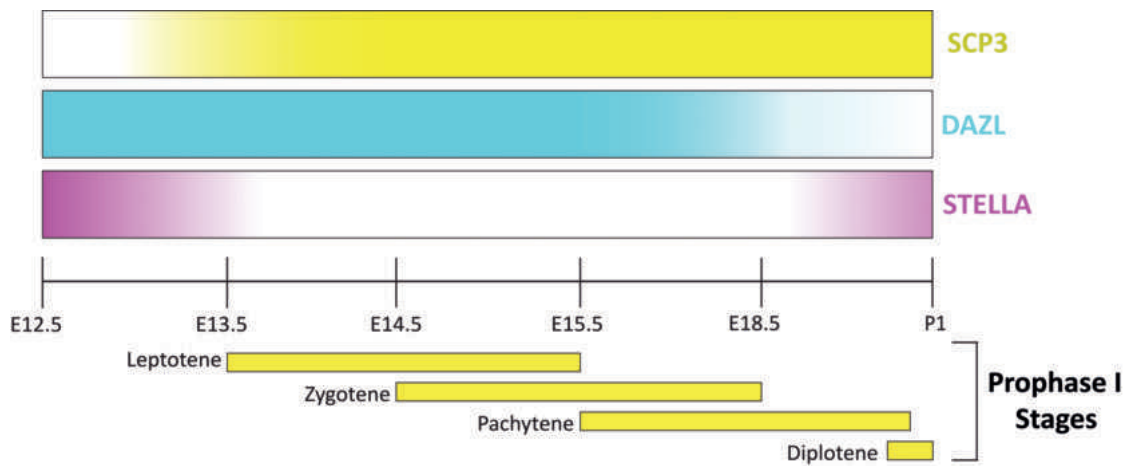


Figure 4: Protein expression summary of SCP3, DAZL, and STELLA from E12.5 to P1.

SCP3 protein expression is upregulated around E13.5. DAZL protein expression is upregulated at E12.5 and downregulated around P1. STELLA protein expression is downregulated around E13.5, then upregulated between E18.5 and P1. The leptotene stage of prophase I is between E13.5 and E15.5. The zygotene stage is between E14.5 and E18.5. The pachytene stage is between E15.5 and P1. The diplotene stage is at P1.

proteins are critical to the process, especially during meiosis like RAD51, which indicates the number of unrepaired DNA breaks, or SCP1, which recruits other elements to finish synaptonemal complex assembly (16). Future directions include using other germ cell marker combinations for immunofluorescence to further characterize germ cell identity and development. Despite these limitations, observing the protein expression of STELLA, DAZL, and SCP3 via immunofluorescent staining reveals the complex and changing identity of mouse PGCs as they arrive at the genital ridge and develop within the ovary into oocytes (Figure 4). This resource provides a timeline to understand how PGCs develop and underlines critical developmental hallmarks of oogenesis that should be considered when generating stem cell-derived germ cells in the rOvary to improve IVO as a reproductive technology, especially the progression of prophase I of meiosis.

ACKNOWLEDGMENTS

A.T.C. supervised the project. A.J.C. performed the experiments. A.J.C. wrote the manuscript with the input of I.R. There is no conflict of interest. The author would like to thank the Microscopy Core at the UCLA Eli and Edythe Broad Center of Regenerative Medicine and Stem Cell Research for confocal microscopy. The author would also like to thank the UCLA Creating Opportunities through Mentorship and Partnership Across Stem Cell Science (COMPASS) Program for funding and support. A.T.C. is supported by grants from the NIH (R01HD058047), which funded the work.

REFERENCES

1. M. V. Borgh, C. Wyns, Fertility and infertility: Definition and epidemiology. *Clin. Biochem.* **62**, 2–10 (2018). doi: 10.1016/j.clinbiochem.2018.03.012
2. E. L. Kelley, S. A. Kingsberg, Sexuality and infertility. *Obstet. Gynecol. Clin. North. Am.* **51**, 311–322 (2024). doi: 10.1016/j.ogc.2024.02.005
3. S. A. Carson, A. N. Kallen, Diagnosis and management of infertility. *JAMA.* **326**, 65–76 (2021). doi: 10.1001/jama.2021.4788
4. A. Le Goff *et al.*, Anticipating *in vitro* gametogenesis: Hopes and concerns for IVG among diverse stakeholders. *Stem Cell Rep.* **19**, 933–945 (2024). doi: 10.1016/j.stemcr.2024.05.002
5. O. Hikabe *et al.*, Reconstitution *in vitro* of the entire cycle of the mouse female germ line. *Nature* **539**, 299–303 (2016). doi:10.1038/nature20104
6. E. Sosa *et al.*, Reconstituted ovaries self-assemble without an ovarian surface epithelium. *Stem Cell Rep.* **18**, 2190–2202 (2023). doi: 10.1016/j.stemcr.2023.10.001
7. B. Payer *et al.*, STELLA is a maternal effect gene required for normal early development in mice. *Curr. Biol.* **13**, 2110–2117 (2003). doi: 10.1016/j.cub.2003.11.026
8. M. Saitou, M. Yamaji, Primordial germ cells in mice. *Cold Spring Harb. Perspect. Biol.* **4**, (2012). doi: 10.1101/cshperspect.a008375
9. M. E. Gill, Y.-C. Hu, Y. Lin, D. C. Page, Licensing of gametogenesis, dependent on RNA binding protein DAZL, as a gateway to sexual differentiation of fetal germ cells. *Proc. Natl. Acad. Sci. U.S.A.* **108**, 7443–7448 (2011). doi: 10.1073/pnas.1104501108
10. P. J. Donovan, D. Stott, L. A. Cairns, J. Heasman, C. C. Wylie, Migratory and post migratory mouse primordial germ cells behave differently in culture. *Cell* **44**, 831–838 (1986). doi: 10.1016/0092-8674(86)90005-X
11. J. Bowles *et al.*, Sex-specific regulation of retinoic acid levels in developing mouse gonads determines germ cell fate. *Science* **312**, 596–600 (2006). doi: 10.1126/science.1125691
12. Y. Lin, M. E. Gill, J. Koubova, D. C. Page, Germ cell-intrinsic and -extrinsic factors govern meiotic initiation in mouse embryos. *Science* **322**, 1685–1687 (2008). doi: 10.1126/science.1166340
13. R. Reichman, B. Alleva, S. Smolikove, Prophase I: Preparing chromosomes for segregation in the developing oocyte. Signaling-Mediated Control of Cell Division. *Results Probl. Cell Differ.* **59**, 125–173 (2017). doi: 10.1007/978-3-319-44820-6_5
14. D. M. Burks *et al.*, Molecular analysis of the effects of steroid hormones on mouse meiotic prophase I progression. *Reprod. Biol. Endocrinol.* **17**, 105 (2019). doi: 10.1186/s12958-019-0548-x
15. J. Schindelin *et al.*, Fiji: An open-source platform for biological-image analysis. *Nat. Methods* **9**, 676–682 (2012). doi: 10.1038/nmeth.2019
16. X. Wang, M. E. Pepling, Regulation of meiotic prophase one in mammalian oocytes. *Front. Cell Dev. Biol.* **9** (2021). doi: 10.3389/fcell.2021.667306
17. K. T. Jones, Meiosis in oocytes: Predisposition to aneuploidy and its increased incidence with age. *Hum. Reprod. Update* **14**, 143–158 (2008). doi: 10.1093/humupd/dmm043
18. M. J. Faddy, R. G. Gosden, A. Gougeon, S. J. Richardson, J. F. Nelson, Accelerated disappearance of ovarian follicles in mid-life: Implications for forecasting menopause. *Hum. Reprod.* **7**, 1342–1346 (1992). doi: 10.1093/oxfordjournals.humrep.a137570

Differential Effects of Iron Chelation on Ferroptosis and Neuroprotection

Caterina Stoica¹, Rajiv Ratan²

¹Department of Psychology, University of California, Los Angeles. ²Brain and Mind Institute, Burke Neurological Institute, Weill Cornell Medicine.

ABSTRACT

The rising global prevalence of neurodegenerative diseases presents a significant challenge to public health, characterized by neuronal damage frequently caused by iron dyshomeostasis and ferroptosis, a form of oxidative-stress-induced cell death. Iron chelators have shown promise in preventing ferroptosis in preclinical and clinical studies, offering a potential treatment for neurodegenerative conditions involving excess iron. This study investigates the mechanisms behind the neuroprotective effects of iron chelators, focusing on their engagement in hypoxia stress response pathways and ferroptosis inhibition. In this study, the effectiveness of iron-chelating drugs in preventing ferroptosis in HT22 cells was explored using an *in vitro* model. Four iron chelators—dipyridyl (DP), 1,10-phenanthroline (PHT), deferoxamine (DFO), and deferiprone (DFP)—were chosen based on their unique molecular characteristics, such as iron selectivity and membrane permeability. Cell viability was measured using live/dead and MTT assays in the presence of erastin, a ferroptosis inducer. The study's results showed that the Fe²⁺ chelators, DP and PHT, provided neuroprotection at moderate concentrations (50–100 μ M), as confirmed by significant increases in cell viability ($p = 3.8 \times 10^{-5}$ for DP; $p = 1.27 \times 10^{-6}$ for PHT) and reduced ferroptotic cell death. However, at higher concentrations (>100 μ M for DP and >50 μ M for PHT), both chelators became cytotoxic, leading to decreased cell viability. Among the Fe³⁺ chelators, DFO exhibited moderate neuroprotection at 50–100 μ M ($p = 0.011$) but was toxic at 200 μ M, as indicated by increased cell death. In contrast, DFP provided little to no protection and showed significant toxicity at all tested concentrations ($p = 0.0014$). DFO, which targeted extracellular iron, specifically demonstrated more neuroprotective effects, suggesting that early-stage iron modulation may be more effective in treating neurodegenerative diseases. DFO is also known to inhibit oxygen-sensing enzymes called hypoxia-inducible factor-prolyl hydroxylase domain-containing proteins (HIF-PHDs), leading to the expression of HIF-1, a transcription factor involved in the hypoxia stress response that prevents cell death. Future research should further explore HIF-1 inhibitors, as these enzymes may have clinical applications in treating neurodegenerative conditions. More research in these areas is required to understand the role of iron chelators in the process of ferroptosis before they can be promoted as a widespread therapeutic approach to treating neurodegenerative diseases.

INTRODUCTION

Neurodegenerative diseases, including Parkinson's Disease, Alzheimer's Disease, and stroke, affect up to one billion people worldwide (1). These conditions are frequently linked to neuronal damage caused by an imbalance of iron, also known as iron dyshomeostasis. This dyshomeostasis can lead to ferroptosis, a form of cell death driven by oxidative stress. With an increase in studies that investigate taking preventative measures earlier rather than repairing neurological damage at a later stage of the disease, iron chelators have become more prevalent in treating neurodegenerative diseases involving the excess of iron. Previous studies have indicated the drawbacks of iron chelation therapy in neurodegenerative conditions. For example, one study demonstrates how the progression of Parkinson's disease significantly worsened with the treatment of an iron chelator and led to severe adverse effects in some participants (2). Although the promise of iron-chelating drugs and iron chelation therapy has been observed in preclinical and clinical studies, there is a growing need to discover non-toxic treatment measures for neurological disease (3).

Iron Chelators and Hypoxia Stress Response in Neurons

By investigating iron chelators as a potential therapeutic approach to treating neurological diseases, previous studies have observed a link between iron in deleterious redox reactions and the pathogenesis of such diseases. While iron is essential for numerous cellular functions, it can also catalyze harmful processes. Iron can convert certain substances, such as superoxide (O_2^-) and hydrogen peroxide (H_2O_2), into highly reactive free radicals through a sequence of reactions, causing oxidative stress. However, iron chelators can diminish the formation of these damaging radicals and reduce oxidative stress. Furthermore, iron chelators impact oxygen-sensing mechanisms by inhibiting hypoxia-inducible factor prolyl hydroxylases (HIF-PHDs) (3). This inhibition results in the increased expression of hypoxia-inducible factor 1 (HIF-1), a crucial transcription factor for oxygen homeostasis that activates a cellular response to hypoxic stress and prevents oxidative stress-induced cell death (4).

Role of Iron in Ferroptosis

The link between iron dyshomeostasis and ferroptosis is especially relevant in the context of neurodegenerative disease. Iron

accumulation within cells promotes the oxidation of membrane lipids, generating harmful lipid peroxides that impair cellular functions and reduce cell viability (5). In addition to iron accumulation, ferroptosis can also be triggered by the depletion of glutathione via the cystine/glutamate (Xc) transporter, a crucial regulator of oxidative stress. The Xc-transporter facilitates the uptake of cystine, which is converted intracellularly to cysteine, a precursor for glutathione synthesis. Glutathione, a powerful antioxidant, it plays a direct role in preventing lipid peroxidation by neutralizing reactive oxygen species (ROS). Inhibition or dysfunction of the Xc-transporter can result in various ways, including due to excess iron, oxidative stress, or cellular signaling disruptions. When the Xc-transporter is blocked, cystine uptake is reduced, leading to a depletion of cysteine and subsequently glutathione. This depletion creates an imbalance between ROS and antioxidants, allowing lipid peroxidation to occur unchecked, leading to cell membrane damage and eventual cell death. Since ferroptosis is a major factor in neurodegeneration, treatments that adjust iron levels and reduce oxidative stress, like iron chelators, could help protect neurons and slow down such disease progression.

The potential of iron chelators in treating neurodegenerative conditions is an area of growing interest. Given the strong association between iron accumulation and the progression of diseases such as Parkinson's, Alzheimer's, and stroke (2), understanding how iron chelation can modulate neurodegenerative processes is crucial. Research on iron metabolism in the central nervous system has highlighted the dual effects of iron, emphasizing the need for precise regulation to prevent ferroptosis without disrupting essential cellular functions (7). By further investigating the effects of iron chelators on neuronal health, this study contributes valuable insights into developing targeted therapeutic strategies that could mitigate iron-driven neurodegeneration while minimizing unintended consequences. There is a need for a better understanding of the mechanisms of iron chelators and how they impact the process of ferroptosis before drugs incorporating them can be effectively used to treat neurological conditions.

Molecular Properties and Function of Iron Chelators: Overview of Hypotheses

There is a significant lack of data on how iron chelation at different stages impacts the progression of ferroptosis. Little is known about the significance of the various ionic forms of iron during the pathway, which is critical in understanding how to inhibit ferroptosis. To better examine the mechanisms by which iron chelators might prevent neuronal injury by binding iron, this research aims to observe the effects of four iron-chelating drugs on ferroptosis in HT22 cells using an *in vitro* model. HT22 cells are an immortalized cell line derived from mouse hippocampal neurons and lack functional ionotropic glutamate receptors (iGluRs), which are proteins that allow glutamate to be properly taken up and used for signaling (8). In HT22 cells, excess glutamate builds up outside the cells and can lead to oxidative stress by interfering with the cell's ability to manage harmful reactive oxygen species. HT22 cells are commonly used in laboratory settings to study oxidative stress. In this study, ferroptosis will be triggered through the drug erastin, which blocks cysteine uptake and depletes glutathione, increasing reactive oxygen species.

The chelators were selected based on their varying molecular characteristics, such as iron selectivity, membrane permeability, and intracellular modifications. Four iron-chelating drugs were tested on

HT22 cells. Dipyridyl (DP) and 1,10-phenanthroline (PHT) are both Fe^{2+} chelators and membrane permeable. They bind to intracellular Fe^{2+} , decreasing iron-dependent lipid peroxidation and inhibiting ferroptosis. Deferoxamine (DFO) is an Fe^{3+} chelator and membrane impermeable due to the large size of its molecules, preventing intracellular uptake of extracellular iron. Deferiprone (DFP) is also an Fe^{3+} chelator and acts similarly to DFO, but its molecules are membrane-permeable.

We hypothesize that chelators that bind to Fe^{3+} , both those with membrane-permeable and impermeable molecular structure, would prevent the intracellular uptake of extracellular iron. On the other hand, chelators that bind to Fe^{2+} , referring strictly to the drugs with membrane-permeable molecules, should be able to chelate iron successfully and inhibit ferroptosis, since the Fe^{2+} form of iron only exists inside the cell once it has been converted from Fe^{3+} . Therefore, it is proposed that the chelating drugs that bound to iron most effectively to decrease iron-dependent lipid peroxidation during ferroptosis would be the most ideal in treating neurological conditions involving deleterious effects caused by excess iron.

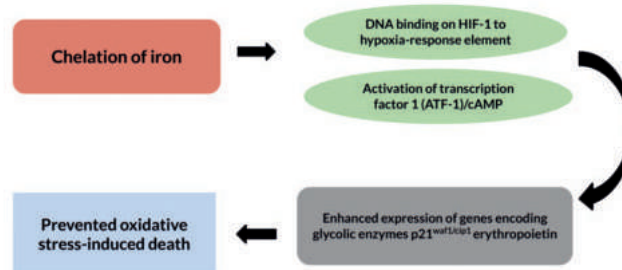


Figure 1: The chelation of iron has been shown to enhance the expression of genes activating a hypoxia stress response pathway, preventing oxidative stress-induced death in neurons.

Iron chelation inhibits hypoxia-inducible factor prolyl hydroxylases (HIF-PHDs), leading to the stabilization and increased expression of hypoxia-inducible factor 1, or HIF-1. HIF-1 is a crucial transcription factor that regulates gene expression in response to low oxygen (or hypoxia). Once stabilized, HIF-1 translocates to the nucleus, where it binds to specific DNA sequences called hypoxia-response elements (HREs), activating genes that encode glycolytic enzymes, p21, and erythropoietin. These genes play protective roles against oxidative stress as p21 induces cell cycle arrest, allowing cells to repair damage, and erythropoietin helps mitigate the effects of oxidative stress.

MATERIALS AND METHODS

HT22 Cell Culturing

The HT22 cells hippocampal cell line was cultured *in vitro* in media containing Dulbecco's modified Eagle's medium (DMEM), fetal bovine serum (FBS), and penicillin/streptomycin (PEN-STREP), which are all sourced from Gibco, Thermo Fisher Scientific. The cells were split upon reaching 80% confluency to prevent over-confluency and cell death. HT22 cells have a doubling time of 15 hours. For experimental treatments, cells were seeded at 7.5×10^5 cells/well in 96-well plates and treated at >50% confluence to best observe results. Cell counting was performed using a Fein Optic RB40 light microscope and bromothymol blue staining from Sigma-Aldrich to ensure accurate cell density measurements.

Erastin Treatment and Lethal Dose 50% (LD50) Determination

Erastin, obtained from MedChemExpress, was used to induce ferroptosis. To ensure consistency, the LD50 of erastin was re-evaluated prior to each experiment with a kill curve in a 96-well plate from CELLTREAT. After erastin had induced ferroptotic cell death through lipid peroxidation (18 hours), MTT (3-(4,5-Dimethylthiazol-2-yl)-2,5-Diphenyltetrazolium Bromide) cell viability assays were performed to assess cell survival and determine the LD50. The MTT kit was sourced from Sigma-Aldrich.

Iron Chelating Treatments

Four iron-chelating drugs were tested on HT22 cells: dipyrldyl (DP), 1,10-phenanthroline (PHT), and deferiprone (DFP), sourced from Sigma-Aldrich, and deferoxamine (DFO) from SelleckChem. Solutions were created with erastin, holding its concentration constant at its LD50, and varying concentrations of each iron chelator including 0, 25, 50, 75, 100, and 200 μM . 12-well sterile basins from CELLTREAT were used to prepare the various concentrations of each iron chelator. HT22 cells that were >50% confluent were treated with increasing doses of a 10 mM stock of the Fe^{2+} -chelating drugs DP and PHT as well as a 10 μM lethal dose of erastin. Other HT22 cells were treated with increasing doses of 10 mM stocks of DFO and DFP, both of which are Fe^{3+} chelators. The treatments with the iron chelator and erastin were conducted 24 hours after plating the cells.

Cells with no treatment were used as negative controls throughout the experimentation. Positive controls were treated with erastin at its LD50, along with N-acetyl cysteine (NAC) from Sigma-Aldrich, which replenishes cellular cysteine to counteract ferroptosis. 200 μM NAC was used, which is the optimal protective dose identified in prior research (4). Each iron chelator was also tested alone at increasing concentrations to test for any cytotoxic effects.

Viability Assays

Live/dead imaging was conducted using a RB40-fluorescence microscope from Fein Optic to qualitatively observe cell viability after exposure to the iron-chelators. Green-fluorescent calcein-AM (1 μM) and red-fluorescent ethidium homodimer (2 μM) from Sigma-Aldrich were added to each well and cells were imaged at 10x magnification. The cells fluoresced either red or green based on membrane integrity and metabolic activity. Red fluorescence indicated dead cells and green fluorescence indicated metabolically active cells. The MTT assay was conducted on the plates 18 hours post-treatment to ensure the effects of the erastin and iron chelator would be observed. This assay is a quantitative measure of cell viability. 0.2 mg/mL of MTT, a water-soluble, cell-permeable yellow tetrazolium salt, was added directly to cells in culture and incubated for four hours. During this time, it was reduced by a mitochondrial enzyme complex to its insoluble form, purple formazan. Dimethyl sulfoxide (DMSO), sourced from Sigma-Aldrich, was used to dissolve the formazan crystals formed by the reduction of MTT by living cells. A plate-reading spectrophotometer from Thermo Fisher was used to measure the quantity of formazan after being dissolved by DMSO, which is directly proportional to the number of viable cells. The spectrophotometer measured absorbance at 570 nm to quantify the amount of formazan produced by viable cells. A reference wavelength of 690 nm was used to account for any differences in solution color or background color in each well.

Data Processing and Image Analysis

Live/dead images were processed and merged using the software Fiji (14). MTT assay data was uploaded into the software GraphPad Prism 10, which was used for graphing and preliminary statistical analysis. Spectrophotometric data was normalized to 100% and sorted into the respective columns for the concentrations of erastin and the iron chelator used. Graphs were then generated, and statistical analysis was conducted.

From the MTT assay data, the means and standard deviation were calculated for each column with varying concentrations of iron chelator. Error bars were created through standard error of the mean (SEM) and plotted on graphs. In the MTT assay, color formation served as a useful and convenient marker of the viable cells, but since cell viability is equated with mitochondrial activity in the MTT, it can overvalue the quantity of living cells compared to other cell-viability assays because full mitochondrial remains may be present in the solution after cells lyse and are no longer living. The interpretation of MTT assay results must consider such factors and qualitative assays should be referenced for a more comprehensive assessment of cell viability. Thus, certain statistical analysis was conducted after a side-by-side comparison to live/dead imaging. Two-tailed t-tests were performed on the MTT data for the conditions where wells treated with an iron chelator and erastin showed significant improvement in survival compared to the negative control (or cells treated with no iron chelator and 10 μM of erastin) in the live/dead images. In addition to the live/dead images, p-values of both columns were calculated to confirm significant differences appeared in the MTT data. P-values of <0.05 and <0.01 were considered statistically significant.

All experiments were performed in triplicate.

RESULTS

Iron Chelator Protection Varies According to Live/Dead Imaging

The live/dead assays showed that the Fe^{2+} chelators, dipyrldyl (DP) and 1,10-phenanthroline (PHT), increased cell viability when used in increasing concentrations in cells undergoing ferroptosis (Figure 2). Treating cells with low concentrations (<25 μM) of each iron chelator resulted in unviable cells, as indicated by the red fluorescence (Figure 2). Protective effects, as indicated by the green fluorescence, appeared at concentrations of 100 μM of DP (Figure 2A). Tested concentrations above 100 μM continued to grant protective benefits against ferroptosis. As for PHT, protection began at concentrations of 25 μM . The concentration of 50 μM seemed to offer the best protection out of the tested concentrations. This outcome is shown by the majority of cells fluorescing green alongside a greater confluence of cells in the live/dead imaging relative to the conditions containing other concentrations of PHT. Cell viability decreased with higher doses of 100 and 200 μM PHT (Figure 2B).

Conversely, the Fe^{3+} chelator deferoxamine (DFO) showed protection at moderate concentrations from 50 μM to 100 μM but exhibited toxicity at higher concentrations, such as at 200 μM DFO, the cells appeared shriveled and sparse (Figure 3A). As for DFP, cells fluoresced red at tested concentrations from 25 μM to 200 μM , signifying that treated cells were not viable and the drug did not protect cells from ferroptosis at these concentrations (Figure 3B).

Live/Dead Imaging Findings Supported by MTT P-Values

In the DP and PHT dose responses with erastin, cell viability showed an upward trend with increasing concentrations of the iron chelator

used. The findings of the live/dead assays were confirmed with statistical analysis of the MTT assays. The protective effects of PHT against erastin-induced cell death were confirmed to be significant with a p-value of 1.27×10^{-9} (Figure 4A), while the protective effects of DP against erastin were confirmed to be significant with a p-value of 3.8×10^{-5} (Figure 4B). Both significant effects are indicated in the figures by three asterisks, signifying $p < 0.001$.

Additionally, the moderate protection of DFO was confirmed by a p-value of 0.011, indicated by two asterisks, signifying $p < 0.01$ (Figure 5A), and the effects of DFP were confirmed with a p-value of 0.0014, indicated by three asterisks (signifying $p < 0.001$) (Figure 5B). The DFO and DFP dose responses with erastin also generally showed increasing cell viability with increasing concentrations of the iron chelator used, but high concentrations of DFO caused cell viability to decrease. All graphs displayed $< 50\%$ average survival for cells treated with low iron chelator concentrations of $< 25 \mu\text{M}$ and a $10 \mu\text{M}$ killing dose of erastin. (Figure 3B).

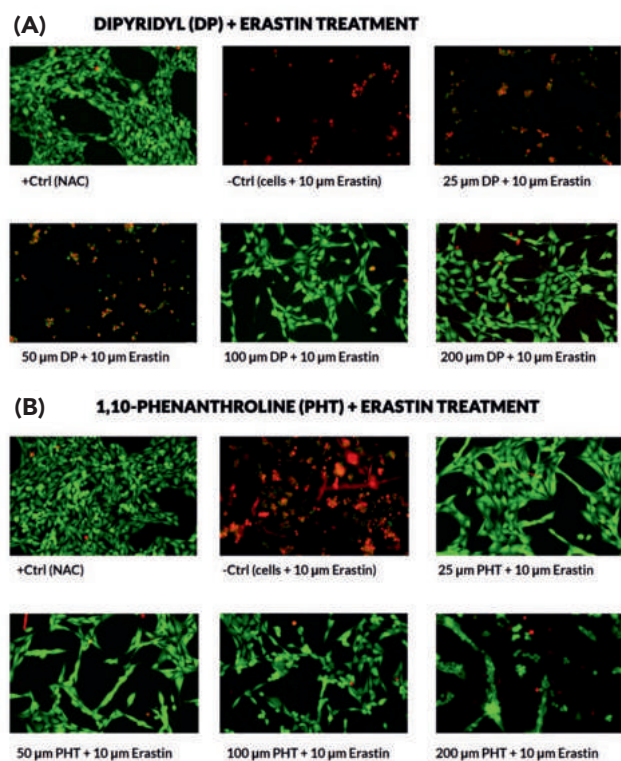


Figure 2: Live/dead assays of HT22 cells treated with two chelators of Fe^{2+} , Dipyrldyl (DP) and 1,10-Phenanthroline (PHT).

Live/dead assays were used to evaluate cell viability and differentiate between live and dead cells within a sample, typically using fluorescent markers like calcein-AM and ethidium homodimer. Calcein-AM, metabolized by living cells, emits a green fluorescence, while ethidium homodimer stains dead cells, producing a red fluorescence. In panel A, HT22 cells were exposed to dipyrldyl (DP) and erastin. The viability of the cells increased with higher DP concentrations, as indicated by a greater number of green-fluorescent cells at elevated DP levels. In panel B, HT22 cells were treated with 1,10-phenanthroline (PHT) and erastin, where cell viability also improved with increasing PHT concentrations. Moderate doses of PHT resulted in a greater appearance of green-fluorescent healthy cells.

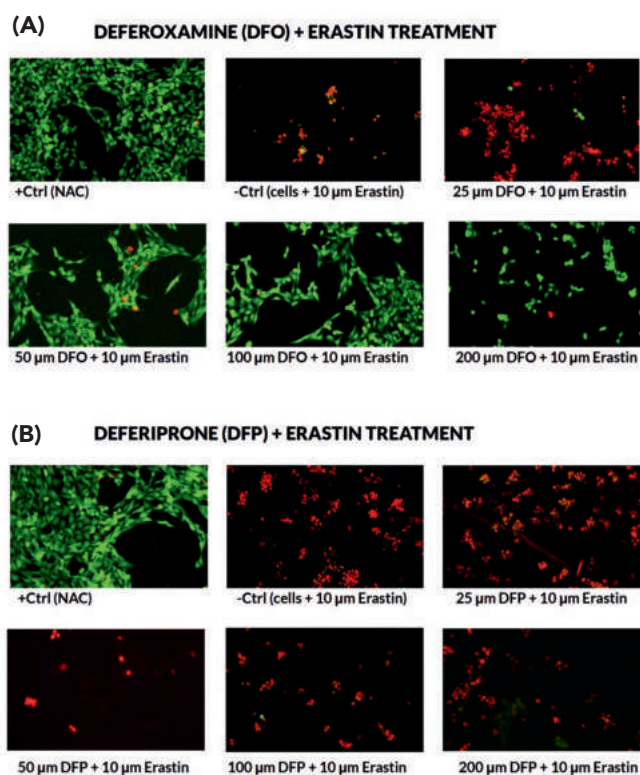


Figure 3: Live/dead assays of HT22 cells treated with Deferoxamine (DFO), a chelator of extracellular iron, and Deferiprone (DFP), a chelator of intracellular Fe^{3+} .

These assays are employed to measure cell viability and distinguish live cells from dead ones using fluorescent stains such as calcein-AM and ethidium homodimer. Calcein-AM is metabolized in living cells, yielding a green fluorescence, while ethidium homodimer binds to DNA in dead cells, emitting red fluorescence. In panel A, HT22 cells were treated with deferoxamine (DFO) and erastin, and cell viability improved with increasing DFO concentrations, though higher viability was observed at moderate DFO levels, evidenced by more green fluorescence. In panel B, HT22 cells were treated with deferiprone (DFP) and erastin. The majority of cells appeared dead, as shown by the red fluorescence and minimal green fluorescence, except in the positive control wells.

DISCUSSION

This study investigated the differential effects of four iron chelators with varying molecular characteristics on ferroptosis in HT22 cells, aiming to understand the role of iron chelators in neuroprotection. It was demonstrated that Fe^{2+} chelators, such as dipyrldyl (DP) and 1,10-phenanthroline (PHT), provide protection against erastin-induced ferroptosis at moderate concentrations. These findings are consistent with previous studies, indicating that reducing intracellular Fe^{2+} can inhibit lipid peroxidation, a key event in ferroptosis (5). The effectiveness of these chelators is linked to their membrane permeability and ability to bind to intracellular iron Fe^{2+} . On the other hand, high concentrations of DP and PHT reduced cell viability. These results align with the understanding that, while excessive iron can be detrimental, iron is still crucial for many cellular processes (6), including electron transport within the mitochondria, cellular respiration, and synthesizing key neurotransmitters, such as dopamine and norepinephrine (9). Hence, the processes iron is involved in highlight the importance of maintaining iron homeostasis.

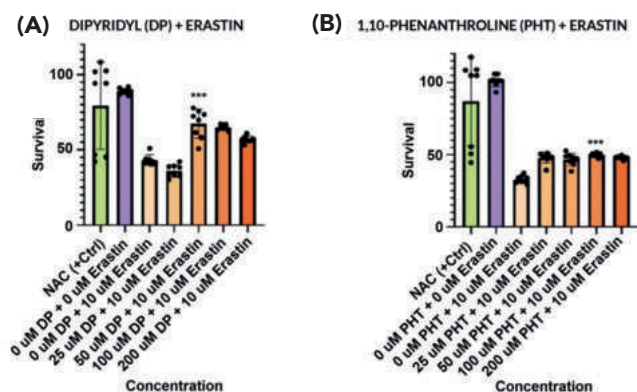


Figure 4: MTT assays of HT22 cells treated with dipyrldyl (DP) and 1,10-phenanthroline (PHT) were produced.

In the MTT assay, the reduction of yellow tetrazolium salt into a purple formazan product by metabolically active cells reflects cell viability. The amount of formazan produced is directly proportional to the number of viable cells, making it a reliable indicator of cell survival. Data points represent individual measurements, while the bars indicate the average of the total values. Error bars represent variability from the three treatments, each repeated on three separate plates, for each iron chelator. Both chelators provided protection against erastin at 50–100 μM concentrations, but higher doses of the chelators reduced cell survival. Error bars represent the mean \pm one standard deviation. P-values were calculated for conditions showing significant differences in the live/dead assays to verify statistical significance. The p-value for PHT against erastin-induced cell death was 1.27×10^{-9} , as shown in graph A, and for DP against erastin, the p-value was 3.8×10^{-5} , as seen in graph B.

Interestingly, the observed toxicity at higher concentrations of Fe^{2+} chelators may be explained by the dual role of iron in cellular function. While moderate iron chelation can protect against ferroptosis by preventing the accumulation of reactive oxygen species (ROS), excessive iron depletion could disrupt essential iron-dependent processes, such as mitochondrial function and oxidative phosphorylation. This disruption could potentially impair cellular metabolism and increase susceptibility to cell death. The balance between iron sequestration and maintaining necessary cellular functions may be critical to achieving neuroprotective effects without inducing toxicity. Further research should investigate the mechanisms by which high doses of Fe^{2+} chelators affect cellular processes and explore potential dose-dependent effects on mitochondrial function.

The findings relating to the Fe^{3+} chelators, deferoxamine (DFO) and deferiprone (DFP), are more complex and contradicting. The MTT assay data indicates that DFO showed protection at moderate concentrations (50–100 μM), but showed toxicity at higher concentrations. These results contrast with other studies that demonstrate DFO to have neuroprotective effects at higher concentrations (10). This study also found a consistent discrepancy between MTT results and the live/dead assay data. Live/dead assay data showed successful protection against ferroptosis at moderate concentrations of DFO. The MTT data for DFP, on the other hand, revealed mostly poor cell viability overall and increased survival at very high concentrations of 200 μM, instead of showing consistent toxicity as in the live/dead assays. One hypothesis for this discrepancy is that MTT may have overestimated living cells compared to live/dead assays by sensing mitochondrial activity

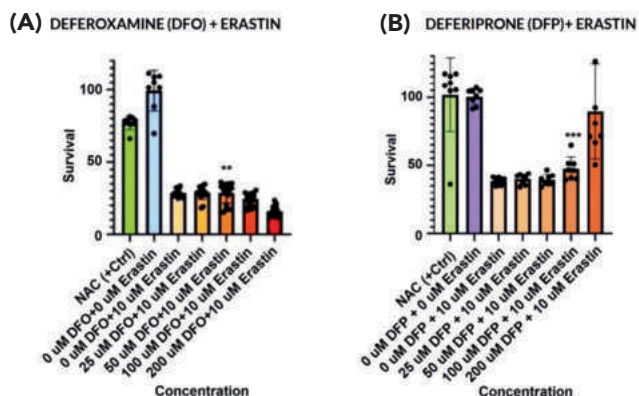


Figure 5: MTT assays of HT22 cells treated with deferoxamine (DFO) and deferiprone (DFP) were produced.

In this assay, the conversion of yellow tetrazolium salt to purple formazan by metabolically active cells indicates cell viability. The formazan amount correlates directly with viable cell numbers. Points represent individual data values, while bars show the mean of the total values. Error bars indicate variability across the three treatments, each performed on three separate plates for each chelator. DFO showed protective effects at moderate concentrations (50–100 μM) but became toxic at higher doses. In contrast, DFP exhibited increasing protective effects with higher concentrations. Error bars represent the mean \pm one standard deviation. P-values were calculated for conditions that showed significant differences in the live/dead assays to confirm statistical significance. The p-value for DFO against erastin-induced cell death was 0.011, as shown in graph A, and the p-value for DFP against erastin was 0.0014, as seen in graph B.

that may have persisted after cell death. This could explain the observed increase in cell viability at high DFP concentrations in the MTT assay, as it may have detected residual mitochondrial activity rather than actual survival. Future research should cross-validate these results with qualitative methods, such as live/dead imaging.

In regards to treating neurological conditions with iron chelators, the results of this study demonstrate that certain qualities of the chelators might yield more protective benefits without toxicity than others. Chelators that are able to most effectively bind to iron during the process of ferroptosis and decrease iron-dependent lipid peroxidation as a result could be more ideal in treating such conditions. However, it is still necessary to investigate iron chelators with the most favorable properties and pharmacokinetics that enhance their protective benefits and minimize toxicity (11). Although iron chelators have been investigated as a possible therapeutic approach to neurological conditions involving the excess of iron, much is still unknown about the role of different chelators in the mechanism of ferroptosis. However, by studying the differential effects of iron chelators with various characteristics *in vitro*, it was possible to learn how chelators' different molecular characteristics impact their cellular function. From the varying successes of the Fe^{2+} and Fe^{3+} chelators tested in this study, targeting forms of iron during its early signaling role or in extracellular stages of ferroptosis may yield more robust protective results than attempting to prevent lipid peroxidation in later stages of the process.

Iron is also essential for hydroxylase activity and the hypoxia stress response pathway, and iron chelators could impact the function of this pathway as well and affect the abilities of cells to adapt to oxidative stress. Iron induces the expression of genes

that act to maintain biological homeostasis and prevent oxidative stress-induced cell death (12). It triggers the expression of HIF-1, a transcription factor that plays a central role in oxygen homeostasis and activates a hypoxia stress response (5). Previous studies have indicated that while iron chelation may offer general neuroprotective potential, the efficacy and safety of the iron chelating drugs vary. Certain drugs have yielded different levels of success, such as DFP in one clinical trial that revealed very poor results protecting against oxidative stress-induced cell death and causing more neuronal damage overall (2).

Consistent with these findings, it was demonstrated in this study that Fe^{2+} chelators, such as DP and PHT, bind to intracellular iron, decreasing iron-dependent lipid peroxidation and inhibiting ferroptosis. These chelators showed protective effects at moderate concentrations but showed less positive results at high concentrations, such as decreased cell confluence and viability. For example, Fe^{3+} chelators, such as DFO and DFP, which bind to extracellular iron, had less success in inhibiting cell death. DFP, an intracellular chelator, showed toxicity in HT22 cells, suggesting that ferric iron may not play a key role in the process of ferroptosis and that chelating this form of iron has little impact on cell viability. However, DFO was protective in HT22 cells at moderate concentrations. DFO is known to mimic hypoxia in cells by inhibiting HIF-1, a transcription factor that activates a stress response to preserve oxygen homeostasis (4). Due to the limited success of Fe^{2+} chelators and the protection of DFO from ferroptosis, it is possible that this drug plays a larger role in targeting HIF-PHDs, not lipid peroxidation in ferroptosis. Testing the effects of Fe^{2+} and Fe^{3+} chelators on cell viability in ferroptosis indicated that iron chelation may be a key mechanism of hydroxylase inhibition rather than the direct binding of iron.

A limitation of the study is the use of an *in vitro* model with HT22 cells, which may not have fully represented the complexity of *in vivo* conditions. The HT22 cell line, while convenient, may not have fully replicated the behavior of primary cortical neurons, which should be addressed in future studies. The dose-response relationship was also not linear, indicating that different concentrations of the iron chelators may have produced varying effects. There may be a specific, optimal concentration at which iron chelation is most effective, maintaining the delicate balance of iron metabolism, while higher or lower doses could be less effective or even disruptive. Further research should test a broader range of concentrations over extended periods of time. Additional studies should also include a wider variety of iron chelators, specifically HIF-1 inhibitors (like DFO, which showed varied results). If the mechanism of action of these drugs is related to hydroxylase inhibition rather than the direct binding of enzymes, it could lead to the identification of iron chelators that are more successful in treating neurological conditions that involve oxidative stress and excess iron.

Given the significant role of iron dyshomeostasis and ferroptosis in neurodegenerative diseases such as Parkinson's Disease, Alzheimer's Disease, and stroke, the findings of this study underscore the potential of iron chelation therapy as a targeted intervention. The observed neuroprotective effects of extracellular iron chelators highlight the importance of early-stage iron modulation in preventing neuronal damage before it occurs. Unlike treatments that focus on repairing degeneration at later stages, early intervention with specific chelators could mitigate oxidative stress and delay disease progression.

These results contribute to the growing body of research supporting iron-targeting therapeutics as a promising strategy in neurodegeneration. The differential effects observed among Fe^{2+} and Fe^{3+} chelators emphasize the necessity of selecting compounds based on their specific iron-binding properties and cellular interactions. Future studies should aim to refine dosing strategies and assess long-term efficacy in disease models to further explore their therapeutic potential. By integrating iron chelation into early treatment approaches, it may be possible to slow disease onset and improve patient outcomes, offering a novel avenue for intervention in conditions currently lacking effective neuroprotective strategies.

ACKNOWLEDGMENTS

CS: Conducted the research and performed all splitting of cells, treating of cells, imaging, and viability assays. IC: Trained the student researcher in wet lab techniques, including culturing HT22 cells, ordering drugs, and running treatment procedures. RR: Provided mentorship and guidance throughout the research project. The authors declare no conflicts of interest.

REFERENCES

1. V. L. Feigin *et al.*, The global burden of neurological disorders: Translating evidence into policy. *Lancet Neurol.* **19**, 255–265 (2020). doi: 10.1016/S1474-4422(19)30411-9
2. D. Devos, *et al.*, Trial of Deferiprone in Parkinson's disease. *N. Engl. J. Med.* **387**, 2045–2055 (2022). doi: 10.1056/NEJMoa2209254
3. S. S. Karuppagounder *et al.*, Therapeutic targeting of oxygen-sensing prolyl hydroxylases abrogates ATF4-dependent neuronal death and improves outcomes after brain hemorrhage in several rodent models. *Sci. Transl. Med.* **8**, 328ra29 (2016). doi: 10.1126/scitranslmed.aac6008
4. K. Zaman, *et al.*, Protection from oxidative stress-induced apoptosis in cortical neuronal cultures by iron chelators is associated with enhanced DNA binding of hypoxia-inducible factor-1 and ATF-1/CREB and increased expression of glycolytic enzymes, p21(waf1/cip1), and erythropoietin. *J. Neurosci.* **19**, 9821–9830 (1999). doi: 10.1523/JNEUROSCI.19-22-09821.1999
5. R. R. Ratan, The chemical biology of ferroptosis in the central nervous system. *Cell Chem. Biol.* **27**, 479–498 (2020). doi: 10.1016/j.chembiol.2020.03.007
6. S. Zuo, J. Yu, H. Pan, L. Lu, Novel insights on targeting ferroptosis in cancer therapy. *Biomark. Res.* **8**, 50 (2020). doi: 10.1186/s40364-020-00229-w
7. T. A. Rouault, Iron metabolism in the CNS: Implications for neurodegenerative diseases. *Nat. Rev. Neurosci.* **14**, 551–564 (2013). doi: 10.1038/nrn3453
8. J. Zhang *et al.*, Neuroprotective mitochondrial remodeling by AKAP121/ PKA protects HT22 cells from glutamate-induced oxidative stress. *Mol. Neurobiol.* **56**, 5586–5607 (2019). doi: 10.1007/s12035-018-1464-3
9. C. Berthou, J. P. Iliou, D. Barba, Iron, neuro-bioavailability and depression. *EJHaem.* **3**, 263–275 (2021). doi: 10.1002/jha2.321
10. Y. Zhang *et al.*, Neuroprotective effect of deferoxamine on erastin-induced ferroptosis in primary cortical neurons. *Neural Regen. Res.* **15**, 1539–1545 (2020). doi: 10.4103/1673-5374.27434
11. L. Kupersmidt, M. B. H. Youdim, The neuroprotective activities of the novel multi-target iron-chelators in models of Alzheimer's disease, amyotrophic lateral sclerosis, and aging. *Cells* **12**, 763 (2023). doi: 10.3390/cells12050763
12. E. A. Cho, *et al.*, Differential *in vitro* and cellular effects of iron chelators for hypoxia-inducible factor hydroxylases. *J. Cell. Biochem.* **114**, 864–873 (2013). doi: 10.1002/jcb.24423
13. X. Chen, R. Kang, G. Kroemer, D. Tang, Ferroptosis in infection, inflammation, and immunity. *J. Exp. Med.* **218**, e20210518 (2021). doi: 10.1084/jem.20210518
14. J. Schindelin, *et al.*, Fiji: An open-source platform for biological-image analysis. *Nat. Methods* **9**, 676–682 (2012). doi: 10.1038/nmeth.2019

Collatz Conjecture: Odd Integer Sequences do not Strictly Increase

Jiali Chen¹, Maya Ybarra²

¹Department of Electrical and Computer Engineering, University of California, Los Angeles. ²West Covina High School.

ABSTRACT

The Collatz conjecture is one of the most fascinating unsolved problems in modern mathematics. This unsolved conjecture presents the following statement: for any positive integer x : if the integer is odd or divide it by 2 if it is even, 1 will eventually be reached after a finite number of iterations. By providing new insights into this open problem, more tools for a long-awaited proof and novel mathematical techniques can be provided. To investigate the iterations of the algorithm, an alternative method for computing iterations up to the iteration where an integer is divisible by 2 more than once will be provided. By induction, consecutive odd iterations can be simplified into an analytic equation. Then, it will be demonstrated that there exists a relationship between the initial input of the Collatz conjecture and the number of successive odd iterations. By applying this relationship, it was discovered that for any odd positive integer, the occurrence of a number that is divisible by 2 more than once can be predicted. Through this fact, this will show that any odd integer sequence does not strictly increase and provides another path to prove the conjecture that relates to the Fundamental Theorem of Arithmetic, p -adic numbers and the behavior of the Collatz conjecture.

INTRODUCTION

The Collatz conjecture is also known as the $3x+1$ problem, the Syracuse problem, and Kakutani's problem. The conjecture's arguably straightforward set of instructions amounts to mathematical challenges that have perplexed mathematicians for decades. Jeffery Lagarias cites two reasons for the conjecture's complexities. The first is from the apparent "pseudorandomness" and chaotic nature of the algorithm. The second is how "Conway's undecidability result indicates that the problem could be close to the unsolvability threshold." The mathematician Paul Erdos even once said, "mathematics may not be ready for such problems" (1). The following equation states the conjecture more formally by defining the *Collatz function*

$$C(x) = \begin{cases} 3x + 1 & \text{if } x \equiv 1 \pmod{2}, \\ \frac{x}{2} & \text{if } x \equiv 0 \pmod{2}. \end{cases}$$

The Collatz conjecture proposes that for any positive integer, after some number of iterations of the Collatz function, the number 1 is reached.

The Collatz function can be rewritten into the $3x+1$ function

$$T(x) = \begin{cases} \frac{3x+1}{2} & \text{if } x \equiv 1 \pmod{2}, \\ \frac{x}{2} & \text{if } x \equiv 0 \pmod{2}. \end{cases}$$

The $3x+1$ function (except when otherwise stated) will be referred to explicitly and implicitly instead of the Collatz function for simplicity (1).

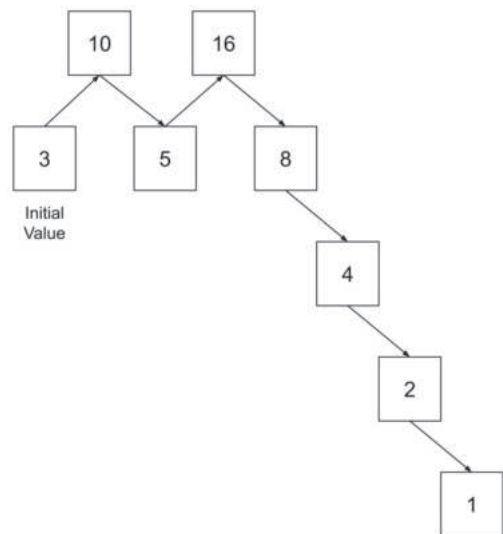


Figure 1: A visual representation of the Collatz conjecture starting at an initial value.

Given the initial integer 3, since $3 \bmod 2$ is 1, the Collatz function multiplies by 3 and adds 1. This is followed by a division of 2, which is represented by a downwards arrow until 8 is reached. At that point, a division of 2 continuously occurs until 1 is reached. Adapted from Terence Tao (2), with additional labeling of the initial value, a decrease from the previous number in the sequence being displayed with a downwards arrow, and termination at 1 instead of a loop between 1, 4, and 2 for organization and to better depict the claim that 1 is reached.

A proof of this conjecture can be used to study similar problems that have “expanding” and “contracting” domains (1). As a result, new techniques for studying such characteristics may arise for these problems in the vicinity.

Although a full proof has yet to emerge, there has been considerable progress, including Terence Tao’s paper titled “Almost all orbits of the Collatz map attain almost bounded values” and Wei Ren showing that the Collatz conjecture is known to be true up to $2^{100000-1}$ (3, 4).

There are numerous methods that may lead to a proof to the Collatz conjecture. Some examples include determining generalized Collatz functions and analyzing special cases, utilizing probabilistic models, and brute-force computer algorithms (3). To understand the Collatz conjecture, a few terms need to be defined. An “odd iteration” is the computation of the algorithm when x is odd, while an “even iteration” is the computation of the algorithm when x is even. An odd iterative sequence contains only the odd iterations in succession, while a “Collatz sequence” contains every iteration in succession, with the last iteration containing 1.

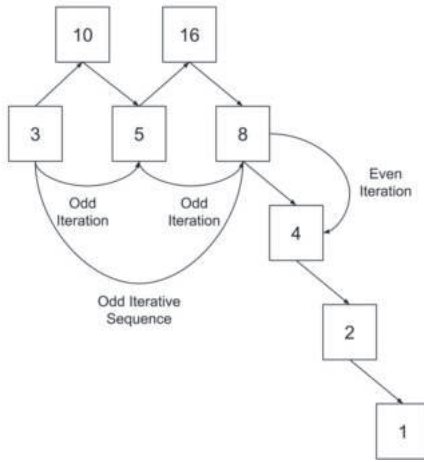


Figure 2: A visual representation of a Collatz sequence and its component parts.

This example depicts two odd iterations, an odd iterative sequence, and an even iteration. An odd iteration is the multiplying of x by 3 and adding 1 when it is odd. An odd iterative sequence is the combination of consecutive odd iterations. An even iteration is the division of x by 2 when it is even. Adapted from Terence Tao (2), with the addition of odd and even iteration labels, a decrease from the previous number in the sequence being displayed with a downwards arrow, and termination at 1 instead of a loop between 1, 4, and 2 for organization and to better depict the claim that 1 is reached.

First, the Collatz conjecture will be generalized for an odd iterative sequence by finding the number that is half of the first value divisible by 2^b ($b \geq 2$) in the Collatz sequence. Next, it will be exemplified that the iteration at which the odd integers do not increase within an odd iterative sequence can be predicted. Then, it will reason that odd integers in any Collatz sequence do not strictly increase. Afterwards, it shall be rationalized that every positive odd integer will decrease for any initial value of an iterative sequence. Lastly, how the results suggest the conjecture’s relationship to the Reduced Collatz Conjecture (5) and how they provide other directions to verify the conjecture will be discussed.

METHODS

Characterizing Iterations of the Collatz Conjecture

Because the algorithm stipulates that an even number must be divided by 2, it is unnecessary to consider even initial integers. This guarantees that the algorithm will reach an odd number. This will avoid any unneeded complexity of considering two distinct cases where the initial value is even or odd when one case suffices.

Take x_n to be the value outputted by $T(x)$ after n iterations. Also define $N(x)$, which will be referred as N hereafter, as the number of consecutive odd iterations starting from x . Furthermore, x_N is the output of that sequence. If the notion that every initial value will reach x_{N+1} after a finite number of iterations is proven, it can be concluded that there will be at least one decrease in the odd integers utilizing the inequality

$$x_{N+1} = \frac{x_N}{2} = \frac{3x_{N-1} + 1}{4} \leq x_{N-1} \quad (3)$$

Theorem 1 begins the proof of Inequality 3.

THEOREM 1. Let x_0 be a positive odd integer representing the initial value of an odd iterative sequence, and N be the number of consecutive odd iterations. Then we can denote

$$X_N = \left(\frac{3}{2}\right)^N x_0 + \frac{1}{2} \sum_{j=0}^{N-1} \left(\frac{3}{2}\right)^j \quad (4)$$

Theorem 1 can be proved through induction.

To prove by induction, first represent the computations of the odd iteration as a recursive formula in the form of

$$a_0 \begin{cases} a_0 = x_0 \\ a_n = \frac{3a_{n-1} + 1}{2} \end{cases}$$

The aim is to show that $\left(\frac{3}{2}\right)^c x_0 + \frac{1}{2} \sum_{j=0}^{c-1} \left(\frac{3}{2}\right)^j = x_N$ using induction.

Base case: $\left(\frac{3}{2}\right)^0 x_0 + \frac{1}{2} \sum_{j=0}^{0-1} \left(\frac{3}{2}\right)^j = x_0$. The base case is true.

Inductive step: Suppose that $\left(\frac{3}{2}\right)^c x_0 + \frac{1}{2} \sum_{j=0}^{c-1} \left(\frac{3}{2}\right)^j = x_N$.

The goal is to show that $\frac{1}{2} \left(3 \left(\left(\frac{3}{2}\right)^c x_0 + \frac{1}{2} \sum_{j=0}^{c-1} \left(\frac{3}{2}\right)^j \right) + 1 \right) = x_{N+1}$.

$$\frac{1}{2} \left(3 \left(\left(\frac{3}{2}\right)^c x_0 + \frac{1}{2} \sum_{j=0}^{c-1} \left(\frac{3}{2}\right)^j \right) + 1 \right) = \left(\frac{3}{2}\right)^{c+1} x_0 + \frac{1}{2} \sum_{j=0}^c \left(\frac{3}{2}\right)^j$$

$$\left(\frac{3}{2}\right)^{c+1} x_0 + \frac{3}{4} \sum_{j=0}^{c-1} \left(\frac{3}{2}\right)^j + \frac{1}{2} = \left(\frac{3}{2}\right)^{c+1} x_0 + \frac{1}{2} \sum_{j=0}^c \left(\frac{3}{2}\right)^j$$

$$\frac{3}{2} \sum_{j=0}^{c-1} \left(\frac{3}{2}\right)^j + 1 = \sum_{j=0}^c \left(\frac{3}{2}\right)^j$$

$$\frac{3}{2} \left(\frac{1 - \left(\frac{3}{2}\right)^c}{1 - \frac{3}{2}} \right) + 1 = \left(\frac{1 - \left(\frac{3}{2}\right)^{c+1}}{1 - \frac{3}{2}} \right)$$

$$\frac{3^{c+1}}{2^c} = \frac{3^{c+1}}{2^c}$$

Every step is reversible, so this concludes the proof by induction of Theorem 1. ■

At this point, the relationship between x_0 and x_N was derived. But to make Equation 5 more useful, a link between x_0 and N should be established. Lemma 1 presents a useful formulation of x_N that is an intermediate step towards determining the connection between x_0 and N .

LEMMA 1. *Let N be the number of consecutive odd iterations. Then*

$$x_N = x_0 + \sum_{m=1}^N \frac{x_0 + 1}{2^N} (2^{N-m})(3^{m-1}) \quad (5)$$

Lemma 1 can be proving that verifying the equivalency of Equations 4 and 5

$$x_0 + \sum_{m=1}^N \frac{x_0 + 1}{2^N} (2^{N-m})(3^{m-1}) = \left(\frac{3}{2}\right)^N x_0 + \frac{1}{2} \sum_{j=0}^{N-1} \left(\frac{3}{2}\right)^j \quad (6)$$

We can simplify the equation through the following steps

$$\begin{aligned} x_0 + \frac{x_0 + 1}{2^N} \sum_{m=1}^N (2^{N-m})(3^{m-1}) &= \left(\frac{3}{2}\right)^N x_0 + \left(\left(\frac{3}{2}\right)^N - 1\right) \\ x_0 + (x_0 + 1) \left(\left(\frac{3}{2}\right)^N - 1\right) &= (x_0 + 1) \left(\frac{3}{2}\right)^N - 1 \\ (x_0 + 1) \left(\frac{3}{2}\right)^N - 1 &= (x_0 + 1) \left(\frac{3}{2}\right)^N - 1 \end{aligned}$$

Both sides of the equation reduce to

$$x_0 + \sum_{m=1}^N \frac{x_0 + 1}{2^N} (2^{N-m})(3^{m-1}) = \left(\frac{3}{2}\right)^N x_0 + \frac{1}{2} \sum_{j=0}^{N-1} \left(\frac{3}{2}\right)^j \quad (7)$$

This proves Lemma 1. ■

With Lemma 1 verified, Theorem 2 presents an equation that gives x_0 as a function of N .

THEOREM 2. *Consider any*

$$x_0 = p(2^N) - 1 \quad (8)$$

where $p, N' \in \mathbb{N}$. Let p be a positive odd integer, N' be the set of natural numbers, and N be the number of consecutive odd iterations starting from the initial value x_0 . Then, $N'=N$.

Theorem 2 can be proven noticing that Equation 5 contains the

term $\frac{x_0 + 1}{2^N}$. It can be assumed that

$$p = \frac{x_0 + 1}{2^N} \quad (9)$$

Rearranging Equation 9 to

$$x_0 = p(2^N) - 1 \quad (10)$$

Equation 10 matches the form of Equation 8. Before concluding that $N'=N$, the assumption for p must be resolved. This can be shown to be true by recognizing that if p was any positive odd integer, $p(2^N)$ in Equation 10 would uniquely represent all positive even integers. This is because every positive integer except for 1 has a unique prime factorization by the Fundamental Theorem of Arithmetic. Thus, if 1 is subtracted, that will provide us with all the positive odd integers, which is the definition of x_0 . Therefore, Theorem 2 is proven. ■

With the proof of Theorem 2 demonstrating that $x_0 = p(2^N) - 1$ the following corollary emerges when substituting Equation 10 into Equation 7 and simplifying to

$$x_N = p(3^N) - 1 \quad (11)$$

COROLLARY 1. *Let x_0 be a positive odd integer representing the initial value of an odd iterative sequence, p be a positive odd integer, and N be the number of consecutive odd iterations. Then if*

$$x_0 = p(2^N) - 1 \quad (10B)$$

$$x_N = p(3^N) - 1 \quad (11B)$$

RESULTS

Behavior of Positive Odd Integers at the End of Iterative Sequences

The previous section justified that all positive odd integers would reach x_N . This section will demonstrate that the odd integers in a Collatz sequence do not strictly increase.

At this point, refer back to Inequality 3, which states that

$$x_{N+1} = \frac{x_N}{2} = \frac{3x_{N-1} + 1}{4} \leq x_{N-1} \quad (3B)$$

surmising that x_{N+1} is less than or equal to x_{N-1} . Proving that inequality will illustrate that odd integer sequences do not monotonically increase.

THEOREM 3. Let N be the number of consecutive odd iterations starting from the initial value x_0 , then the output of the $N+1$ iteration, x_{N+1} , is less than or equal to the output of the $N-1$ iteration, x_{N-1} .

Rearrange Inequality 3 as follows:

$$1 \leq x_{N-1} \quad (12)$$

Referring to Inequality 12, since 1 is less than or equal to x_{N-1} , and x_{N-1} will always be a positive integer, Inequality 3 is true for all x_{N-1} and consequently true for all x_0 . Furthermore, the only time when the odd integer sequence stays the same is when x_{N-1} is equal to 1. Therefore, Theorem 3 is true, and a decrease in an odd integer sequence is guaranteed except for 1. ■

DISCUSSION

Recall that the Collatz conjecture claimed that for a positive integer x , if the integer is odd, multiply x by 3 and add 1. If it is even, divide it by 2, repeatedly iterate, and 1 will be reached. After analyzing this problem, it was evaluated whether there is always a decrease in the odd integers for any positive initial value.

Based on the result in Section 1, it can be concluded that for an initial value of the iterative sequence $p(2^N)-1$, there is a number that is half of the value in the Collatz sequence that is divisible by 2^b is given by $p(3^N)-1$. Also, it can be stated that all initial values of a Collatz sequence reach an output of x_N or $p(3^N)-1$.

Building on Section 1, the findings from Section 2 lead to the conclusion that x_{N-1} is greater than x_{N+1} apart from when x_{N-1} is 1. More generally, it can be claimed that the odd integers in the Collatz sequence do not strictly increase. Also, this implies that all Collatz sequences with initial odd positive integers except for 1 will display a decrease in the odd integers at least once.

For future investigation, the conclusions can be linked to the Reduced Collatz Conjecture. The results can be expressed in a similar structure in that all x_o reach x_N and all x_N return to an integer less than x_N (except for 1). However, this is not equivalent to the Reduced Collatz Conjecture—any natural number x will return to an integer that is less than x (1). This is because the Reduced Collatz Conjecture relies on the intuition that if every natural number returns to a number less than itself, the number it returns to also reaches a number less than itself until 1 is reached. The former statement does not make the same suggestion because if the Collatz sequence were split into iterative sequences, there would be an intermediate x_o at the beginning of each iterative sequence, which might lead to larger and larger values of x_n in future iterative sequences. Although the previously mentioned statements do not have the same implications, future analyses could entail attempts to refine the statement to show that all x_N return to an output of $p(3^N)-1$ less than x_N (except for 1) for equivalency since the scope of search can be reduced to outputs of $p(3^N)-1$.

Moreover, if it can be determined how the values of p and N for $p(2^N)-1$ of the next iterative sequence from the output of $p(3^N)-1$ from the current iterative sequence can be predicted, the traditional method of computing the Collatz algorithm can be bypassed. And if $p=1$ and $N=1$, it would be equivalent to reaching 1. Considering this representation could be advantageous as the $p(2^N)$ and $p(3^N)$ terms suggest that there is a relationship between 2-adic and 3-adic numbers within the Collatz conjecture. This correspondence to p -adic numbers could lead advancements on how 2-adic and 3-adic numbers can be mapped to each other and provide insights into the field of p -adic analysis in general.

ACKNOWLEDGMENTS

I would like to express my sincere gratitude to my mentor, Maya Ybarra, for guiding me through my exploration of the Collatz conjecture. From her mathematical expertise and correspondence from the very beginning to my first draft, she has played a tremendous role in this journey. The author declares that they have no conflicts of interest.

REFERENCES

1. J. C. Lagarias, The $3x+1$ problem: An overview. *American Mathematical Society* **2010**, 2–23 (2010). doi: 10.48550/arXiv.2111.02635
2. T. Tao, The notorious Collatz conjecture. *WordPress*. <https://terrytao.files.wordpress.com/2020/02/collatz.pdf>
3. T. Tao, Almost all orbits of the Collatz map attain almost bounded values. *Forum Math. Pi.* **10**, 1–56 (2022). doi: 10.1017/fmp.2022.8
4. W. Ren *et al.*, Collatz Conjecture for $2^{100000}-1$ is true - Algorithms for verifying extremely large numbers. *IEEE SmartWorld* **2018**, 411–416 (2018). doi: 10.1109/SmartWorld.2018.00099
5. W. Ren, A new approach on proving Collatz Conjecture, *J. Math.* **2019**, 6129836 (2019). doi: 10.1155/2019/6129836

Investigating Mitochondrial Evolution in Advanced Prostate Cancer

Kylie Heering¹, Andrew Goldstein¹

¹Department of Molecular, Cell and Developmental Biology, University of California, Los Angeles.

ABSTRACT

A significant challenge in advanced prostate cancer is the development of resistance to androgen inhibition therapy, known as castration resistance. Cancer cell survival and proliferation are closely associated with altered mitochondrial dynamics, which play a crucial role in the metabolic reprogramming that drives cancer progression. The modulation of mitochondrial fission and fusion helps regulate the metabolic flexibility that is a hallmark of cancer cells, enabling them to adapt to changing energy demands and survive therapeutic stress. Using *in vitro* models, prostate cancer progression was genetically induced by transducing prostate cancer cells with oncogenic mutations. Across four genetic models of disease progression, distinct mitochondrial phenotypes associated with changes in N-MYC and RB1 expression, key drivers of late-stage disease, were identified. Specifically, regulation of the mitochondrial fission protein DRP1 mediates N-MYC-driven mitochondrial fragmentation linked to enhanced glycolysis, while RB1 loss induces mitochondrial elongation and altered Citric Acid Cycle metabolism. This research demonstrates that mitochondrial elongation and downregulation of glycolysis contribute to the emergence of Enzalutamide-driven castration-resistant prostate cancer. By examining the interplay between therapeutic resistance and genetic drivers of advanced prostate cancer, this study substantially contributes to the understanding of mitochondrial adaptations that occur during disease progression, highlighting potential targets for therapeutic intervention.

INTRODUCTION

Prostate cancer (PCa) is the most common cancer in men in the United States and remains a leading cause of morbidity and mortality among men worldwide (1). In prostate cells, androgens, like testosterone, bind to the androgen receptor (AR) in the cytosol, triggering its translocation to the nucleus where it functions as a transcription factor to activate genes that promote prostate growth and survival. In PCa, this pathway is upregulated, driving tumor persistence (2). While initially treatable with androgen deprivation therapy, PCa can overcome androgen depletion and progress to metastatic castration-resistant prostate cancer (CRPC), an incurable stage. To understand CRPC progression, current research primarily focuses on genetic mechanisms of receptor reactivation, such as AR amplification and alternative splicing of AR mRNA (3). However, AR signaling also plays a crucial role in shifting PCa toward mitochondrial metabolism as the disease advances (4). Despite the influence of AR signaling on metabolic reprogramming, the role of mitochondrial dynamics in facilitating this transition within the context of CRPC remains largely unexplored.

Mitochondria are highly dynamic organelles that undergo continuous fusion and fission to regulate their size, shape, and function in response to cellular energy demands and stress (Figure 1). Mitochondrial fission is the process of dividing a single mitochondria into two to create new punctate mitochondria. Mitochondrial fragmentation is regulated by dynamin-related protein 1 (DRP1), which assembles at mitochondrial constriction sites and mechanically constricts both the inner and outer

membranes, leading to organelle division. This process is induced by the phosphorylation of DRP1 at serine 616 by ERK1/2 and has been implicated in K-Ras-driven tumor growth (5). Mitochondrial fusion, on the other hand, is the merging of two mitochondria into one elongated mitochondria. Outer membrane fusion is mediated by mitofusin 1 and mitofusin 2 (MFN2), while inner membrane fusion is regulated by optic atrophy 1 (6, 7). Mitochondrial elongation has been associated with increased oxidative phosphorylation by preserving both the structural and functional integrity of the electron transport chain (6).

This dynamic is crucial for the metabolic flexibility that allows cancer cells to adapt to changing microenvironments and support rapid proliferation. An imbalance in mitochondrial fission and fusion drives tumor progression by adversely altering cell growth, metabolism, and invasive potential (8). This dysregulation enables cancer cells to meet bioenergetic demands and resist apoptosis, highlighting the importance of studying mitochondrial fission and fusion in advanced PCa.

It is hypothesized that the progression of PCa requires a specific mitochondrial phenotype. Furthermore, it is proposed that two key factors contribute to the mitochondrial changes observed in advanced stages of the disease: (1) the cellular response to therapeutic interventions, and (2) the acquisition of novel driver gene mutations.

To investigate mitochondrial changes associated with AR inhibition, the 16D CRPC cell line was treated with androgen receptor pathway inhibitors (ARPIs), which block key steps in the AR signaling pathway to treat CRPC (Figure 2). To better

understand how the mitochondria adapts to late stage disease, common mutations seen in advanced PCa, specifically N-MYC and RB1, were induced. N-MYC overexpression was evaluated for its impact on mitochondrial phenotype due to its role as a MYC family transcription factor frequently mutated in various cancers. Previous studies have identified N-MYC as an oncogenic driver of neuroendocrine PCa and aggressive prostate adenocarcinoma, making it a valuable model for studying PCa progression (9). Likewise, RB1 loss-of-function is a late-stage event associated with aggressive and metastatic PCa (10). Metabolic enzyme expression was assessed, mitochondrial fission-fusion dynamics were evaluated, and mitochondrial morphology was analyzed using confocal imaging.

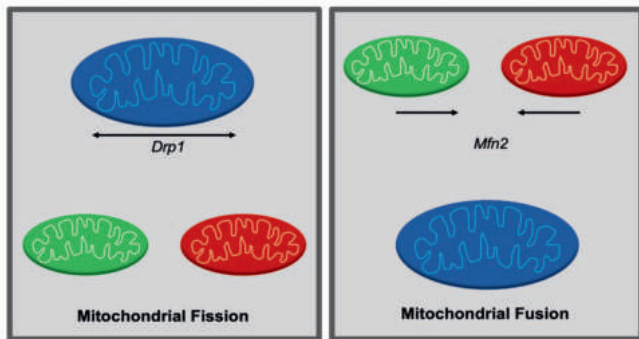


Figure 1: Mitochondrial fission-fusion dynamics.

The left panel of the figure illustrates mitochondrial fission, a process regulated by dynamin-related protein 1 (DRP1). DRP1 is activated into its pDRP1 form upon phosphorylation at serine 616, leading to its oligomerization and assembly into helical structures around the outer mitochondrial membrane, which constrict the membrane to facilitate scission and the formation of two daughter mitochondria. The right panel of the figure depicts mitochondrial fusion, a process mediated by mitofusin 2 (MFN2). MFN2 is localized to the outer mitochondrial membrane, and facilitates tethering and subsequent membrane merging between adjacent mitochondria. This promotes the formation of a single, larger organelle.

METHODS

Cell Culture

The 16D CRPC cell line was cultured to model CRPC behavior *in vitro*. Cells were grown in Roswell Park Memorial Institute (RPMI) 1640 media (Gibco, 11965118) containing 10% Fetal Bovine Serum (Sigma, F0926-500ML) and 1% Penicillin-Streptomycin (Thermo Fisher Scientific, 15140122). Tissue culture plates were coated with 0.01% Poly-L-Lysine (Sigma, P4832) to enhance cell adhesion and washed with 1X phosphate-buffered saline (PBS) (Thermo Fisher Scientific, 14-190-250) once. Cells were divided into different conditions to be treated with one of the following: 10 μ M dimethyl sulfoxide (DMSO) (Thermo Fisher Scientific, BP231-100) as a vehicle control, 10 μ M Enzalutamide (Selleck Chemicals, S1250), 10 μ M Apalutamide (Cayman Chemicals, 17132), 0.1 μ M ARCC-4 (Tocris, 7254), or 1 μ M ARCC-4 (Tocris, 7254) for 1 week *in vitro*.

Lentiviral Transduction

The 16D CRPC cell line was transduced with lentivirus to generate late-stage disease models. Cells were seeded at 30–50% confluence on a 10 cm plate. 24 hours after seeding, media was replaced with

RPMI 1640 media containing 10 μ L virus and 8 μ g/mL Polybrene (Thermo Fisher Scientific, NC0663391) to facilitate viral entry into the cell. The lentiviruses generated in-house for specific genetic modifications include FU-CRW (control), FU-NMYC-CRW (N-MYC overexpression), FU-shRB1-TP53DN-CYW (RB1 and p53 dual disruption), FU-TP53DN-CYW (dominant-negative p53), FU-shRB1-CRW (RB1 knockout), and a scramble GFP short hairpin RNA (shRNA) control lentivirus (containing a non-targeting scrambled shRNA sequence). Following loss of biosafety level 2 plus (BSL2+) status after 72 hours, cell media was changed every 48 hours. Transduced cells were cultured for 7 days and treated with either 10 μ M Enzalutamide (Selleck Chemicals, S1250) or DMSO (Thermo Fisher Scientific, BP231-100) (vehicle control) to investigate how key hallmarks of PCa progression influence mitochondrial dynamics in the context of AR inhibition.

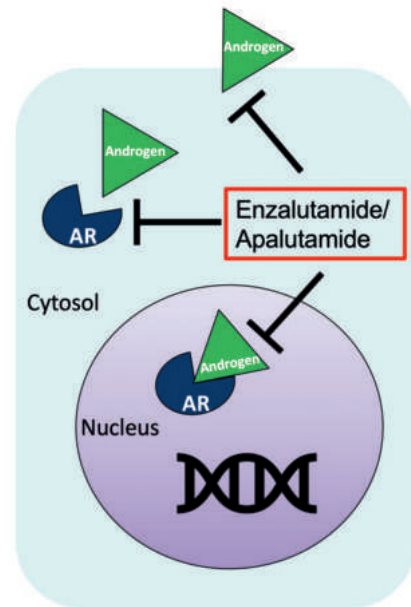


Figure 2: Androgen receptor therapy alters mitochondrial dynamics and increases reliance on oxidative phosphorylation.

Diagram detailing the mechanism of androgen receptor (AR) inhibitors Enzalutamide and Apalutamide in prostate cancer (PCa).

Microscopy

Microscopy was performed to visualize mitochondrial morphology. Cells were plated onto 8-well iBidi slides at a density of 22,500 cells/well, fixed in 4% paraformaldehyde/PBS for two minutes, and then washed with PBS. The cells were stained with Alexa Fluor 488 (green, 488 nm) for mitochondrial translation elongation factor tu (TUFM) to highlight the mitochondrial membrane, Alexa Fluor 647 (far-red, 647 nm) for phospho-pDRP-Ser(616) to co-localize DRP1 phosphorylation with the mitochondria, and 4',6-diamidino-2-phenylindole (DAPI) (blue) to label DNA. Signals were visualized using a Zeiss LSM 880 confocal scanning microscope with Airyscan through a 63x oil immersion lens to collect a pinhole-plane image at every scan position.

Western Blot

Western blot was performed to qualify relative protein expression levels. Cells were plated at a density of 225,000 cells/well into

6-well plates, harvested, and lysed in radioimmunoprecipitation assay buffer (50mM Tris-HCl pH8.0, 150mM NaCl, 1% NP-40, 0.5% sodium deoxycholate, 0.1% sodium dodecyl-sulfate (SDS)). Cell lysates were then sonicated with a sonic dismembrator (Thermo Fisher Scientific, FB120) for two 20-second cycles to maximize protein extraction. A green-to-purple (562 nm) bicinchoninic acid assay (Thermo Fisher Scientific, 23225) was performed to determine and normalize protein concentrations. For the polyacrylamide gel electrophoresis, samples were run on NuPAGE 4%–12% Bis-Tris Gels (Thermo Fisher Scientific, NP0335). 10 µg of protein were loaded per lane. Invitrogen™ XCell SureLock™ Mini-Cell contained running buffer (5% 20x MOPS NuPAGE SDS Running Buffer) in the outer chamber and running buffer + 0.25% of NuPAGE antioxidant filled the inner chamber. The gel was run at 200V for 50 minutes. Protein was transferred from the gel to polyvinylidene difluoride transfer membranes (Thermo Fisher Scientific, IPV00010) using transfer buffer (5% 20x NuPAGE Transfer Buffer, 0.06% NuPAGE antioxidant, 10% methanol). The transfer was run at 30V for 1 hour. Total protein was fluorescently qualified using SYPRO Ruby protein blot stain (Thermo Fisher Scientific, S11791). Membranes were blocked in PBS + 0.1% Tween-20 (Thermo Fisher Scientific, BP337-500) + 5% w/v non-fat milk (Thermo Fisher Scientific, BC9121673) and incubated with primary antibody overnight (Table 1). Then, membranes were washed in PBS + 0.1% Tween-20 and incubated

| Primary Antibody | Company | Catalog Number |
|------------------|-----------------|----------------|
| DRP1 | Cell Signaling | 5391S |
| pDRP1 | Cell Signaling | 3455S |
| C-MYC | Abcam | ab32072 |
| N-MYC | Santa Cruz | sc-53993 |
| RB1 | Abcam | ab181616 |
| MFN2 | Abcam | ab56889 |
| IDH1 | Cell Signaling | 3997S |
| p53 | Santa Cruz | sc-126 |
| ERK | Cell Signaling | 4696 |
| p-ERK | Cell Signaling | 4370 |
| CS | Cell Signaling | 14309S |
| OGDH | Proteintech | 15212-1-AP |
| HK2 | Cell Signaling | 28675 |
| LDHA | Millipore Sigma | MABC-150 |
| NSE | Proteintech | 66150-1-Ig |
| AR | Cell Signaling | 5153S |
| PSA | Cell Signaling | 5877S |
| Actin | Invitrogen | MA1-140 |
| Vinculin | Abcam | Ab129002 |

Table 1: Primary antibodies used in this study.

This table lists the primary antibodies used for western blot and immunofluorescence analysis, along with their respective vendors and catalog numbers.

in either anti-mouse (Thermo Fisher Scientific, 31430) or anti-rabbit secondary antibodies (Thermo Fisher Scientific, 31463) for 1 hour. Membranes were washed and imaged via fluorescence or horseradish peroxidase chemiluminescence.

Cell Cycle Assay

Cell cycle assays were performed to quantify cell proliferation and viability. 16D cells were cultured in 6-well plates. The cells were pretreated for 7 days to allow the drugs to exert their effects, using one of the following ARPIs: 10 µM DMSO, 10 µM Enzalutamide, 10 µM Apalutamide, 0.1 µM ARCC-4, or 1 µM ARCC-4. Following pre-treatment, cells were exposed to 30 nM IACS-010759 (ChemieTek CT-IACS107) (IACS), a complex I inhibitor of oxidative phosphorylation, or DMSO (control) for 72 hours. Media changes were performed every 48 hours and contained the corresponding small molecule inhibitors for each group.

Cell cycle analysis was conducted by staining the DNA with fluorescent dye to measure how many cells in a population are actively dividing. To do this, a 5-ethynyl-2'-deoxyuridine (EdU)-based kit (Thermo Fisher Scientific, C10635) was used according to the manufacturer's protocol. EdU labeling was performed for 2 hours, and flow cytometry was used to determine the percentage of EdU-positive cells.

Metabolite Extraction

Given the role of mitochondrial morphology in metabolic reprogramming, a metabolomics assay was performed to analyze metabolite abundance in RB1-KO and control 16D cells. 16D cells transduced with RB1 knockdown (FU-shRB1-CRW) and a scramble GFP shRNA lentivirus (control) were plated in a 6-well plate at 250,000 cells/well, with three technical replicates per condition. Cells were incubated with 13C-labeled glucose tracer media for 24 hours prior to metabolite extraction. To extract metabolites, cells were first washed with cold 150 mM ammonium acetate, then scraped off in 500 µL of cold 80% methanol containing 2 µM Norvaline. The suspension was transferred to a 1.5 mL Eppendorf tube, vortexed three times, and then spun at 800g for 5 minutes at 1°C. The samples were centrifuged again at 17,000g for 5 minutes. The supernatant volume was standardized and transferred to glass vials, and the remaining pellets were saved for DNA normalization. Samples were evaporated at 30°C, then stored at -80°C until they were sent to the UCLA Metabolomics Center for analysis.

Clinical Dataset

The SU2C Prostate Cancer Metastatic CRPC dataset was analyzed to assess the correlation between DNM1L mRNA expression (encodes DRP1 protein) and RB1 in patient PCa samples. DNM1L mRNA was examined in RB1-low and RB1-high tumors. Statistical analysis was performed using an unpaired t-test with Welch's correction.

RESULTS

Androgen Receptor Therapy Alters Mitochondrial Dynamics to Drive Castration Resistance

ARPI drug treatments reduced DRP1-serine 616 (pDRP1) phosphorylation. Western blot also revealed a reduction in band size for hexokinase 2 (HK2) and lactate dehydrogenase A (LDHA),

two key glycolytic enzymes (Figure 3A, 3B). Cells treated with both AR blockade and IACS exhibited reduced proliferation compared to those treated with AR blockade alone (control) (Figure 3C).

Shifts in pDRP1 expression suggest alterations in mitochondrial morphology, and pDRP1 was successfully detected and colocalized with mitochondria (Figure 3D). Microscopy images revealed that FU-CRW 16D cells treated with Enzalutamide exhibited more elongated mitochondria compared to vehicle-treated FU-CRW 16D cells (Figure 3E).

N-MYC Upregulates Mitochondrial Punctuation and Glycolysis

Successful lentiviral transduction of N-MYC overexpression in 16D cells was validated by Western blot, which showed prominent bands for N-MYC protein in FU-NMYC-CRW cells, while no bands were detected in the FU-CRW control (Figure 4A). Additionally, Western blot analysis confirmed reduced PSA and AR expression in Enzalutamide-treated 16D cells, validating the Enzalutamide-mediated decrease in AR signaling (Figure 4A). Furthermore, Western blot revealed that N-MYC overexpression rescued

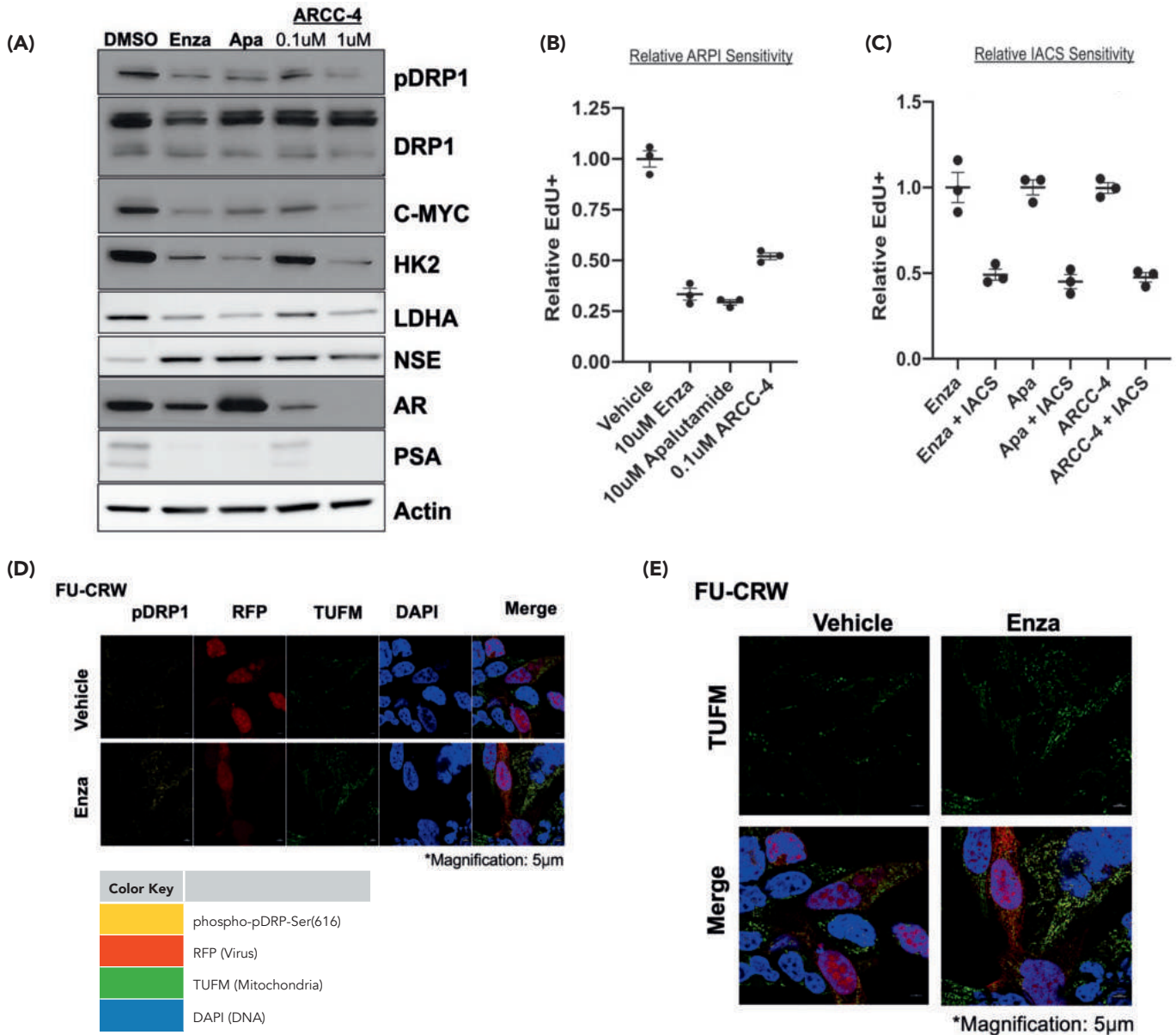


Figure 3: Androgen receptor therapy alters mitochondrial dynamics and increases reliance on oxidative phosphorylation.

(A) Western blot showing protein expression levels of dynamin-related protein 1 (DRP1), phosphorylated dynamin-related protein 1 (pDRP1), cellular myelocytomatosis oncogene (C-MYC), hexokinase 2 (HK2), lactate dehydrogenase A (LDHA), neuron-specific enolase (NSE), and androgen receptor (AR), and prostate-specific antigen (PSA), and actin as a loading control in 16D cells treated with either 10 µM DMSO, 10 µM Enzalutamide, 10 µM Apalutamide, 0.1 µM ARCC-4, or 1 µM ARCC-4 for 1 week. (B) Cell cycle analysis quantifying the relative sensitivity of 16D cells to various AR pathway inhibitors (ARPIs). (C) Cell cycle analysis quantifying relative proliferation of 16D cells treated with 10 µM DMSO, 10 µM Enzalutamide, 10 µM Apalutamide, 0.1 µM ARCC-4 with or without 30 nM IACS, a complex I inhibitor of oxidative phosphorylation. (D) Immunofluorescence analysis of mitochondrial morphology in 16D cells transduced with FU-CRW (RFP represents that the virus has entered the cells) and treated with 10 µM Enzalutamide (Enza) or vehicle for 72 hours. (E) Representative immunofluorescence images of FU-CRW 16D cells were stained for TUFM (green), DAPI (blue), and DRP1S616 (far red).

pDRP1 expression in Enzalutamide-treated 16D cells (Figure 4A). Consistent with previous findings, LDHA protein levels decreased with Enzalutamide treatment in the FU-CRW control group (Figure 4A). Interestingly, N-MYC overexpression rescues LDHA expression in the context of Enzalutamide treatment (Figure 4A). Confocal microscopy analysis revealed that N-MYC overexpression maintained punctate mitochondria in both vehicle- and Enzalutamide-treated FU-NMYC-CRW-transduced 16D cells, contrasting with the mitochondrial elongation observed induced by Enzalutamide treatment in the FU-CRW 16D cells (Figure 4D).

Loss Of Tumor Suppressor RB1 Reduces DRP1 Activity and Elongates Mitochondria

Successful lentiviral transduction of RB1 knockout in 16D cells was validated by Western blot, which showed no RB1 protein in FU-shRb1-CRW cells, and successful Enzalutamide treatment was confirmed via observed reduction in AR and

PSA protein (Figure 5A). Loss of RB1 reduced expression of DRP1 and its active form pDRP1-S616 (Figure 5A). Upstream mitogen-activated protein kinase regulators of DRP1, ERK1 and ERK2, exhibited reduced phosphorylation (Figure 5B). Imaging showed that RB1 loss produced elongated mitochondria (Figure 5D–5F). Statistical analysis of RB1-low and RB1-high tumors revealed a positive correlation between RB1 and DRP1 expression, indicating that RB1-low tumors clinically exhibit reduced DRP1 levels (Figure 5C).

Altered TCA Cycle Dynamics and OGDH Downregulation In RB1-KO Cell

Metabolite extraction revealed a trend toward increased alpha-ketoglutarate abundance in the RB1-KO cells compared to the scrambled control (Figure 6A, 6B). While M0 labeling remained consistent, M2 labeling in alpha-ketoglutarate showed a strong upward trend in RB1-KO cells (Figure 6C). In contrast, M2

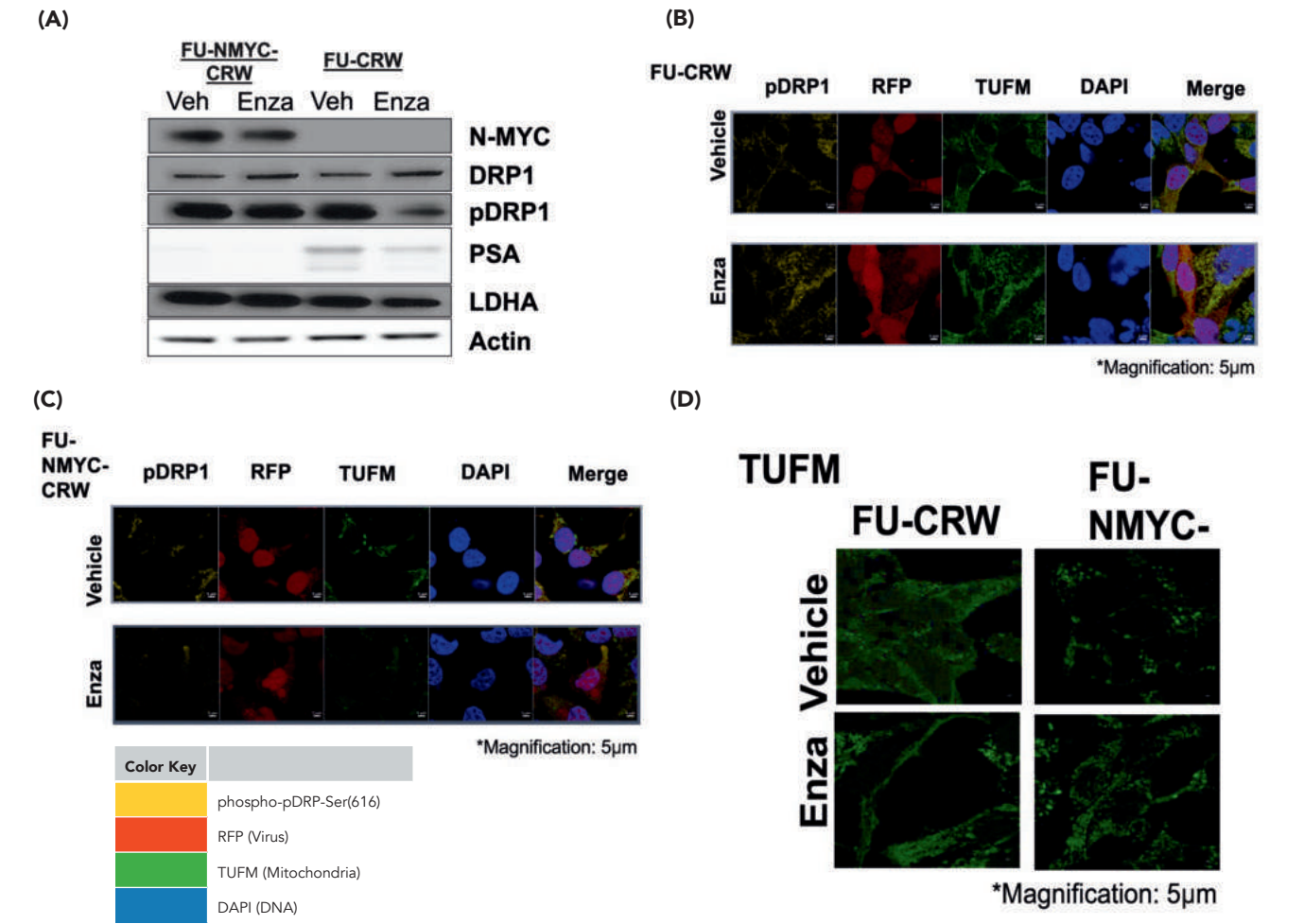


Figure 4: N-MYC upregulates mitochondrial punctation and glycolysis. (A) Western blot indicating protein level expression of nuclear myelocytomatosis oncogene (N-MYC), dynamin-related protein 1 (DRP1), phosphorylated dynamin-related protein 1 (pDRP1), prostate-specific antigen (PSA), lactate dehydrogenase A (LDHA), and actin (loading control) in 16D cells transduced with N-MYC overexpression lentivirus FU-NMYC-CRW or control virus FU-CRW and treated with 10 µM Enzalutamide or 10 µM DMSO (vehicle control) for 72 hours. (B) Representative immunofluorescence images of FU-CRW 16D cells treated with 10 µM Enzalutamide or vehicle for 72 hours. Cells were stained for TUFM (green), DAPI (blue), and DRP1S616 (far red). (C) Representative immunofluorescence images of FU-NMYC-CRW 16D cells treated with 10 µM Enzalutamide or vehicle for 72 hours. Cells were stained for TUFM (green), DAPI (blue), and DRP1S616 (far red). (D) Analysis of mitochondrial morphology in FU-CRW and FU-NMYC-CRW 16D cells.

labeling in succinate remained stable, while M2 labeling in malate was reduced. Western blot analysis of RB1-KO cells revealed decreased expression of oxoglutarate dehydrogenase (OGDH), an enzyme responsible for converting alpha-ketoglutarate to succinyl-CoA (Figure 6D).

DISCUSSION

ARPIs, including Enzalutamide, Apalutamide, and ARCC-4, downregulate DRP1 phosphorylation, HK2, and LDHA in 16D cells (Figure 3A). These protein-level changes indicate a

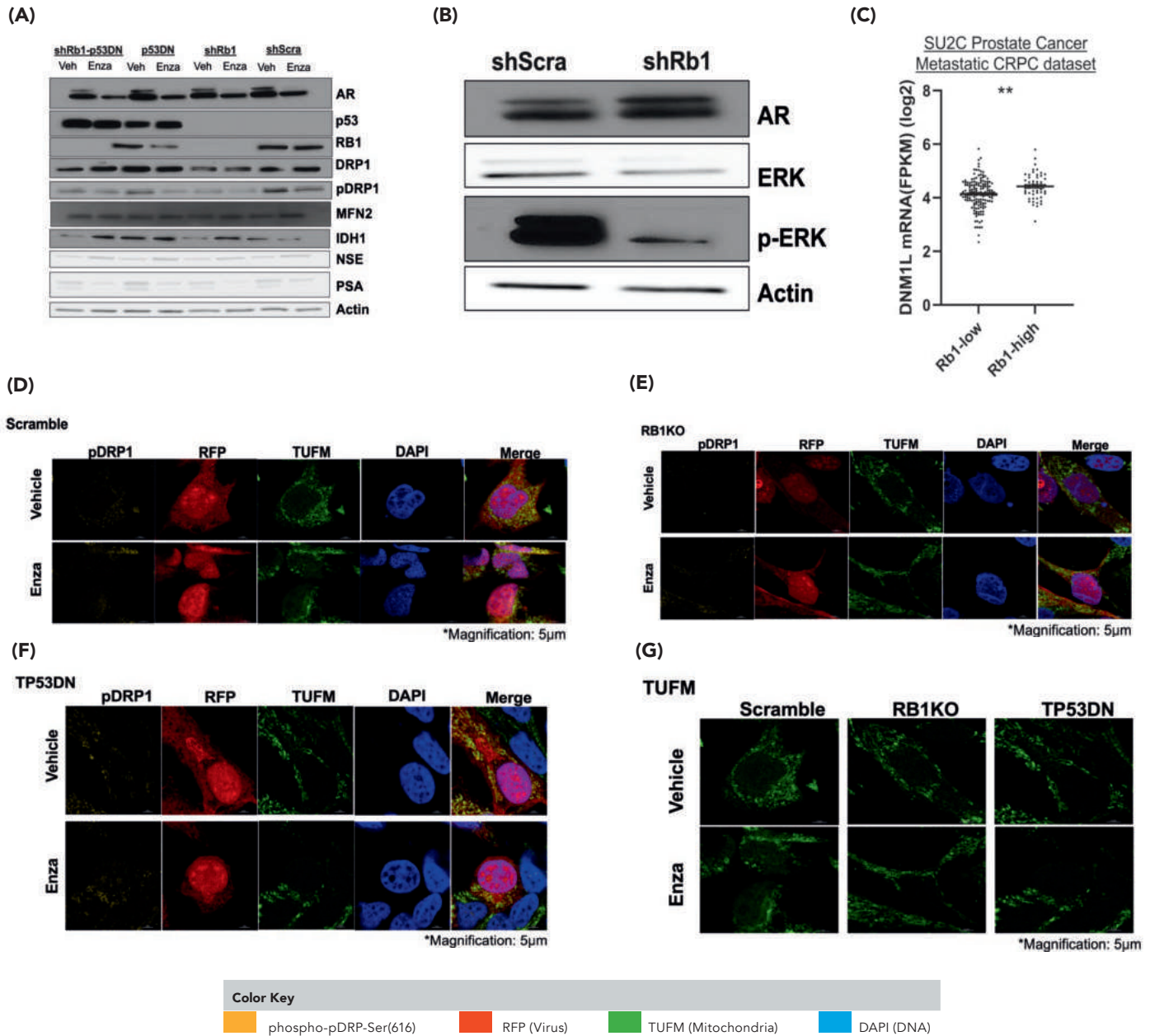


Figure 5: Loss of tumor suppressor RB1 decreases DRP1 expression.

(A) Western blot indicating protein level expression of androgen receptor (AR), tumor protein p53 (P53), retinoblastoma protein 1 (RB1), dynamin-related protein 1 (DRP1), phosphorylated dynamin-related protein 1 (pDRP1), mitofusin 2 (MFN2), isocitrate dehydrogenase 1 (IDH1), neuron-specific enolase (NSE), prostate-specific antigen (PSA) and actin (loading control) in 16D cells transduced with FU-shRB1-TP53DN-CYW, FU-TP53DN-CYW, FU-shRB1-CRW, and scramble shRNA control lentivirus (containing a non-targeting scrambled shRNA sequence) and treated with or without 10 μ M Enzalutamide for 72 hours. Results validate the successful knockout of Rb1. (B) Western blot indicating protein level expression of AR, ERK, pERK, and actin (loading control) in FU-shRB1-CRW and scramble shRNA transduced 16D cells. (C) Clinical positive correlation between DNM1L mRNA (encodes DRP1) and RB1 in PCa assessed using the SU2C Prostate Cancer Metastatic CRPC dataset. The p-value was calculated from an unpaired t-test with Welch's correction; $p = 0.0008$. (D-G) Analysis of the effect of RB1-KO and TP53DN on Enzalutamide effects on mitochondrial morphology. Representative immunofluorescence images of 16D cells transduced with control Scramble (green), RB1-KO (red), or TP53DN (green), treated with Enzalutamide or vehicle for 72 hours, and stained for TUFM (green), DAPI (blue), and DRP1S616 (far red).

reduction in mitochondrial fission and glycolysis, suggesting a metabolic shift toward enhanced oxidative phosphorylation to fulfill cellular bioenergetic demands. Consistently, Enzalutamide-treated cells that survived treatment exhibited elongated mitochondria, a feature that has been linked to increased oxidative phosphorylation necessary for cell proliferation (Figure 3A) (11). This metabolic reprogramming was further evidenced by the greater dependence of ARPI-treated cells on oxidative phosphorylation, as ARPI-treated cells exhibited heightened sensitivity to complex I inhibition compared to controls (Figure 3C).

Conversely, N-MYC overexpression preserves mitochondrial punctation and sustains glycolytic activity despite AR inhibition. In 16D cells, N-MYC overexpression increased mitochondrial punctation and upregulated LDHA, a key glycolytic enzyme (Figure 4A–4D). Even in Enzalutamide-treated 16D cells, N-MYC restored pDRP1 expression, counteracting the mitochondrial elongation induced by treatment (Figure 4A–4D). Given that mitochondrial fission via DRP1 is closely linked to glycolytic reprogramming in cancer cells, these findings suggest that N-MYC promotes a metabolic shift toward glycolysis by driving mitochondrial fragmentation (12, 13).

This metabolic reprogramming may also contribute to lineage plasticity and the emergence of neuroendocrine PCa (NEPC), an aggressive and treatment-resistant subtype. As a key driver of NEPC (14), N-MYC facilitates neuroendocrine lineage reprogramming by inducing histone acetylation, which increases DNA accessibility to support the expression of neuroendocrine-specific genes (4). Elevated glycolysis further promotes NEPC differentiation by generating pyruvate, the precursor for acetyl-CoA, a critical cofactor for histone acetyltransferases that drive the epigenetic modifications required for lineage conversion (4). By coupling mitochondrial dynamics with metabolic shifts, N-MYC overexpression not only sustains cancer cell survival under AR inhibition but also provides a potential mechanistic link between glycolytic reprogramming and the neuroendocrine phenotype, ultimately supporting cancer persistence despite AR inhibition.

In a separate model of late-stage PCa, the loss of tumor suppressor RB1 was found to be associated with reduced DRP1 and ERK phosphorylation (Figure 5A, 5B). Morphologically, RB1-KO cells exhibited mitochondrial elongation (Figure 5G). Given that ERK is an upstream kinase of DRP1 and has been shown to promote mitochondrial fission, this suggests a potential regulatory link. In mouse embryo fibroblasts, inactivation of RB1 eliminates

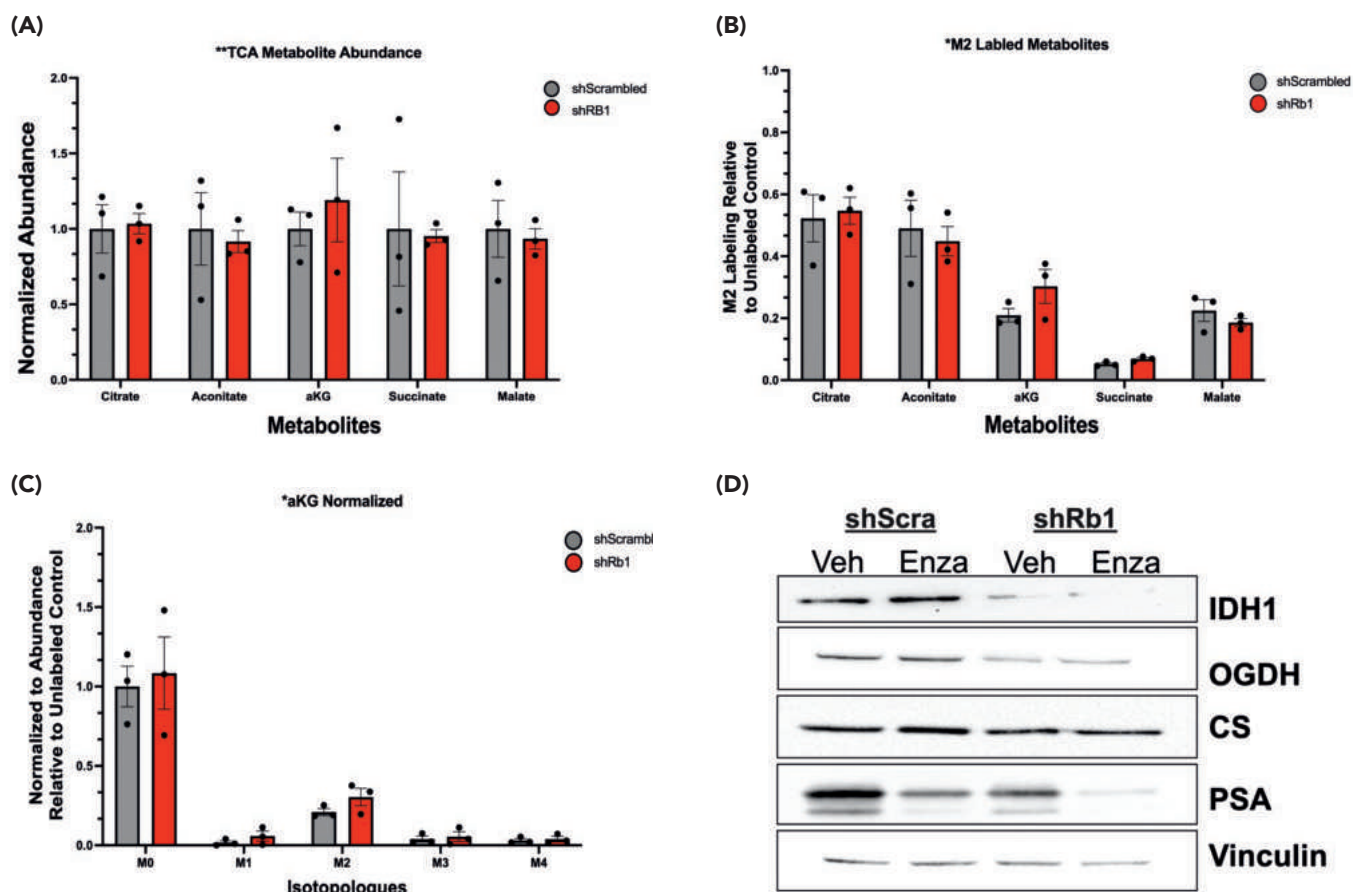


Figure 6: Increased alpha-ketoglutarate abundance in PCa cells with RB1 loss.

(A) Relative measures of overall TCA metabolite abundance in 16D cells transduced with FU-shRB1-CRW or scrambled shRNA virus. (B) Alpha-ketoglutarate isotopologue data. (C) M2 isotopes in TCA enzymes. (D) Western blot indicating protein level expression of isocitrate dehydrogenase 1 (IDH1), oxoglutarate dehydrogenase (OGDH), citrate synthase (CS), prostate-specific antigen (PSA), and vinculin (loading control) in FU-shRB1-CRW and scramble shRNA transduced 16D cells treated with or without 10 μ M Enzalutamide.

ERK signaling as a requirement for proliferation, as important cell cycle genes are still expressed (5). This raises the possibility that RB1 loss directs mitochondrial elongation through disrupting ERK activity, potentially altering their metabolic phenotype without compromising proliferation.

Clinically, analysis of the SU2C Prostate Cancer Metastatic CRPC dataset revealed a positive correlation between DRP1 and RB1 expression, with RB1-low tumors exhibiting reduced DRP1 levels (Figure 5C). In our study, experimental downregulation of RB1 led to decreased DRP1 expression, indicating that RB1 loss is not just statistically associated with changes in DRP1 levels, but likely plays a direct role in regulating them.

A metabolomics assay showed more alpha-ketoglutarate in RB1-KO cells compared to the controls, while the abundance of downstream metabolites did not increase. Metabolite trends coincide with a reduction in OGDH, the enzyme responsible for metabolizing alpha-ketoglutarate in the TCA cycle. These results suggest that alpha-ketoglutarate may be accumulating or be redirected. Alpha-ketoglutarate has previously been associated with aggressive PCa (15). Given the secondary role of alpha-ketoglutarate in epigenetic regulation through histone demethylation, it would be valuable to conduct a chromatin immunoprecipitation sequencing experiment to determine whether RB1-KO PCa cells exhibit differential methylation patterns that regulate genes involved in PCa progression (16). Since RB1 loss has also been linked to NEPC development, elevated alpha-ketoglutarate levels may provide an alternative mechanism for promoting neuroendocrine reprogramming.

Overall, this study highlights DRP1 as a key regulator of mitochondrial dynamics in the progression toward a more aggressive PCa phenotype. By elucidating the interplay between AR inhibition, genetic drivers, and mitochondrial dynamics, this research provides a framework for understanding the metabolic evolution of PCa and identifying mitochondria-centered therapeutic targets for combating castration-resistant disease.

Firstly, the observed decrease in DRP1 expression following ARPI treatment co-occurs with increased sensitivity to IACS, suggesting AR inhibition shifts PCa metabolism toward a greater reliance on oxidative phosphorylation.

This aligns with patient tumor profiles, which demonstrate upregulated oxidative phosphorylation in malignant prostate tumors (17, 18). Similarly, studies on chemotherapy-resistant CRPC have shown that surviving cells undergo a metabolic shift toward oxidative phosphorylation (19, 20). Building on this, Ippolito *et al.* tested whether chemotherapy-resistant cells became more vulnerable to oxidative phosphorylation inhibition using metformin, a mitochondrial complex I inhibitor. Their results demonstrated that metformin impaired both the proliferation and invasiveness of cells that survived chemotherapy (19).

The therapeutic potential of targeting oxidative phosphorylation extends beyond CRPC, as both metformin and IACS have been shown to inhibit tumor growth in breast, pancreatic, and ovarian cancer cell lines, as well as in xenograft models in mice (21). These findings highlight oxidative phosphorylation as a promising target for enhancing treatment efficacy in ARPI-resistant CRPC.

Secondly, this study indicates that the mitochondria's response to new PCa mutations is context-dependent, with hormone therapy and different driver genes selectively influencing DRP1 expression. When N-MYC was overexpressed, an upregulation of DRP1 and its active form, pDRP1, was observed, leading to more punctate mitochondria and enhanced glycolysis. In contrast, AR inhibition and

RB1 loss reduce DRP1 activity, resulting in elongated mitochondria and metabolic shift toward oxidative phosphorylation.

Mitochondrial morphology is tightly linked to nutrient utilization and metabolic adaptation. Studies show that forced mitochondrial elongation through DRP1 depletion decreases fatty acid oxidation (22), while nutrient depletion sustains mitochondria in an elongated state (23). These findings emphasize that mitochondrial dynamics are not merely structural changes but important regulators of metabolic reprogramming.

These findings provide compelling evidence that PCa progression is closely associated with dynamic changes in mitochondrial phenotypes, driven by both therapeutic responses and genetic alterations. As advanced PCa often develops resistance to multiple lines of treatment, understanding how mitochondrial morphology adapts to oncogenic drivers and therapeutic pressures is essential for uncovering new vulnerabilities for targeted therapies.

ACKNOWLEDGMENTS

Thank you to the Eli and Edythe Broad Center of Regenerative Medicine and Stem Cell Research (BSCRC) for funding this work. Thank you to Takao Hashimoto for his help in imaging the cells with confocal microscopy.

REFERENCES

1. S. P. Kelly, W. F. Anderson, P. S. Rosenberg, M.B. Cook, Past, current, and future incidence rates and burden of metastatic prostate cancer in the United States. *Eur. Urol. Focus.* **4**, 121–127 (2018). doi: 10.1016/j.euf.2017.10.014
2. D. T. Hoang, K. A. Iczkowski, D. Kilari, W. See, M. T. Nevalainen, Androgen receptor-dependent and -independent mechanisms driving prostate cancer progression: Opportunities for therapeutic targeting from multiple angles. *Oncotarget* **8**, 3724–3745 (2017). doi: 10.18632/oncotarget
3. T. Chandrasekar, J. C. Yang, A. C. Gao, C. P. Evans, Mechanisms of resistance in castration-resistant prostate cancer (CRPC). *Transl. Androl. Urol.* **4**, 365–380 (2015). doi: 10.3978/j.issn.2223-4683.2015.05.02
4. F. Ahmad, M. K. Cherukuri, P. L. Choyke, Metabolic reprogramming in prostate cancer. *Br. J. Cancer* **125**, 1185–1196 (2021). doi: 10.1038/s41416-021-01435-5
5. J. A. Kashatus *et al.*, Erk2 phosphorylation of Drp1 promotes mitochondrial fission and MAPK-driven tumor growth. *Mol. Cell* **57**, 537–551 (2015). doi: 10.1016/j.molcel.2015.01.002
6. P. Mishra, D. C. Chan, Metabolic regulation of mitochondrial dynamics. *J. Cell Biol.* **212**, 379–387 (2016). doi: 10.1083/jcb.201511036
7. R. Youle, A. M. van der Bliek, Mitochondrial fission, fusion, and stress. *Science* **337**, 1062–1065 (2012). doi: 10.1126/science.1219855
8. S. Vyas, E. Zaganjor, M. C. Haigis, Mitochondria and cancer. *Cell* **166**, 555–566 (2016). doi: 10.1016/j.cell.2016.07.002
9. J. K. Lee *et al.*, N-Myc drives neuroendocrine prostate cancer initiated from human prostate epithelial cells. *Cancer Cell* **29**, 536–547 (2016). doi: 10.1016/j.ccell.2016.03.001
10. D. L. Burkhardt, K. L. Morel, A.V. Sheahan, Z. A. Richards, L. Ellis, The role of RB in prostate cancer progression. *Adv. Exp. Med. Biol.* **1210**, 301–318 (2019). doi: 10.1007/978-3-030-32656-2_13
11. C. H. Yao *et al.*, Mitochondrial fusion supports increased oxidative phosphorylation during cell proliferation. *eLife* **8**, e41351 (2019). doi: 10.7554/eLife.41351
12. C. Guido *et al.*, Mitochondrial fission induces glycolytic reprogramming in cancer-associated myofibroblasts, driving stromal lactate production, and early tumor growth. *Oncotarget* **3**, 798–810 (2012). doi: 10.18632/oncotarget.574
13. T. Sun *et al.*, Activated DRP1 promotes mitochondrial fission and induces glycolysis in ATII cells under hyperoxia. *Respir. Res.* **25**, 443 (2024). doi: 10.1186/s12931-024-03083-8
14. Y. Yamada, H. Beltran, Clinical and biological features of neuroendocrine prostate cancer. *Curr. Oncol. Rep.* **23**, 15 (2021). doi: 10.1007/s11912-020-01003-9

15. A. M. Mondul *et al.*, Metabolomic analysis of prostate cancer risk in a prospective cohort: The alpha-tocopherol, beta-carotene cancer prevention (ATBC) study. *Int. J. Cancer* **137**, 2124–2132 (2015). doi: 10.1002/ijc.29576
16. K. A. Tran, C. M. Dillingham, R. Sridharan, The role of α -ketoglutarate-dependent proteins in pluripotency acquisition and maintenance. *J. Biol. Chem.* **294**, 5408–5419 (2019). doi: 10.1074/jbc.TM118.000831
17. R. S. Kelly *et al.*, The role of tumor metabolism as a driver of prostate cancer progression and lethal disease: Results from a nested case-control study. *Cancer Metab.* **4**, 22 (2016). doi: 10.1186/s40170-016-0161-9
18. E. Reznik *et al.*, A landscape of metabolic variation across tumor types. *Cell Syst.* **6**, 301–313.e3 (2018). doi: 10.1016/j.cels.2017.12.014
19. L. Ippolito *et al.*, Metabolic shift toward oxidative phosphorylation in docetaxel resistant prostate cancer cells. *Oncotarget* **7**, 61890–61904 (2016). doi: 10.18632/oncotarget.11301
20. G. Petrella *et al.*, Metabolic reprogramming of castration-resistant prostate cancer cells as a response to chemotherapy. *Metabolites* **13**, 65 (2022). doi: 10.3390/metabo13010065
21. K. B. Punter, C. Chu, E. Y. W. Chan, Mitochondrial dynamics and oxidative phosphorylation as critical targets in cancer. *Endocr. Relat. Cancer*. **30**, e220229 (2022). doi: 10.1530/ERC-22-0229
22. J. Ngo *et al.*, Mitochondrial morphology controls fatty acid utilization by changing CPT1 sensitivity to malonyl-CoA. *EMBO J.* **42**, e111901 (2023). doi: 10.15252/embj.2022111901
23. M. Liesa, O. S. Shirihai, Mitochondrial dynamics in the regulation of nutrient utilization and energy expenditure. *Cell Metab.* **17**, 491–506 (2013). doi: 10.1016/j.cmet.2013.03.002

Non-Invasive Analysis of Vessel Wall Vibrations During Blood Flow

Ashwath Nayagadurai¹, Jakob Evers^{2,3}, Javier Carmona¹, Katsushi Arisaka¹

¹Department of Physics and Astronomy, University of California, Los Angeles. ²Department of Physics, Freie Universität Berlin. ³Department of Biology, Chemistry and Pharmacy, Freie Universität Berlin.

ABSTRACT

Blood vessels regulate blood flow, relying on both elasticity and resistance for proper circulation. When a blood vessel narrows—a condition known as stenosis—this balance is thrown off. A stenosis is known to disrupt the laminar flow and create turbulent flow patterns which can contribute to the development of vascular diseases such as aneurysms. Aneurysms occur when parts of the vessel wall balloon outward, often in response to abnormal hemodynamic forces. Turbulence in blood flow has been hypothesized to cause vibrations in surrounding blood vessels. However, the precise mechanisms that translate vibrations into potential disease formation remain not completely understood. This study investigates the effect of a vessel model stenosis on the vibrational behavior of the blood vessels through the use of Spectral Domain Optical Coherence Tomography (SD-OCT). SD-OCT is an imaging technique that uses light to generate high-resolution images, allowing for the detection of extremely high vibrational frequencies. The position of the vessel wall was analyzed with a Fast Fourier Transform (FFT) to determine the underlying frequencies of vibration. The stenotic model exhibited significantly greater baseline FFT amplitudes (6.02 ± 0.94) compared with healthy (2.39 ± 1.12 , $p = 0.002$) and control (3.11 ± 1.06 , $p = 0.007$) conditions, indicating that the stenotic models resulted in significantly increased vibrational energy in the vessel wall. These findings support the hypothesis that stenotic regions can induce vibrations, potentially accelerating mechanical stress and the structural weakening that precedes aneurysm formation. By offering a non-invasive and high-resolution method to observe vascular structures, SD-OCT enables professionals to identify progressive diseases and improve patient outcomes.

INTRODUCTION

A stenosis is an abnormal narrowing of a blood vessel (1), which impairs the function of the blood vessel. By forcing blood to move through a smaller opening, the stenosis creates turbulent flow patterns that stress the wall of the blood vessel (Figure 1). Over time, the stress weakens the vessel wall and increases the risk of further damage or rupture (2). Healthy blood flow relies on a delicate balance of elasticity and resistance, and stenosis disrupts this balance.

A stenosis in the brain is a precursor to several neurologic complications (3). For example, brain stenosis can lead to transient ischemic attacks, strokes, and chronic cognitive decline due to reduced blood flow to the brain (4). Cerebral stenoses are challenging to evaluate due to the tightly packed vessels in the brain, which complicate invasive imaging techniques and surgical interventions. Unlike stenoses in other regions of the body, the confined space and intricate vascular structure of the brain make it harder to assess and treat effectively. If the stenotic wall becomes compromised, it can bulge outward, forming an aneurysm. They pose a significant threat given their potential to rupture, which leads to sudden death in approximately 12.4% to 44.7% of cases, depending on the location in the brain (5). Therefore, the early detection of aneurysms is crucial for risk stratification. By identifying stenosis early, healthcare providers can assess the risk of rupture and determine the most appropriate intervention.

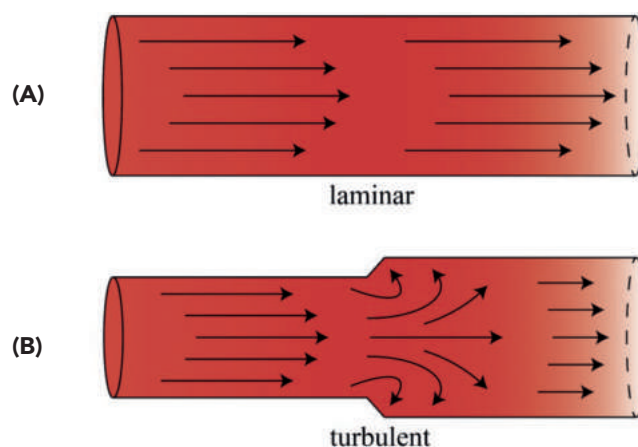


Figure 1: Comparison of laminar flow and turbulent flow caused by vessel geometry differences

(A) A vessel with a constant diameter exhibits laminar flow, characterized by smooth, parallel layers of fluid. In this case, the shear forces on the vessel walls remain relatively uniform. (B) A vessel with a sudden expansion in diameter, indicative of stenosis, disrupts the laminar flow. Turbulent flow is marked by chaotic, irregular fluid motion and the formation of vortices around the expansion site. This transition from laminar to turbulent flow has been hypothesized to generate acoustic vibrations and increased mechanical stress on the vessel walls, which progress into aneurysms.

To characterize the vibrations caused by the stenosis, this study uses Spectral Domain Optical Coherence Tomography (SD-OCT). SD-OCT is a non-invasive imaging technique that uses light to generate high-resolution images of tissues (Figure 2). It is effective for studying blood vessels due to its ability to capture detailed structural information at the micrometer scale with high imaging speed (6). SD-OCT can image the movement of blood vessels without damaging the tissue and with a time resolution far surpassing most microscopes. This time resolution is needed in the data analysis to convert the movement into a full-frequency spectrum of the vibrations. A lower imaging speed would not allow the detection of high frequencies and might result in a loss of important frequencies. By using OCT, the vibrations generated in blood vessels can be quantified, which may reveal the differences in stenotic vessel behavior.

This research aims to bridge the gap between a stenosis and aneurysm formation by analyzing the impact of a stenosis on the vibration of vessel walls. A stenosis causes more turbulent flow with increasingly more severe narrowings. Computational fluid-structure models showed that turbulence in blood flow, specifically around a brain stenosis, resulted in significantly more wall shear stress on blood vessel walls (7). Vibrations induced by turbulent flow may be of relevance in the weakening of blood vessels or may help predict aneurysm formation and guide the

development of preventative treatments for vascular diseases. This study hypothesizes that vessel architecture, and thus the type of blood flow, significantly affects the vibrations of blood vessel walls. In stenotic models, the change in vessel diameter is expected to produce turbulent flow, which induces vibrations in blood vessel walls. The vibrations are anticipated to be more frequent and pronounced in stenotic vessels compared to healthy vessels.

METHODS

Silicone Blood Vessel Models

Two different silicone blood vessel models were used to simulate healthy and stenotic conditions in blood vessels. Silicone possesses mechanical properties—such as elasticity, compliance, and tensile strength—similar to those of vascular tissue (8). Both models had a wall thickness of 0.5 mm. The healthy model had a constant inner diameter of 5.3 mm. The two strands of all models were directly connected by the silicone. The stenotic model was identical in dimensions to the healthy model, except that the bend in the vessel had a diameter change from 4.0 mm to 5.3 mm, which simulates the characteristics of stenosis. All vessel models were manufactured by Dr. Naoki Kaneko's laboratory, mounted in 3D-printed holders and were screwed onto a cushioned optical table for stable imaging during the experiments (Figure 3).

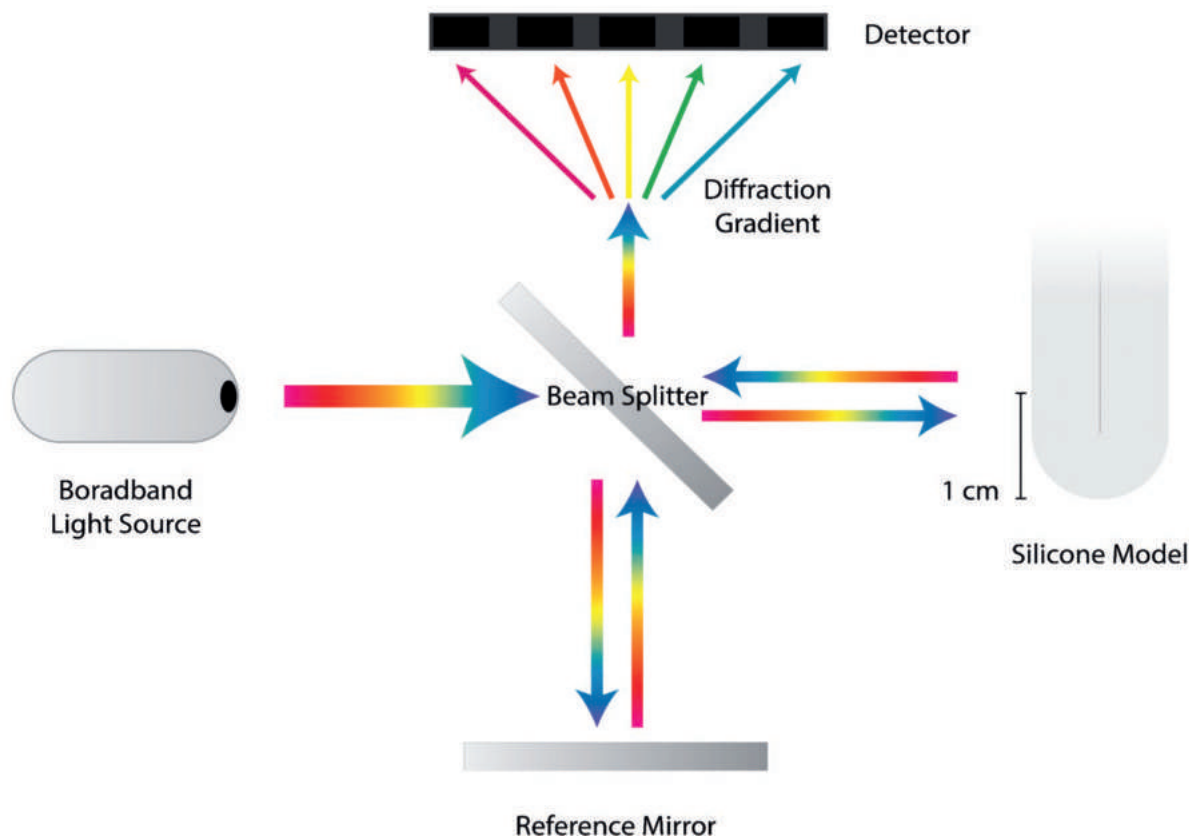


Figure 2: Working principle of Spectral Domain Optical Coherence Tomography (SD-OCT) for imaging vessels

A broadband light source is split by a beam splitter and shot at a sample and reference mirror in equal distance. The returning interference beam from the reference mirror is being dispersed into its wavelength components by a diffraction gradient. The wavelengths are then recorded individually by a detector. The scattered light from the sample, interfering with the original signal from the reference mirror, then gives structural information about the sample. This is because the broadband light is scattered at different depths throughout the sample, creating a shift relative to the reference beam.

Data Acquisition Using Spectral Domain Tomography Microscopy

Spectral Domain Optical Coherence Tomography (SD-OCT) was used to capture one-dimensional cross-sectional images of the vessel walls with a 6 mm depth and a spatial resolution of 6 μm . The interference between the reference and imaging beams allows for 1D cross-sectional imaging at a frequency of 51,200 lines per second, enabling the capture of high-frequency movement in the vessel walls. To ensure reliability, a Thorlabs piezoelectric actuator was used to generate known oscillations at fixed frequencies, verifying that the OCT system accurately detected and recorded vibrations. This calibration ensured that the observed vessel wall movements were not artifacts of the imaging system, but real flow-induced oscillations.

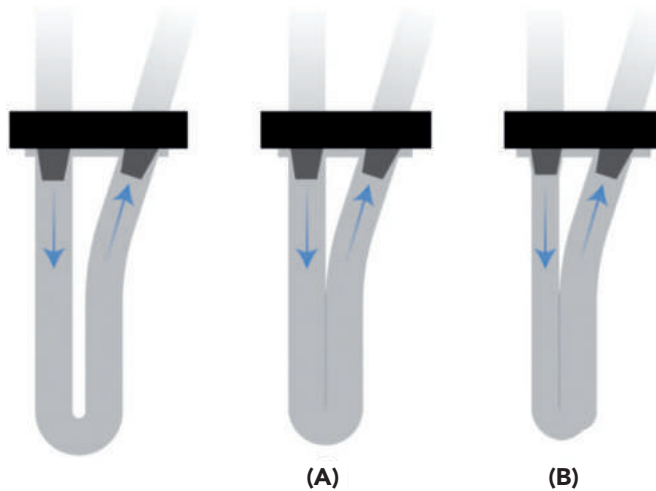


Figure 3: Design of silicone blood vessels are modeled for fluid flow experiments.

The silicone models are shown in light grey beneath the black 3D-printed holders. Water flows through tubes connected to the top of each model. These tubes are insulated to prevent external vibrations from the pump and waste reservoir from interfering with the experimental measurements. (A) The healthy model maintains a uniform diameter at 5.3 mm. (B) The stenotic model with a constricted region where the vessel diameter narrows from 4.0 mm to 5.3 mm.

Spectral Domain Optical Coherence Tomography (SD-OCT) system uses a low-coherence beam for rapid imaging (Figure 4). The low-coherence laser was set up at a fixed height of 1 cm above the bottom of the models, with the first outer vessel wall in focus. The SD-OCT system imaged 204,800 positional data points over 4 seconds per trial. 10 trials were conducted for each model (Stenotic Vessel, Healthy Vessel, and Control Group). Each model was carefully flooded with water so that no air bubbles interfered with the imaging. The control group was identical in structure to the stenotic vessel but with still water. Still water was chosen as the control to ensure measured vibrations were due to water flow and not background noise. Water was pumped at a constant flow rate of 104.4 mL/min with a Harvard Apparatus Pump 11 Elite through the models. The total cerebral blood flow rate is between 717 ± 123 mL/min with 2–21% per artery (9), making the used flow rate within average cerebral flow rates.

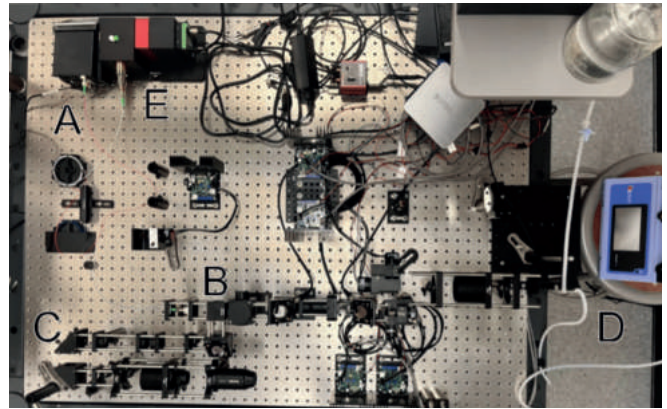


Figure 4: Spectral Domain Optical Coherence Tomography (SD-OCT) system is used for high-resolution imaging.

A broadband laser (A) emits a low-coherence beam used for imaging. The emitted light is split into two paths by a beam splitter (B), one directed toward the sample and the other toward a reference mirror. The reference mirror (C) reflects this light, maintaining a fixed optical path length. The backscattered light from the silicone blood vessel model (D) interferes with the reference beam and is recorded by a spectrometer (E) after being dispersed into wavelength components. The interference pattern generated by the returning light is analyzed to extract structural information. This technique enables real-time imaging of vessel model walls.

Data Analysis using Fast Fourier Transformation

The location of the vessel wall was collected with a center-of-mass analysis. A Fast Fourier Transform (FFT) was applied to the positional data to extract the frequencies in the signal. The FFT is an efficient algorithm for computing the Discrete Fourier Transform (DFT), which is mathematically defined as:

$$X(k) = \sum_{n=0}^{N-1} x(n) e^{-\frac{2\pi i k n}{N}} \text{ for } k = 0, 1, 2, \dots, N-1 \quad (1)$$

where $x(n)$ is the original signal—in this case, the position of the vessel wall. N is the number of data points, and $e^{-2\pi i k n / N}$ is a complex exponential function that “extracts” different frequency components from the signal. While the DFT itself requires a large number of calculations, the FFT algorithm reduces this significantly (10). This technique allows for the study of high-frequency oscillations in vessel walls since it enables the analysis of several data points without overwhelming computing resources.

The baseline FFT amplitude, defined as the average amplitude between 500 Hz and 5,000 Hz, was instead used to quantify the intensity of oscillations in the vessel walls. Frequencies below 500 Hz were excluded from the analysis due to their exponential nature, which introduced artifacts into the data. This is due to the trial time of a few seconds, producing unreliable low frequencies. An analysis over a long period of time would be able to produce more reliable data in this region. Above 5 kHz, the oscillations became too negligible to change the results. This was evident as the FFT remained uniform in this range, showing no significant peaks or variations, making the measurements uninformative. This standardized each comparison, focusing on the main plateau of frequencies. In short, the vibrational energy was analyzed, rather than specific frequencies.

The observed frequencies in the vessel walls were compared between models to determine the impact of stenosis on blood flow dynamics. A two-standard deviation filter was applied to remove any outliers and ensure the reliability of these findings, and the p-value test confirmed the validity of the statistical analysis.

RESULTS

OCT Data Processing and Center of Mass Determination

The position of the vessel model is characterized using a center-of-mass analysis. Center-of-mass analysis identifies all pixels of the vessel wall and calculates their weighted mean position based on the pixel brightness values. This creates a single representative coordinate that captures the object's overall location for each point in time. To achieve this, raw OCT data was processed on the white line representing the detected vessel boundary in each scan (Figure 5). This technique tracks the vessel wall position to a more precise location, ensuring that even minor oscillations could be accurately quantified. This allowed for better subsequent frequency analysis. The center-of-mass of the blood vessel is plotted over time, highlighting the oscillations over time (Figure 6). By applying the Fast Fourier Transform (FFT) to this motion data, the frequency components associated with the vibrational behavior were extracted.

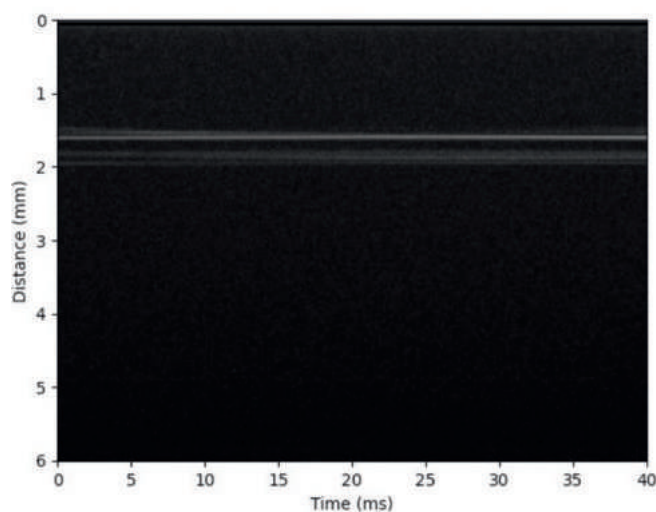


Figure 5: The blood vessel wall is imaged using Spectral Domain Optical Coherence Tomography.

The raw Optical Coherence images were acquired in 40 millisecond intervals; these images were compiled into a continuous dataset for analysis. The y-axis represents depth in millimeters, with deeper regions of the vessel model appearing further down in the image. The bright white lines in the image represent the detected inner and outer boundaries of the silicone vessel wall, allowing for localization of the vessel wall. These boundaries were analyzed to determine vibrational motion.

FFT Analysis on Vessel Wall Position

The Fast Fourier Transform was applied to center-of-mass data to extract the frequency distribution of vibrational behavior. The frequency spectrum of one h experimental trial shows the distribution of amplitudes from 0–1000Hz (Figure 7). Frequencies below 500 Hz and above 5000 Hz were cut off due to artifacts in the data or noise. The healthy vessel shows relatively low vibrational behavior, with lower FFT amplitudes across all relevant frequency bands, indicating minimal turbulence-induced vibrations. In contrast, the stenotic vessel exhibited a two-fold amplification of oscillations in the 500–5000 Hz range (Figure 8).

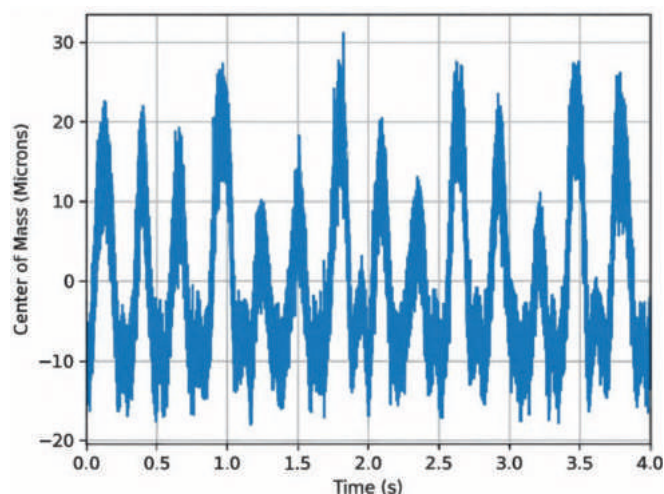


Figure 6: Vessel wall position oscillates with respect to time after center-of-mass analysis.

A center-of-mass analysis was applied to track vessel wall displacement over time, providing a visualization of the oscillatory behavior. The x-axis is time in seconds; the y-axis is the relative displacement of the vessel wall in micrometers. By looking at the position of the center of mass, the frequency and amplitude of oscillatory motion can be measured through a Fourier Transformation.

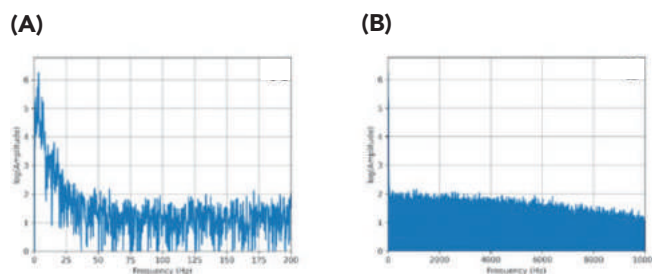


Figure 7: Data analysis of center-of-mass yielded the Fast Fourier Transform graphs.

The Fast Fourier Transform was applied to vessel wall displacement data to analyze the frequency distribution of vibrational behavior. The amplitude represents the relative intensity of vibrations at certain frequencies. It is plotted on a logarithmic scale to show contributions of lower frequencies. (A) The 0–200 Hz plot shows the low-frequency spikes due to the current data acquisition time. (B) The 0–10,000 Hz plot on the right shows frequencies after about 5 kHz decreasing exponentially. They had little effect on the results and were cut off after 5 kHz.

Increasing Vibrational Energy in Stenotic Vessel Model

The stenotic vessel demonstrated significantly elevated oscillatory amplitudes compared to the healthy vessel and control (Figure 9). The Relative FFT amplitude in the stenotic vessel was measured at 6.02 ± 0.94 . This was significantly higher than the healthy vessel (2.39 ± 1.12 , $p = 0.002$) and the control model (3.11 ± 1.06 , $p = 0.007$). The control model with no fluid flow served as a baseline, exhibiting low average oscillatory amplitudes. A p-value analysis showed that the control baseline FFT amplitude was significantly lower than the stenotic Vessel ($p = 0.007$), but not significantly different from the Connected Healthy Vessel ($p = 0.63$).

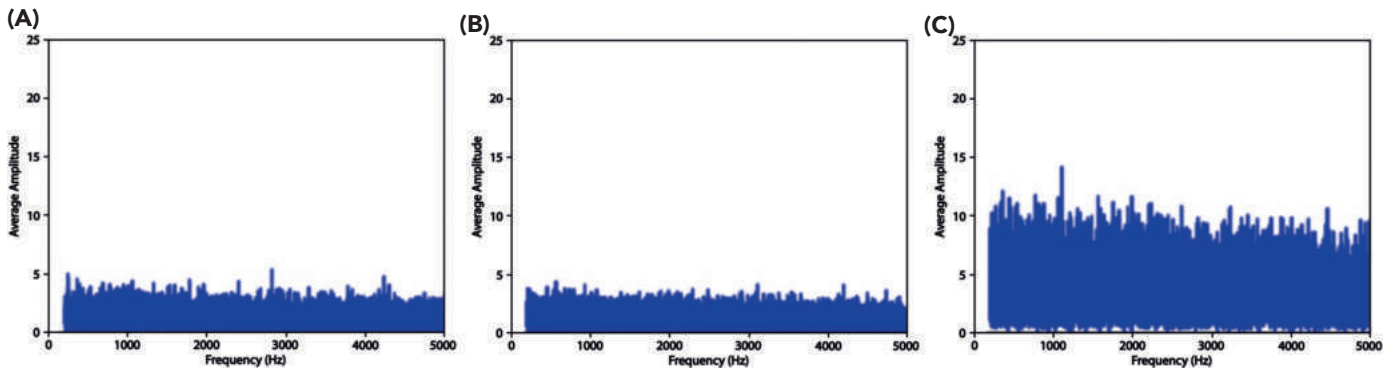


Figure 8: Averaged Fast Fourier Transform amplitudes are the highest for stenotic vessels.

The averaged Fast Fourier Transform graphs from the ten independent trials are shown for each experimental condition: control, healthy vessel, and stenotic vessel. The x-axis represents frequency (Hz), while the y-axis shows relative FFT average amplitude, which quantifies the vibrational energy of the blood vessel. The control (A) and healthy vessel (B) exhibited relatively stable oscillatory behavior with lower relative amplitudes in the 500–5000 Hz range. The stenotic vessel (C) shows a two-fold amplification of oscillations in the same range. Comparing the frequency spectra across different models shows the effect of a stenosis on vibrational behavior.

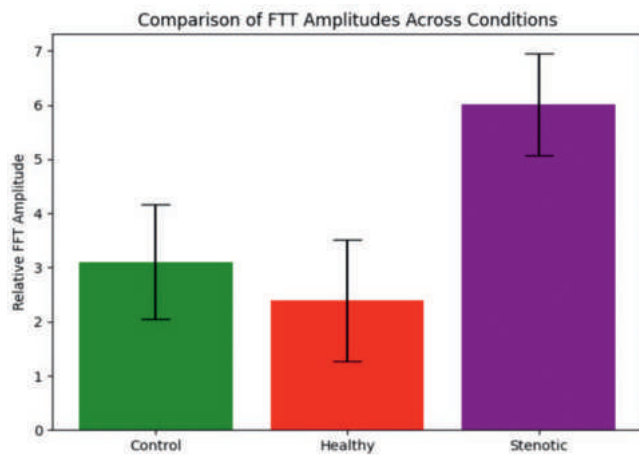


Figure 9: Stenotic vessels have the highest amplitude of average Fast Fourier Transform accounting for error.

This figure presents the FFT amplitude distributions for the control, healthy vessel, and stenotic vessel conditions. The x-axis represents the three experimental conditions, while the y-axis denotes the relative FFT amplitude, quantifying the vibrational energy of the detected vessel wall. Error bars, representing the standard error of the mean, are overlaid on the bars. P-value analysis shows that the stenotic vessel exhibits significantly higher oscillatory amplitudes compared to the healthy and control models.

DISCUSSION

This study set out to better understand how stenosis impacts the vibrational behavior of vessel walls. In particular, this study examined whether the narrowing of the vessel, as modeled by stenotic models, would induce more pronounced vibrations than seen in healthy vessels, a common precursor to aneurysm formation. The results show distinct differences in oscillatory behavior among the models. Notably, the stenotic vessel exhibited almost twice the baseline FFT amplitudes compared to the healthy vessel and the control. This supports our initial hypothesis that a narrowed vessel can indeed produce elevated vibrations in the vessel wall, likely driven by turbulent flow patterns that emerge in stenotic regions (4).

Elevated vibrations may exacerbate stresses on the vessel wall, potentially accelerating pathological processes like intimal thickening or aneurysm formation (12). Detecting these vibrations *in vivo* could offer a preventative approach to vascular conditions before they become life-threatening. Coupled with imaging modalities such as the SD-OCT, clinicians could employ higher frequency vibration-based metrics to screen patients for certain complications.

Several factors may have influenced the observed results. Small inconsistencies in the silicone vessel models, such as variations in wall thickness and elasticity, could have led to differences in how the models responded to flow-induced stresses. While a constant-flow pump was used to maintain a steady fluid velocity, minor fluctuations over time may have subtly affected the measured oscillatory behavior. Additionally, slight misalignments in the OCT focal plane could have introduced variability in the detected vessel wall displacement.

A key limitation of this study is the use of water instead of blood. Unlike water, blood is a non-Newtonian fluid with higher viscosity and complex properties due to the presence of cells and proteins. These factors influence how blood flows, particularly in regions of stenosis, where shear forces and turbulence play a major role in vessel wall dynamics. Water, on the other hand, behaves as a Newtonian fluid with a lower viscosity and lacks the cellular interactions that contribute to the mechanical stresses in real blood vessels. As a result, the measurements may not fully capture the true extent of turbulence-induced vibrations that occur *in vivo*. Furthermore, the study was limited by the relatively small number of vessel models tested and the use of a single flow rate. While silicone models allow for controlled experimentation, they lack the biological complexity of native vascular tissue, including its adaptive mechanical properties and interactions with circulating cells. Future studies should aim to incorporate a wider range of flow conditions and more physiologically relevant materials to better understand vessel wall vibrations in a better context.

Ultimately, this research adds to a growing body of literature aiming to find the link between stenosis and the progression of vascular diseases. By showing that stenotic regions exhibit pronounced vibrational activity, the findings suggest an indicator of compromised vascular health. If further validated, high-frequency vibration-based analyses could serve as a diagnostic tool, potentially halting progressive conditions like aneurysms. Using non-invasive

techniques like SD-OCT allows for detailed characterization of vascular structures, allowing healthcare professionals to detect disease progression and enhance patient outcomes.

ACKNOWLEDGMENTS

This work was supported by the Elegant Mind Club, whose resources and support were indispensable to the successful completion of this research. We thank Dr. Arisaka and Javier for their critical contributions to this study. Dr. Arisaka provided guidance on experimental design and data interpretation, while Javier constructed the OCT microscope and guided the team with data acquisition and analysis. We are also grateful to Dr. Kaneko and his lab for supplying the silicon blood vessel models and sharing their expertise in biomechanical processes. The authors declare that there are no conflicts of interest related to this work.

- **A.N.** Contributed to experiments, analyzed data, and wrote the manuscript.
- **J.E.** Contributed to experimental setup, performed experiments, analyzed data, and wrote the manuscript.
- **J.C.** Conceptualized experiment, constructed the OCT, guided data analysis, and reviewed the manuscript.
- **K.A.** Conceptualized the idea, supervised the study, guided data interpretation, and reviewed the manuscript

REFERENCES

1. J. Gutierrez, T. N. Turan, B. L. Hoh, M. I. Chimowitz, Intracranial atherosclerotic stenosis: Risk factors, diagnosis, and treatment. *Lancet Neurol.* **21**, 355–368 (2022). doi: 10.1016/S1474-4422(21)00376-8
2. M. N. Uddin, K. E. Hoque, M. M. Billah, The impact of multiple stenosis and aneurysms on arterial diseases: A cardiovascular study. *Heliyon* **10** (2024). doi: 10.1016/j.heliyon.2024.e26889
3. L. M. Héman, L. M. Jongen, H. B. Van Der Worp, G. J. E. Rinkel, J. Hendrikse, Incidental intracranial aneurysms in patients with internal carotid artery stenosis: A CT angiography study and a metaanalysis. *Stroke.* **40**, 1171–1176 (2009). doi: 10.1161/STROKEAHA.108.538058
4. G. Viticci, L. Falsetti, E. Potente, M. Bartolini, M. Silvestrini, Impact of carotid stenosis on cerebral hemodynamic failure and cognitive impairment progression: A narrative review. *Ann. Transl. Med.* **9**, 1209 (2021). doi: 10.21037/atm-20-7226
5. J. Huang, J. M. Van Gelder, The probability of sudden death from rupture of intracranial aneurysms: A meta-analysis. *Neurosurgery.* **51**, 1101–1107 (2002). doi: 10.1097/00006123-200211000-00001
6. S. Aumann, Optical Coherence Tomography (OCT): Principle and technical realization. *High Resol. Imaging Microsc. Ophthalmol.* (2019). doi: 10.1007/978-3-030-16638-0_3
7. K. Jain, The effect of varying degrees of stenosis on transition to turbulence in oscillatory flows. *Biomech. Model Mechanobiol.* **21**, 1029–1041 (2022). doi: 10.1007/s10237-022-01579-0
8. A. Larena-Avellaneda, G. Dittmann, C. Haacke, F. Graunke, R. Siegel, U. A. Dietz, E. S. Debus, Silicone-based vascular prosthesis: Assessment of the mechanical properties. *Ann. Vasc. Surg.* **22**, 106 (2008). doi: 10.1016/j.avsg.2007.09.003
9. L. Zarrinkoob, K. Ambarki, A. Wåhlin, R. Birgander, A. Eklund, J. Malm, Blood flow distribution in cerebral arteries, *J. Cereb. Blood Flow Metab.* **35**, 648–654 (2015). doi: 10.1038/jcbfm.2014.241
10. J. W. Cooley, J. W. Tukey, An algorithm for the machine calculation of complex fourier series, *Math. Comput.* **19**, 297–301 (1965). doi: 10.1090/S0025-5718-1965-0178586-1
11. A. Noorani, G. K. El Khoury, P. Schlatter, Evolution of turbulence characteristics from straight to curved pipes, *Int. J. Heat Fluid Flow.* **41**, 16–26 (2013). doi: 10.1016/j.ijheatfluidflow.2013.02.009
12. A. Wahle, J.J. Lopez, M.E. Olszewski, S.C. Vigmostad, K.B. Chandran, *et al.*, Plaque development, vessel curvature, and wall shear stress in coronary arteries assessed by X-ray angiography and intravascular ultrasound. *Med. Image Anal.* **6**, 17–36 (2006). doi: 10.1016/j.media.2006.03.002

2024–2025 USJ STAFF

LEADERSHIP



(From left to right) Top row: Dr. Jorge A. Avila, Sohan Talluri. Second row: Dashrit K. Pandher, Isabel Angres, Malvika Iyer. Not pictured: Archi K. Patel.

ASST. EDITORS



(From left to right) Top row: Kuan Heng (Jordan) Lin, Oliver Wang, Timothy Liu. Second row: Zenya Bian, Chahak Gupta, Tanisha Lakhanpal, Melody Jiang, Nhi H. Pham. Not pictured: Brynn Beatty, Caden Chow, Nyah Zhang.

REVIEW BOARD



(From left to right) Top row: Vedant V. Janapaty, Oliver Wang, Kuan Heng (Jordan) Lin, Aryan Law, Naisha Agarwal. Middle row: Catherine Zhang, Ken Woo, Sumedha M. Shastry, Nathan Abraham Joshua. Bottom row: Melody Jiang, Beverly Luring, Felisha Kuo, Khushi Sharma, Joanna Rhim, Malvika Iyer. Not pictured: Katherine A. Morrisette, Miki Matsuoka, Sofia Ando, Summer Kelso, Caden Chow, Nyah Zhang.

EDITORIAL BOARD



(From left to right) Top row: Ryan Wong, Phillip Tang, Aniket Das, Spencer Bergland, Karch A. Borsa, Andrew Tsui, Vyas Koduvayur. Middle row: Lee Zucker-Murray, Emre Gürdal, Timothy Liu, Chahak Gupta, Eshika Abbaraju, Paul Zhang. Bottom row: Nhi H. Pham, Siddhika Naik, Kavya M. Pandrangi, Priya Ravi, Yubin Kim, Tanisha Lakhapal, Isabel Angres. Not pictured: Brynn Beatty, Gia Boisselier, Marie Yang, Prannay Veerabahu, Truman Ma

LAYOUT BOARD



(From left to right) Top row: Natalia Liang, Lucas J. Kim, Hongbo (Danny) Zhu, Zenya Bian. Bottom row: Katelyn Mak, Megan Huang, Renee Chowdhry. Not Pictured: Ahmad Ismail, Dashrit K. Pandher.



(From left to right) Top row: Dashrit K. Pandher, Truman Ma, Aniket Das, Kuan Heng (Jordan) Lin, Oliver Wang, Aryan Law, Andrew Tsui, Karch A. Borsa, Spencer Bergland, Vyas Koduvayur, Phillip Tang, Sohan Talluri. Second row: Ryan Wong, Sumedha M. Shastry, Lucas J. Kim, Hongbo (Danny) Zhu, Zenya Bian, Paul Zhang, Emre Gürdal, Ken Woo, Naisha Agarwal, Vedant V. Janapaty. Third row: Malvika Iyer, Beverly Luring, Khushi Sharma, Lee Zucker-Murray, Katelyn Mak, Natalia Liang, Eshika Abbaraju, Yubin Kim, Chahak Gupta, Timothy Liu, Catherine Zhang. Fourth row: Felisha Kuo, Isabel Angres, Melody Jiang, Joanna Rhim, Priya Ravi, Kavya M. Pandrangi, Renee Chowdhry, Tanisha Lakhanpal, Siddhika Naik, Megan Huang.

The UCLA Undergraduate Science Journal is a peer-reviewed publication registered with the Library of Congress, featuring top-quality research performed by undergraduates in all STEM fields, including life sciences, engineering, statistics, physics, mathematics, computer science, and more. We aim to provide a multidisciplinary platform that allows students to publish their research and engage with the larger research community at UCLA and also involves students with the peer review process. Submitted manuscripts undergo a rigorous review and publication process run completely by undergraduates.

USJ accepts manuscript submissions and staff applications annually in the fall.

Correspondence should be addressed to Dr. Jorge A. Avila, Life Sciences 2121, 621 Charles E. Young Dr. S. Los Angeles, CA 90095 or the UCLA Undergraduate Science Journal at usj@ucla.edu.

We acknowledge the generous support of the Undergraduate Research Center–Sciences and of the UCLA Clinical and Translational Science Institute (CTSI) grant UL1TR001881 to publish this journal.

